Summer 2018

THE SAUDI ARAMCO JOURNAL OF TECHNOLOGY
A quarterly publication of the Saudi Arabian Oil Company

Saudi Aramco Journal of Technology

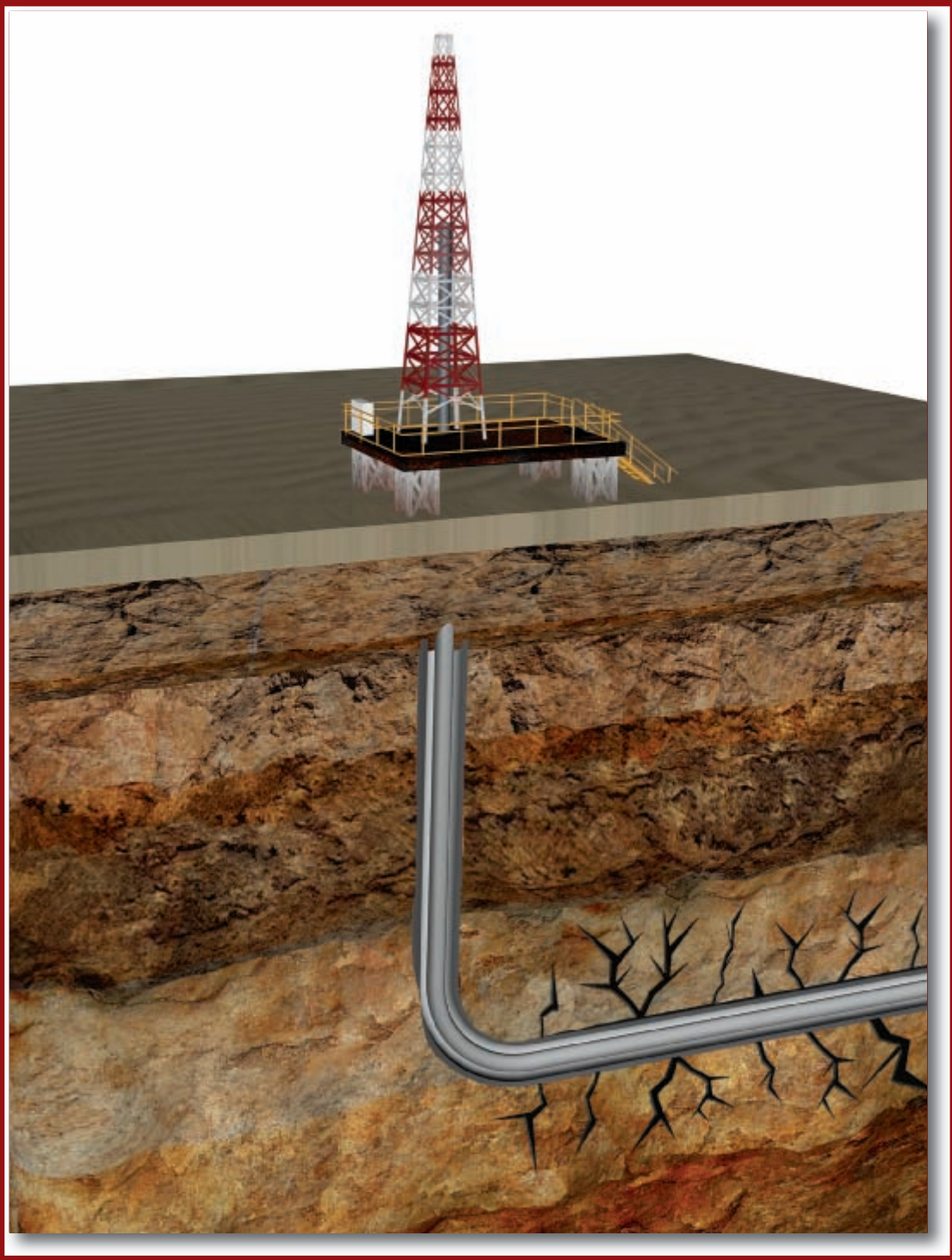

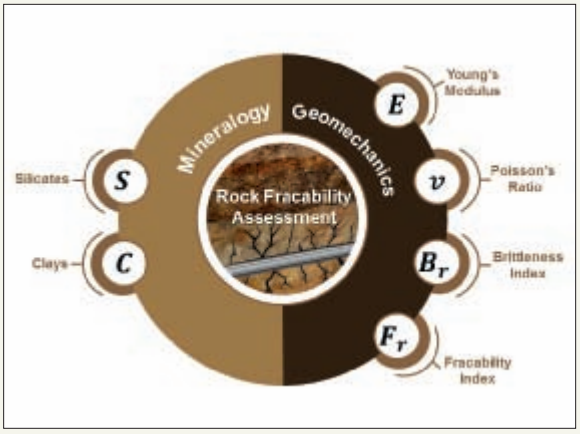

Integration of geomechanical parameters and mineralogical assessment to analyze rock stiffness and hydraulic fracture susceptibility.

On the Cover

A novel stimulation assessment to enhance production in Saudi Arabia: A coupled mineralogy and geomechanics approach to evaluate rock fracability and optimum zones for fracture generation. The study increased the percentage of successful stimulation jobs and had a major contribution to optimizing project economics.

MORE SAUDI ARAMCO JOURNAL OF TECHNOLOGY ARTICLES AVAILABLE ON THE INTERNET.

Additional articles that were submitted for publication in the *Saudi Aramco Journal of Technology* are being made available online. You can read them at this link on the Saudi Aramco internet website: www.saudiaramco.com/jot

The *Saudi Aramco Journal of Technology* is published quarterly by the Saudi Arabian Oil Company, Dhahran, Saudi Arabia, to provide the company's scientific and engineering communities a forum for the exchange of ideas through the presentation of technical information aimed at advancing knowledge in the hydrocarbon industry.

Complete issues of the Journal in PDF format are available on the internet at: http://www.saudiaramco.com (click on "publications").

SUBSCRIPTIONS

Send individual subscription orders, address changes (see page 75) and related questions to:

Saudi Aramco Public Relations Department
JOT Distribution
Box 5000
Dhahran 31311, Saudi Arabia
Website: www.saudiaramco.com/jot

CONTRIBUTIONS

Relevant articles are welcome. Submission guidelines are printed on the last page. Please address all manuscript and editorial correspondence to:

EDITOR

William E. Bradshaw
The *Saudi Aramco Journal of Technology*
C-11B, Room AN-1080
North Admin Building #175
Dhahran 31311, KSA
Tel: +966-013-876-0498
E-mail: william.bradshaw.1@aramco.com.sa

Unsolicited articles will be returned only when accompanied by a self-addressed envelope.

PRODUCTION COORDINATION

Richard E. Doughty

DESIGN

Graphic Engine Design Studio,
Austin, Texas, U.S.A.

ISSN 1319-2388.

The *Saudi Aramco Journal of Technology* gratefully acknowledges the assistance, contribution and cooperation of numerous operating organizations throughout the company.

أرامكو السعودية
saudi aramco

Summer 2018

THE SAUDI ARAMCO JOURNAL OF TECHNOLOGY
A quarterly publication of the Saudi Arabian Oil Company

Saudi Aramco Journal of Technology

Contents

Mineralogy and Geomechanical Analysis for Hydraulic Fracturing: An Integrated Approach to Assess Rock Fracability in Sandstone Reservoirs

Noor A. Alsaif, Ahmad R. Hage, and Dr. Hassan H. Hamam

ABSTRACT

A comprehensive integrated methodology is presented that assesses rock hydraulic fracability using rock geomechanics, mineralogy, and chemical compositions. This petrophysical multiple mineralogy-based approach utilizes sonic and density log data to relate mineralogy and geomechanics to rock stiffness and its susceptibility to fracture.

Rock fracability is assessed in terms of compressional and shear transit times from borehole acoustic logging. These transit times are used to calculate both Poisson's ratio and Young's modulus, which provide an indication of the tendency of a rock to fracture while preserving the opening of the fracture. The lower the Poisson's ratio, the more brittle the rock is, and the higher the value of Young's modulus. The brittleness index (B_r) and fracability index (F_r) are introduced to predict fracable rocks; sands with a B_r of 50 and higher, and a F_r above 0 and less than 1 are fracable candidates.

This geomechanical analysis is combined with rock mineralogy to make conclusive predictions about rock fracability. Rocks rich in silicates and sufficient clay volumes exhibit high rock fracability while ductile rocks negatively impact fracability. The success of the hydraulic fracturing jobs was observed to be directly related to rock mineralogy. The mineralogy groups for the wells in study were silicates — quartz and orthoclase — and clays — illite, kaolinite, and chlorite. Quartz associated with sufficient illite volumes promoted fracability; however, high contents of kaolinite led to unfavorable results, whereas small quantities of chlorite positively impacted fracability and promoted well deliverability. The integrated approach showed good predictability and consistency of rock fracability with a certain degree of error — within 10%.

This approach has been applied successfully on different sands with a wide variation in chemical compositions. It can predict wells with the highest success rate of the fracturing operation, save the injectivity test, minimize the fracturing costs and optimize the economics of tight reservoirs.

INTRODUCTION

Unconventional reservoirs are characterized by their ultra-low permeability albeit having an enormous potential for commercial production if successfully stimulated. Hydraulic fracturing has been extensively used in the oil and gas industry to unlock the trapped potential in tight formations. A large hydraulic fracture treatment is required to create pathways through which hydrocarbons can flow economically to the wellbore; however, the success of the hydraulic fracturing treatment remains a challenge. It is important to consider an effective operational procedure, optimum well placement and design and selection of zones that are prone to hydraulic fracturing to increase the chance of success of the hydraulic fracturing treatment.

This article presents an approach to help propose wells that are likely to be successful candidates for a hydraulic fracturing job. It evaluates rock fracability and selects zones that are susceptible to the generation of fractures based on rock geomechanics, mineralogy, and chemical compositions.

Several approaches have been proposed to assess rock fracability. Rickman et al. (2008)[1] used the elastic moduli of Young and Poisson to derive a relationship that is used extensively as a brittleness indicator. Glorioso and Rattia (2012)[2] established a brittleness indicator that is based solely on rock lithological compositions. Jin et al. (2014)[3] studied brittleness and their work integrated other parameters, including fracture toughness and energy dissipation during hydraulic fracturing to define a rock strength indicator, termed fracability index. Mullen (2012)[4] proposed another definition of fracability by integrating the sedimentary fabric, stratigraphic properties, mineral distribution, and the presence and orientation of preexisting planes of weakness to present the complex fracability index.

This article initially studies Young's modulus and Poisson's ratio to evaluate if a rock can be a candidate for hydraulic fracturing. It then uses the brittleness correlations defined[1] and introduces a fracability index based on the Lamé parameters to assess rock brittleness. This geomechanical analysis is integrated with mineralogical analysis for rock fracability evaluation.

STUDY MOTIVATIONS

Hydraulic fracturing is one of the most popular stimulation techniques; however, there is a chance that the stimulation job fails. Furthermore, a well can be successfully stimulated without reporting any fluids flowing to the surface. This unpredictable

performance can impact rig time, cost, and project economics. This study provides a viable method to assess rock fracability and provides an explanation regarding the success or failure and the flow potential of hydraulically fractured wells.

PETROPHYSICS

Bulk density (g/cc), ρ, compressional wave transit time (μs/ft), *DTC*, and shear wave transit time (μs/ft), *DTS*, are important for the evaluation of formation geomechanical properties. They are used to calculate rock elastic properties, i.e., Young's modulus and Poisson's ratio, and for stress estimations.

Density log data is converted to a gradient (psi/ft) by multiplying by the freshwater gradient: 1 g/cc = 0.433 psi/ft. At the top treatment depth, overburden pressure is obtained by multiplying by the overburden — geostatic/lithostatic — pressure gradient of 1.1 psi/ft. The overburden gradient is commonly assumed as 1 psi/ft[5]; however, 10% of this value is added as a safety factor since the assumption can vary based on many factors, including the geographic area and geologic timeline. The vertical overburden stress and horizontal stresses are then obtained for the entire treated interval.

In this article, the objective is not to present how to obtain formation stresses since it is well established in the industry, and there are several commercial and in-house developed types of software that can perform the subject calculations correctly. Nevertheless, relying on stress calculations only may not necessarily lead to a successful hydraulic fracturing job. To increase the chance of success, stresses should be accompanied by the understanding of rock fracability, which is the main objective in this study.

The petrophysical ultrasonic wave measurements — *DTC* and *DTS* — are used as the basis for the dynamic method. One of the key parameters in the developed method is the travel ratio (TR), which is the ratio of the *DTS* to *DTC* as shown in Eqn. 1.

$$TR = \frac{DTS}{DTC} \tag{1}$$

Measurements of densities and acoustic wave transit times are associated with some degree of uncertainty, e.g., shear data may require corrections in a rock with permeability of less than 1 millidarcy.

GEOMECHANICS

Identification of a fracable formation interval to achieve effective fracturing requires an assessment of rock brittleness. Brittleness could be defined in terms of elastic properties (Young's modulus and Poisson's ratio), strength parameters (compressive and tensile strengths), frictional properties (cohesion and friction coefficients), hardness, or the energy or strain budget (ratio of reversible to the total energy or strain, respectively[6]). In this article, elastic properties have been adopted to define rock brittleness, which is one of the indicators to ensure a successful hydraulic fracturing job.

Young's modulus and Poisson's ratio are essential parameters for the determination of rock stiffness. Young's modulus is defined as the ratio of tensile stress to tensile strain, where stress is the external force applied per unit area and strain is the resulting distortion — change in shape. Young's modulus describes the tendency of a material to deform along an axis as a result of opposing forces acting along that axis. Poisson's ratio, however, is defined as the ratio of lateral strain to longitudinal strain[7]. The degree to which the material will distort under stress is a function of Poisson's ratio.

Young's Modulus

The dynamic Young's modulus (psi), *E*, is the main parameter of elasticity and is related to the dynamic shear modulus (psi), *G*, and dynamic Poisson's ratio (υ) by the following equation:

$$E = 2G\ (1 + \upsilon) \tag{2}$$

Shear modulus is defined as the ratio of shear stress to shear strain. It describes the tendency of a material to shear — deform in shape at constant volume — when acted upon by opposing forces and it is calculated as follows[7]:

$$G = \frac{1.34\times10^{10}\ \rho}{DTS^2} \tag{3}$$

Poisson's Ratio

The dynamic Poisson's ratio is a function of the TR, and is calculated as follows:

$$\upsilon = \frac{0.5TR^2-1}{TR^2-1} \tag{4}$$

Dynamic properties are derived from well log data, whereas static properties are derived from lab core tests. The relationships between the dynamic and static Young's modulus and Poisson's ratio have been established using in-house core data analysis and they are used to determine the static elastic properties as shown in Eqns. 5 and 6:

$$E_{static} = 0.0001646742\ E^{1.5606} \tag{5}$$

$$\upsilon_{static} = 1.15\ \upsilon \tag{6}$$

where E_{static} is the static Young's modulus and υ_{static} is the static Poisson's ratio.

A plot of the *E* vs. E_{static} provides a symptom of rock stiffness, Fig. 1. Based on international standards, an E_{static} above 5×10^6 psi is an indication of hard sand and a value between 0.1×10^6 psi and 5×10^6 psi is the range of soft to medium sand. The typical Young's modulus values for sands and other rocks are presented in Table 1[7]. Accordingly, Fig. 1 shows that the

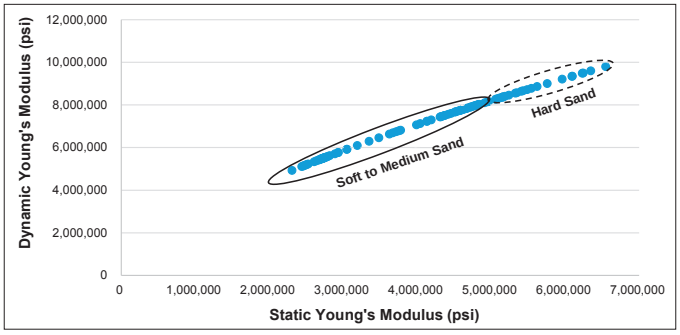

Fig. 1. The E *vs.* E_{static} *as an indicator of rock stiffness.*

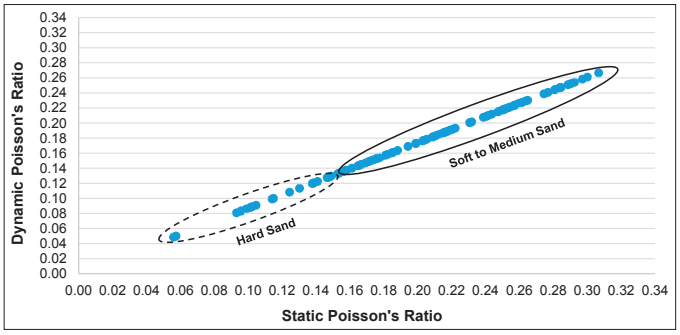

Fig. 2. The v *vs.* v_{static} *as an indicator of rock stiffness.*

Rock Type	Young's Modulus (psi)	Poisson's Ratio
Soft sandstone	0.1 – 1 × 10^6	0.2 – 0.35
Medium sandstone	2 – 5 × 10^6	0.15 – 0.25
Hard sandstone	6 – 10 × 10^6	0.1 – 0.15
Limestone	8 – 12 × 10^6	0.30 – 0.35
Coal	0.1 – 1 × 10^6	0.35 – 0.45
Shale	1 – 10 × 10^6	0.28 – 0.43

Table 1. Typical range of values for Young's modulus and Poisson's ratio for different rock types[7]

rock is a mixture of soft, medium and hard sands.

Figure 2 shows a plot of the v vs. v_{static}, which provides another indicator of the stiffness of the rock. The typical Poisson's ratio values for sands and other rocks are also presented in Table 1[7]. A decrease in Poisson's ratio below 0.15 indicates a hard rock.

In general, zones with higher Young's modulus and lower Poisson's ratio are more brittle and more fracable. Therefore, the harder the sand, the more likely that it will fracture. The presence of hard sand, as indicated by Figs. 1 and 2, qualifies the rock to be targeted for hydraulic fracturing. Nevertheless, Young's modulus and Poisson's ratio analyses are not conclusive and further analysis is required to study rock brittleness and evaluate fracability.

Rock Brittleness

Several empirical correlations have been developed for rock brittleness. In this article, Rickman's approach is used. Based on laboratory ultrasonic measurements[1], formation brittleness has been correlated to the static Young's modulus and static Poisson's ratio as per the following equation:

$$B_r = \frac{50}{7}\left(E_{static} - 28v_{static} + 10.2\right) \quad (7)$$

where B_r is the rock brittleness index.

Rickman's relationship reflects the tendency of a rock to fail under stress (v) while maintaining the opening of the fracture (E). Based on fracture mechanics, brittle rocks are targeted for fracturing because they are easier to fracture than ductile rocks due to their predominant elastic deformation[8].

Having calculated the static properties of Young's modulus and Poisson's ratio, the brittleness of both moduli is required to quantify rock brittleness. The Young's modulus brittleness, E_{BRIT}, is a function of the E_{static}, and is expressed in Eqn. 8.

$$E_{BRIT} = \frac{E_{static}-1}{7} \times 100 \quad (8)$$

The Poisson's ratio brittleness, v_{BRIT}, is a function of the v_{static} and the relationship is shown in Eqn. 9.

$$v_{BRIT} = \frac{v_{static}-0.4}{-0.25} \times 100 \quad (9)$$

The B_r is an average of the Young's modulus brittleness and Poisson's ratio brittleness as expressed in Eqn. 10.

$$B_r = \frac{E_{BRIT}+v_{BRIT}}{2} \quad (10)$$

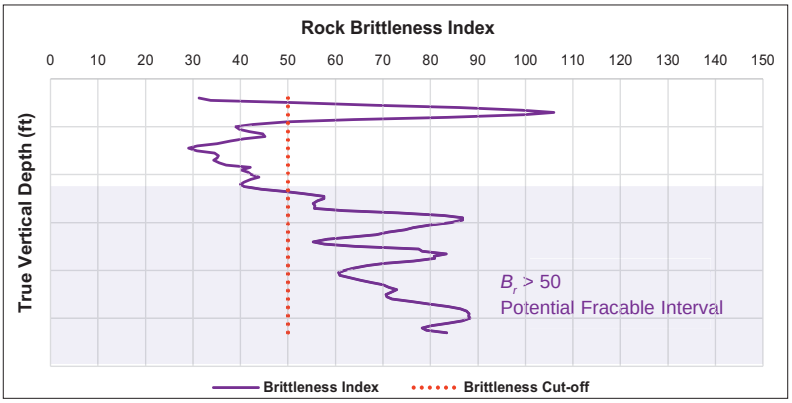

Fig. 3. B_r *to indicate potential fracable intervals.*

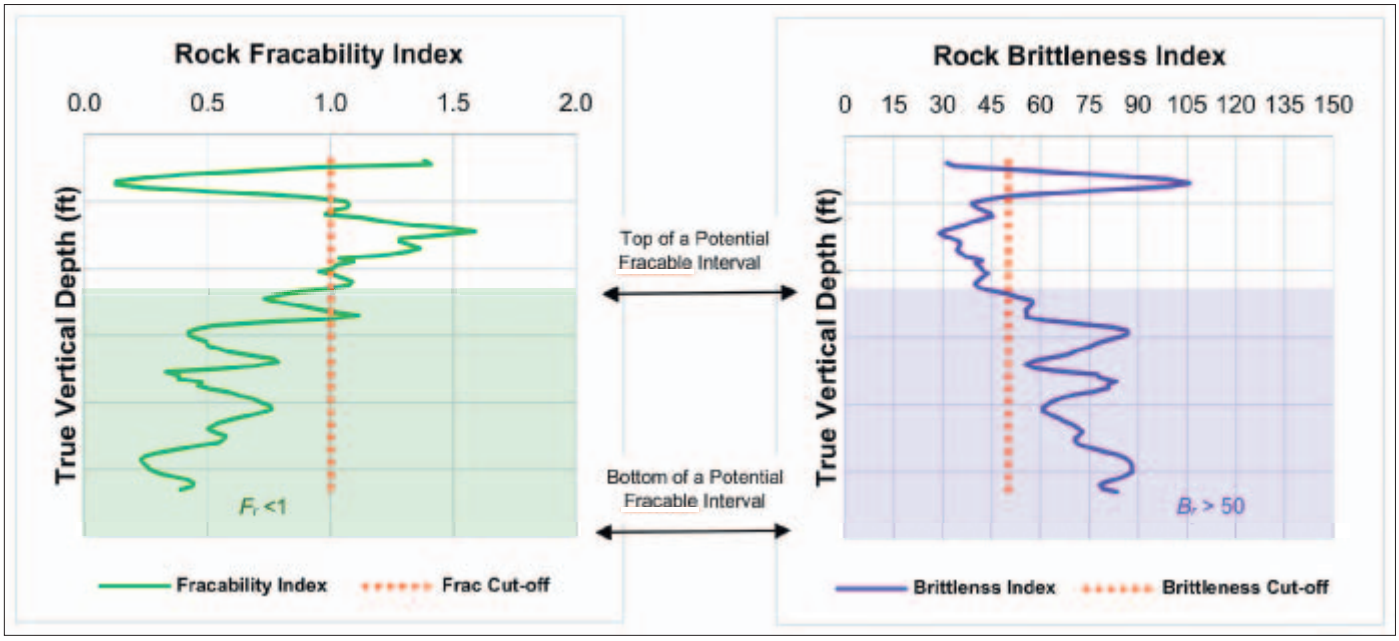

Fig. 4. The combination of F_r *and* B_r *analyses to indicate potential fracable intervals (same depth scale).*

To distinguish a brittle rock from a ductile rock, a brittleness cutoff is applied. Stimulation data shows that a rock is brittle if it has a B_r above 50. A B_r below 50 indicates that the rock becomes more ductile and it may act as a fracture barrier; therefore, it should not be targeted for hydraulic fracturing. Analysis of the B_r shows that the highlighted interval in Fig. 3 is a potential fracable interval.

Rock Fracability

Fracability is another major index that is used conjointly with the B_r analysis to verify fracture prone intervals. The two essential parameters in calculating the fracability index (F_r) are the Lamé parameters of lambda, (psi), λ, and mu, (psi), μ. The λ can be termed incompressibility, Eqn. 11[7], and μ is rigidity, Eqn. 12[9], and their ratio (λ/μ) is the F_r, Eqn. 13. According to Goodway et al. (2007)[10], low incompressibility and high rigidity indicate a brittle zone.

$$\lambda = \frac{E_{static}\, v_{static}}{(1+v_{static})\times(1-2v_{static})} \quad (11)$$

$$\mu = \frac{E_{static}}{2\,(1+v_{static})} \quad (12)$$

$$F_r = \frac{\lambda}{\mu} \quad (13)$$

The F_r for a fracable interval was found to range between 0 and 1. A rock may fail to fracture when the F_r is greater than 1, due to the rock becoming more ductile. Therefore, it should not be taken as a potential candidate. Plotting both brittleness and fracability indices in one chart can provide significant information about possible fracable intervals, which can vary over the thickness of the target reservoir. Figure 4 shows a plot of the F_r vs. depth combined with the preceding B_r analysis to identify an interval that has a significant chance to fracture.

MINERALOGY

Rock fracability estimation using well log and geomechanical data should be coupled with mineralogical analysis — mainly the chemical composition of the rock. A thorough multiple mineral analysis was conducted to derive an understanding of the impact of mineralogy on the susceptibility of a rock to fracture and flow. There were four mineral groups in this study: Silicates, clays, carbonates and others. Calcite, dolomite, and siderite were nearly absent, and therefore, carbonates were not considered. Other discarded mineralogy includes pyrite, anhydrite, apatite, and aragonite. Silicates consist mainly of quartz, K-spar/orthoclase, and albite. On the other hand, clays consist of different chemical compositions, including illite, kaolinite, chlorite, and mixed clays. In general, silicates are considered rock hardening minerals, whereas clays soften the rock.

This study covered two types of sands, and each sand showed a totally different performance based on the chemical composition of the rock. The general understanding in the industry is that a clean sand is a potential successful candidate, although each sand has its own story and should be studied separately. Quantitative assessment of silicates and clay minerals aids in predicting rock fracability.

In addition to geomechanics, rock ductility assessment is one of the main parameters that should be studied before the injectivity test. Clay contents can either increase or decrease rock ductility and having significant or insufficient amounts of clays can lead to unfavorable results. A sufficient amount of illite in a quartz-rich rock tends to soften the rock and promote fracability. Nevertheless, rocks with higher illite volumes increase ductility that may hinder fracability. The transition from a brittle rock

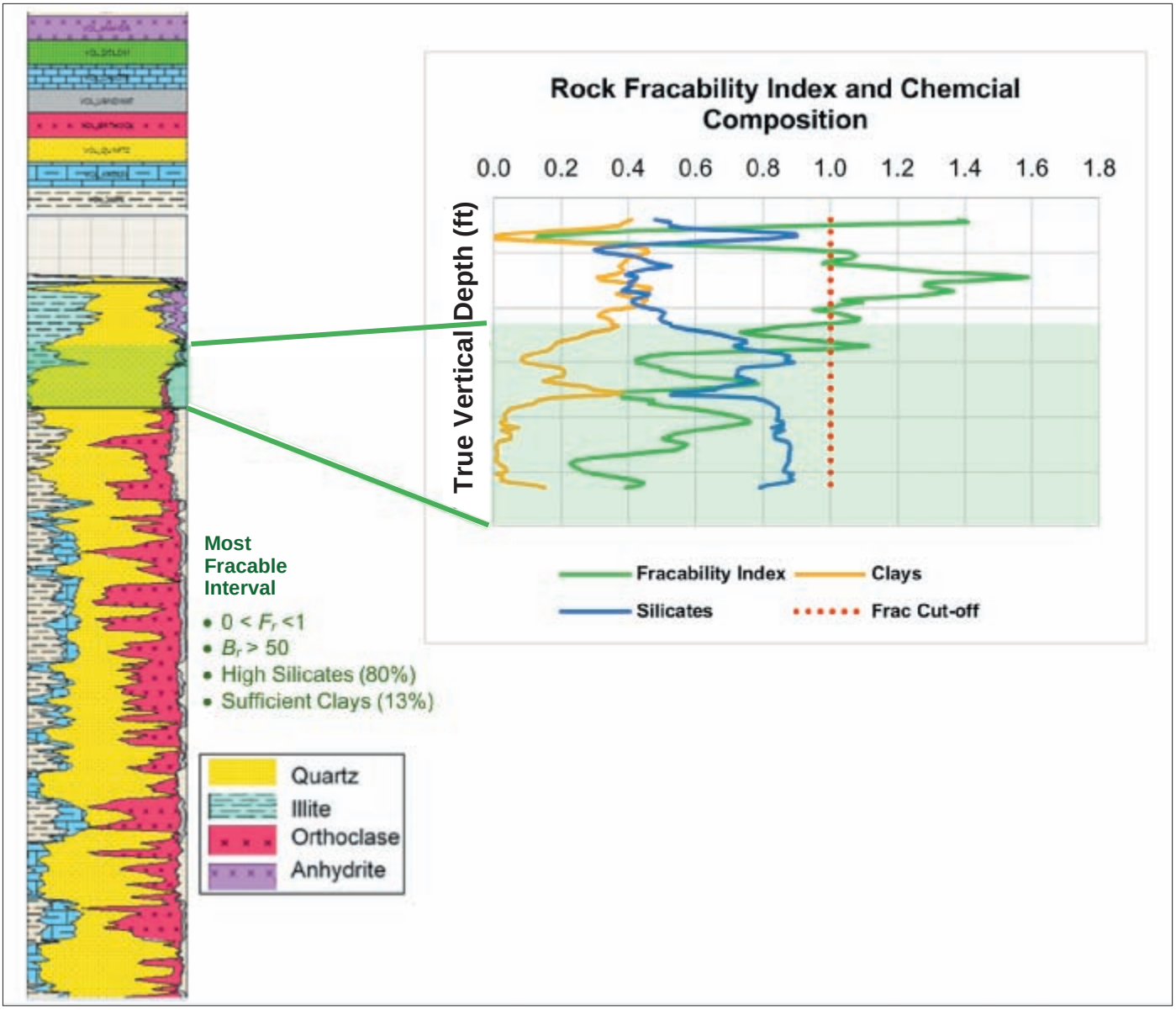

Fig. 5. Integration of mineralogy and geomechanical analysis to indicate potential fracable intervals.

to a ductile rock should be estimated for each sand type.

Moreover, another major constituent is chlorite, which plays an important role in decreasing rock stiffness and lowering the degree of cementation. A successful stimulation job with significant chlorite contents had the tendency to flow, whereas a successful hydraulic fracturing job without chlorite failed to flow. Kaolinite is another constituent that was observed to have a negative impact on fracability, and that could be attributed to the hardening behavior or plasticity of kaolinite.

Applying this understanding in conjunction with the preceding geomechanical analysis can lead to a reliable prediction of rock fracability. Figure 5 illustrates how this integrated method helps to identify an interval with the highest fracturing potential. A F_r of less than 1 associated with high silicates, and sufficient clays indicate that the highlighted interval can be a target for hydraulic fracturing. Moreover, this interval is equivalent to a B_r higher than 50, as previously seen in Fig. 3.

Therefore, both geomechanics and mineralogy give consistent results regarding the zone that is prone to fracturing, which increases our confidence regarding rock fracability predictions. For the rock in this study, the ideal amounts of silicates and clays to fracture the rock were found to be 80% and 10% to 15%, respectively.

Consequently, if the integrated approach indicates potential fracable intervals, the well is a potential successful candidate for hydraulic fracturing and it should be proposed for a hydraulic fracturing job. The potential fracable zones are to be targeted for hydraulic fracturing.

The deviation from this mineralogy may affect the success rate of the hydraulic fracturing job. This mineralogical evaluation acts as a quick indicator of rock fracability in all sands. Nevertheless, the chemical composition enhancing rock fracability varies from one sand to another and it has proven to be a main factor explaining why each sand behaves differently when it comes to hydraulic fracturing.

CONCLUSIONS

A viable approach was presented to evaluate fracability in sandstone reservoirs. This approach entails the use of geomechanical parameters in conjunction with mineralogical assessment to analyze the stiffness of the rock and evaluate its susceptibility to hydraulic fracturing. Petrophysical data was used to derive rock chemical compositions and also calculate Young's modulus and Poisson's ratio as an initial assessment of rock stiffness. The two indices, B_r and F_r, were then obtained and the following outcomes were attained from this study.

1. Sands with a B_r of 50 and higher and a F_r ranging between 0 and 1 are brittle, and they should be taken as potential successful candidates for hydraulic fracturing.
2. Rock ductility assessment is required to tie mineralogy with geomechanics. In general, silicate-rich rocks with a sufficient amount of clays are brittle and have the tendency to fracture. When the rock becomes ductile, it has poor fracability. The transition from brittle to ductile should be estimated for each sand type.
3. Mineralogy alone should not be used to study rock fracability. The chemical compositions enhancing rock fracability vary from one sand type to another, which explains why each type of sand behaves differently when hydraulically fractured.

This approach can be used to assess rock fracability before conducting the injectivity test and the hydraulic fracturing job to determine whether or not a well can be a successful candidate for hydraulic fracturing.

RECOMMENDATIONS

1. The presented approach can be enhanced using production and temperature logs to verify the fractured zones and narrow down the ranges of the B_r and F_r for fracable intervals.
2. This study helps to predict in advance which wells to stimulate to avoid fracturing wells in locations where the rock does not have the tendency to fracture, thereby minimizing the fracturing costs. One extra step to optimize cost savings is enhanced well placement by targeting locations that are most fracable to minimize both drilling and fracturing cost. This can be achieved by constructing 3D models and incorporating stresses, along with the results of this integrated fracability analysis, to extend fracability evaluation beyond well level.

ACKNOWLEDGMENTS

The authors would like to thank the management of Saudi Aramco for their support and permission to publish this article. Special thanks go to Mustafa Abdulmohsin for his support in providing all of the petrophysical data.

This article was presented at the Abu Dhabi International Petroleum Exhibition and Conference, Abu Dhabi, UAE, November 13-16, 2017.

REFERENCES

1. Rickman, R., Mullen, M.J., Petre, J.E., Grieser, W.V., et al.: "A Practical Use of Shale Petrophysics for Stimulation Design Optimization: All Shale Plays Are Not Clones of the Barnett Shale," SPE paper 115258, presented at the SPE Annual Technical Conference and Exhibition, Denver, Colorado, September 21-24, 2008.
2. Glorioso, J.C. and Rattia, A.J.: "Unconventional Reservoirs: Basic Petrophysical Concepts for Shale Gas," SPE paper 153004, presented at the SPE/EAGE European Unconventional Resources Conferece and Exhibtion, Vienna, Austria, March 20-22, 2012.
3. Jin, X., Shah, S.N., Roegiers, J-C. and Zhang, B.: "Fracability Evaluation in Shale Reservoirs — An Integrated Petrphysics and Geomechanics Approach," SPE paper 168589, presented at the SPE Hydraulic Fracturing Technology Conference, The Woodlands, Texas, February 4-6, 2014.
4. Mullen, M.J. and Enderlin, M.B.: "Fracability Index — More Than Rock Properties," SPE paper 159755, presented at the SPE Annual Technical Conference and Exhibition, San Antonio, Texas, October 8-10, 2012.
5. Castagna, J.P. and Backus, M.M.: *Offset-Dependent Reflectivity: Theory and Practice of AVO Analysis*, SEG Books, 1993, 348 p.
6. Rybacki, E., Reinicke, A., Meier, T., Makasi, M., et al.: "What Controls the Strength and Brittleness of Shale Rocks?" Abstract presented at the EGU General Assembly, Vienna, Austria, April 27-May 2, 2014.
7. Crain, E.R.: "Crain's Petrophysical Handbook," 3rd edition, Spectrum 2000 Mindware, 2010.
8. Bai, M.: "Why are Brittleness and Fracability not Equivalent in Designing Hydraulic Fracturing in Tight Shale Gas Reservoirs," *Petroleum*, Vol. 2, Issue 1, March 2016, pp. 1-19.
9. Zhang, D., Ranjith, P.G. and Perera, M.S.A.: "The Brittleness Indices Used in Rock Mechanics and Their Application in Shale Hydraulic Fracturing: A Review," *Journal of Petroleum Science and Engineering*, Vol. 143, July 2016, pp. 158-170.
10. Goodway, B., Varsek, J. and Abaco, C.: "Isotropic AVO Methods to Detect Fracture Prone Zones in Tight Gas Resource Plays," paper presented at the CSPG/CSEG GeoConvention 2007, Calgary, Alberta, Canada, May 14-17, 2007.

BIOGRAPHIES

Noor A. Alsaif joined Saudi Aramco in 2014 as a Petroleum Engineer. She is currently working as a Simulation Engineer in the Event Solutions Center of the Reservoir Description and Simulation Department (RDSD). Noor is a member of a multidisciplinary team dedicated to conducting integrated reservoir studies on Saudi Aramco fields with the objective of devising field development plans that maximize recovery while minimizing cost. Since joining the Event Solutions Center, she has participated in several successful projects, creating eminent value in meeting company objectives.

Before Noor joined the Event Solutions Center, she completed several assignments in the Khurais Reservoir Management Department, Reservoir Description and Data Management divisions.

In 2014, Noor received her B.S. degree in Petroleum Engineering from the University of Leeds, Leeds, U.K.

Ahmad R. Hage is a Petroleum Engineering Specialist working with the Advanced Well Testing Modeling Group in Saudi Aramco's Reservoir Description & Simulation Department. Prior to this, he occupied different senior positions in reservoir engineering and conducted study and research with the Abu Dhabi National Oil Company in Abu Dhabi, Halliburton Asia Pacific, and Petroleum Development Oman (Shell) in Sultanate of Oman.

Ahmad received his B.S. degree in Petroleum Engineering from the American University of Beirut, Beirut, Lebanon, and his M.S. degree in Petroleum Engineering from Heriot-Watt University, Edinburgh, U.K. He has also completed postgraduate research in gas enhanced oil recovery technology.

Dr. Hassan H. Hamam is a Senior Reservoir Engineer who started his career with Saudi Aramco in 2005. He works in the Integrated Reservoir Studies Group of Saudi Aramco's Reservoir Description and Simulation Department.

In 2005, Hassan received his B.S. degree in Petroleum Engineering from West Virginia University, Morgantown, WV, and in 2010, he received an M.S. degree in Petroleum Engineering from Texas A&M University, College Station, TX. In 2016, Hassan received his Ph.D. degree in Petroleum Engineering from Penn State University, State College, PA. His Ph.D. work focused on the applications of the coupling of artificial intelligence and enhanced oil recovery.

Design Transformation of Hydraulically Powered Coiled Tubing Tractors for Matrix Acidizing Stimulations in Extended Reach Carbonate Reservoirs

Laurie S. Duthie, Abubaker S. Saeed, Saud A. Shaheen, Hussain A. Al-Saiood, Dr. Norman B. Moore, and Ernst Krueger

ABSTRACT

The deployment of hydraulically powered coiled tubing (CT) tractors for matrix acidizing stimulations in extended reach carbonate reservoirs have provided critical benefits to well productivity. The technology allows for uniform placement of the matrix acid treatment while ensuring good zonal coverage. There have been several innovative tractor technologies developed over the last few years and the latest advances in design required an "out of the box" solution. For oil producers with electric submersible pump (ESP) completions, including bypass sections, the 2.4" restriction in tubing size requires a large expansion ratio once the tractor enters the 7" cased and 6⅛" open hole sections. The slim size of the tractor and expansion ratio were the main challenges to overcome in designing a tractor capable of delivering a high enough pull force to reach deeper target depths. It was recognized that a radical change in slim tractor design was required if these goals were to be met.

Although 2⅛" slim CT tractors have been used extensively in this field, the results were not always consistent, leading to reduced coverage during the acid stimulation of the well, which resulted in lower production and reservoir optimization. These previous tractors relied upon wheel sections to transfer the pulling force to the casing, or open hole. Although these tractors performed well in the cased hole environment, they were less effective once the wheels came in contact with the reservoir rock. To overcome this deficiency, a completely new approach was taken in designing a slim tractor that could deliver a much higher pull force with improved grip in the open hole section. The new design uses a synchronized gripper system to enable the tractor to have continuous traction in the open hole section. This new compact design, while less than one-half the length, produces almost double the pulling force of the previous wheel-based slim CT tractors.

During the trial test, the tractor delivered a pulling force of up to 3,500 lb to overcome friction and helical buckling forces to reach the target depth. This resulted in an increase in the stimulation coverage from the original lockup depth of around 50% of the open hole, to increase the coverage to 100% of the open hole.

This new design opens a window to ultimately meet the goals of improved well treatment in long horizontals resulting in better productivity and uniform flow distribution in extended reach wells. New generations of the tractor are planned for development with increased pull force, higher expansion ratios for larger open hole sizes, and also to allow real time production logging with the CT.

BACKGROUND

The design of the 2⅛" hydraulically powered tractor began with a feasibility study that resulted in a shortlist of three designs identified as the most applicable. From the three conceptual designs, the first two designs were eliminated within the first month, and work carried on for another two months on the third design, which was selected as the best candidate for development. A prototype version of the tool was built and tested extensively; these early demonstrations proved the potential of the technology. The manufacturing of a set of tools based on the prototype version was completed, and the first field trial was finalized within a year from the start of the project. The process resolving core design issues was addressed with rapid prototyping of key design features, fast shop testing, and adaptive response to field experience.

INTRODUCTION

During coil tubing (CT) well intervention for extended reach wells, the goal of reaching target depth or at least covering a sufficient proportion of the open hole remains one of the most elusive challenges today. The challenges of early lockup in CT interventions due to helical buckling and weight stacking have been covered extensively in technical literature[1]. This is of particular importance in the target field, where over 60% of the wells experience CT lockup before reaching target depth. Since the drilling program started, several types of innovative tractors and vibrating tools — combined with other solutions — have been developed to enhance the reach of the CT.

During matrix acid stimulation treatments, the importance of covering the maximum length of the open hole cannot be understated. Failure to treat the entire wellbore could potentially leave significant portions of the open hole section in a nonproductive condition. Attempting to bullhead the treatment from an early lockup depth to stimulate the section

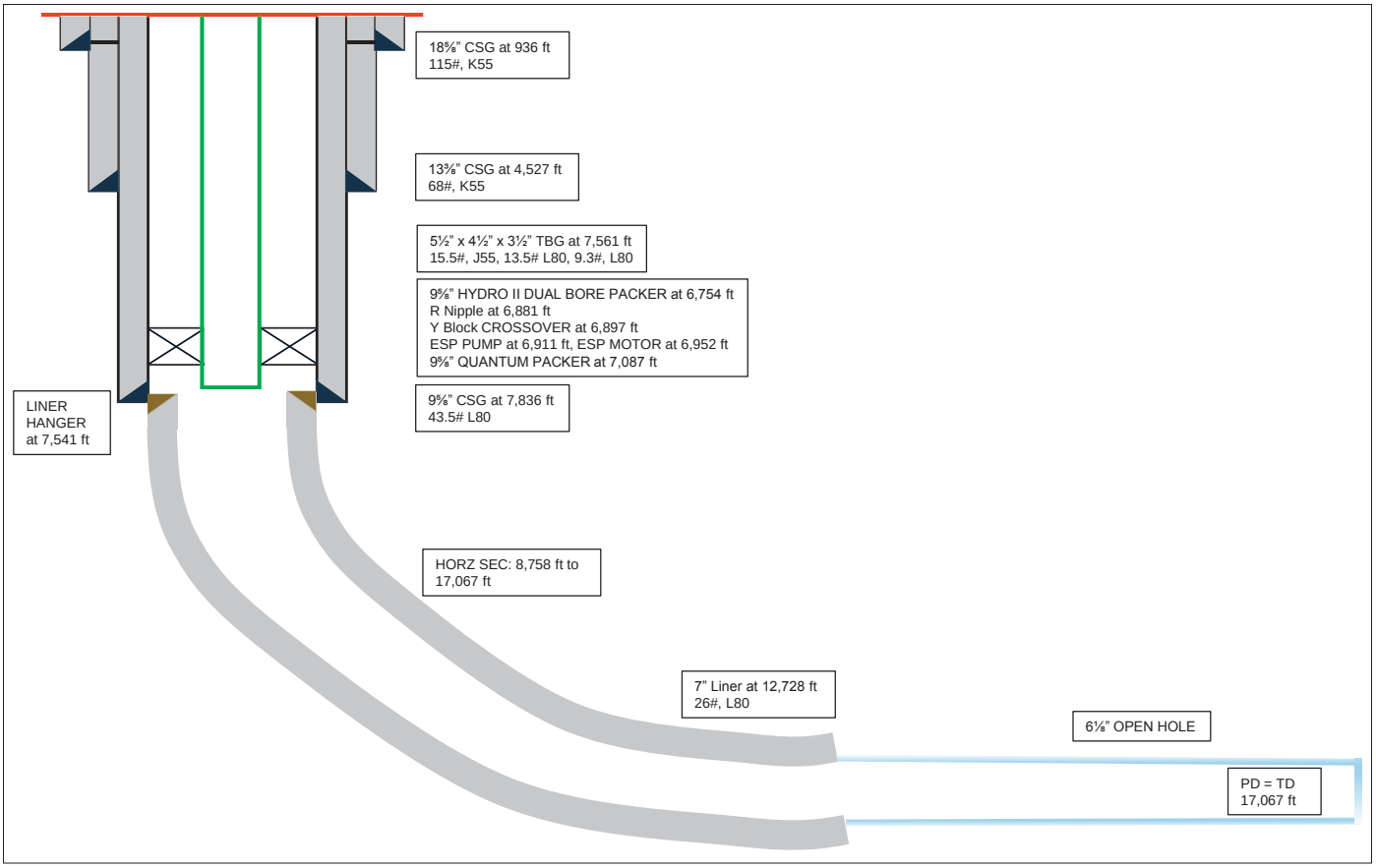

Fig. 1. A diagram of a typical well completion.

where the CT did not reach may not result in the desired outcome. Rather, the treatment fluids will take the path of least resistance to the non-damaged and highly permeable zones, which may not require stimulation, while missing completely the zones that are most in need of the treatment[2]. This is far from a satisfactory outcome. The advantages of drilling extended reach wells — increased reservoir contact, reduced footprint, less wells drilled — quickly becomes a disadvantage, and the additional cost of drilling the extended reach wells may effectively contribute zero benefit.

WELL OVERVIEW

This article will review the actual trial run on one of the extended reach wells that required additional pulling force to reach target depth, and to complete the acid stimulation successfully. The completion diagram, Fig. 1, is typical for the oil producers in this field, with a 9⅝" casing for the upper completion, a 7" liner for the lower completion, and a 6⅛" horizontal open hole section.

The well is completed with a 4½" tubing, a Y-block assembly, an electric submersible pump (ESP), and a 2⅞" bypass tubing to allow well intervention, Fig. 2. The minimum restriction in the bypass tubing is 2.441", as this restriction limits the diameter of the collapsable tractor to pass through with adequate clearance. The 3D plot in Fig. 3 illustrates the well profile in terms of azimuth, trajectory, and inclination of the wellbore.

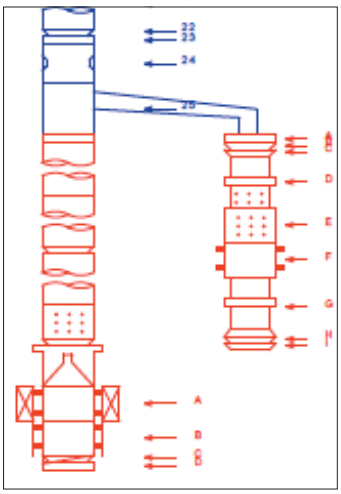

Fig. 2. ESP bypass system.

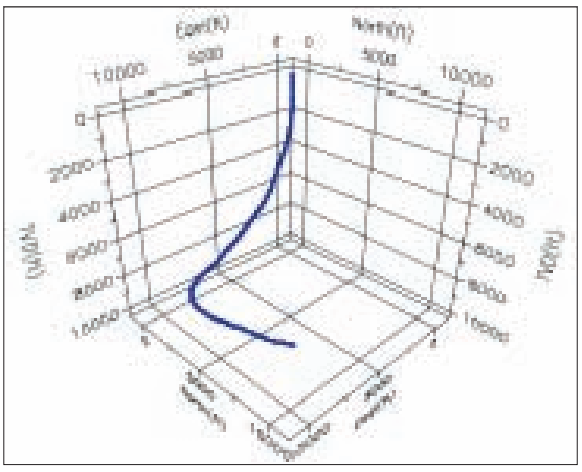

Fig. 3. A 3D well profile illustrating the azimuth, trajectory, and inclination of the wellbore.

ALTERNATIVE TRACTOR DESIGNS AND PERFORMANCE

Several iterations of slim-hole tractors have been developed and deployed in the field with varying degrees of success.

All of these previous designs relied upon wheels to grip the side of the casing or open hole, and to pull the CT along the hole. The single-stage hydraulically powered tractor had limited success with insufficient pull force to make a significant impact on the distance traversed along the hole.

The second generation of the slim-hole wheel-based CT tractor added a second section to increase the pull force. The tandem tractor is a hybrid construction and consists of a single hydraulically powered tractor and a second electrically powered tractor to form the tandem tractor. Turbine and generator subs are included to generate the electricity for the second section. The tandem tractor was a definite improvement on the single-stage tractor and was deployed successfully in several wells. The pulling force in the open hole was significantly less than the pulling force inside the 7" liner section, and the tandem tractor reduced the pulling force in the open hole, proving a limitation for longer extended reach wells[3].

The third generation of the slim-hole wheel-based CT tractor added a third section to further increase the tractor pulling force. A second electrically powered section was added, together with the hydraulically powered section, to form the tridem tractor. The third section increased the overall rig up height for the blowout preventers, lubricator and CT injector head, making it unsafe to proceed as a stand-alone rig up. An eight-level tower structure was erected to safely support the complete rig up. The tridem tractor performed as expected in the 7" liner, delivering the desired pulling force over multiple runs, showing excellent consistency. The tridem tractor was unable to make significant progress in the open hole with a significant drop in pulling force.

The performance of a wheel-based tractor in the open hole, specifically for CT applications, as opposed to wireline, so far has not resulted in delivering the required pull force to provide confidence to use this technology for the longer extended reach wells. The length of the tool and subsequent rig up height requiring a tower structure increased the cost and duration of the job considerably, and is not considered a viable long-term solution.

STRATEGIES TO INCREASE REACH

One key objective during the well intervention in extended reach wells is to delay the onset of helical buckling of the CT as far as possible. This will not only guarantee that more of the open hole section will be covered, but will also reduce the overall workload on the tractor, greatly increasing the likelihood of reaching the target depth. Several techniques are used to attain this, including tapered tubing, friction reducers, organic solvents, and hole clean out procedures.

Tapered tubing has been used extensively in this field, the external diameter of the CT is constant at 2" and the internal diameter has been tapered with the minimum metal thickness — lightest — at the end of the CT. The basic premise for the tapered tubing is to have the lighter section of the tapered tubing in the horizontal section, and the heavier walled tubing in the vertical section. The maximum compression forces will occur on the vertical and near vertical sections; these forces will be transmitted through the reel to allow the lightest part of the reel to reach the furthest possible distance. All of the wells in the field have been grouped into five categories determined by the length of the well. Depending on the category of the well, a tapered CT reel is selected that is matched to the category.

One of the most recent tools to be used to extend the CT reach has been the use of a high-pressure blasting tool on the end of the CT to clean out the downhole liner from around a 60° deviation point to the end of the horizontal liner section. Any fine solids that have accumulated along the horizontal section will increase the frictional forces; the disturbance and removal of these fine solids reduces the overall frictional forces acting against the CT. During this clean out procedure, the well is flowed back to the surface where possible, and the solids are captured in a solids filter. This action alone has reduced the friction coefficient by up to 15% on some of the treated wells, resulting in a considerable additional distance covered before lockup. If there is evidence of high viscosity fluids such as tar, organic solvents are applied and allowed time to dissolve the material. The presence of tar downhole can be identified based on a few factors, such as higher than expected weights seen when pulling out of the hole (POOH) — caused by higher drag forces — evidence of tar on the tools when pulled back to the surface, and the actual well placement in the reservoir. The entire 7" liner section from around a 60° deviation to the end of the horizontal liner is fully cleaned out with several passes, if required.

Once the friction coefficient is at the expected level as determined by previous experience and the simulations run for that particular well, the CT is POOH to the surface and the tractor is connected for the actual stimulation run. To further reduce the frictional forces, a friction reducer agent is introduced while being run in hole (RIH) with the tractor. Typically, a layer of this metal to metal friction reducer is pumped over the same section of the 7" liner that was cleaned out on the previous run. The chemical selection and concentration of the friction reducer was selected to provide the optimum level for reducing the frictional drag forces. No friction reducer is used in the open hole section, to avoid contributing to formation damage[4].

CT TRACTOR TRANSFORMATION

A continuing effort to push the envelope in maximizing the pull force for slim-hole CT tractors has required a transformation in design to meet the objectives. A CT mechanical tractor typically consists of a main body, with arms that collapse, allowing the tool to pass through completion restrictions, and then extend out to engage with the wellbore to commence tractoring in horizontal sections. Once the tool is in tractoring

Fig. 4. A 4.7" hydraulically powered tractor.

mode, the body of the tool is centralized in the horizontal hole with arms extended, making contact with the casing or rock face, Fig. 4.

For tractors designed to work in completions with larger through bore sizes, this design performs well and is the logical design choice. The main body of the tractor is of sufficient size to allow a good expansion ratio while maintaining the required material density, providing material strength for the arms to deliver a high pulling force. This design runs into limitations once constraints in the completion demand a slimmer sized tractor. With the maximum outer diameter of the tractor tool at 2⅛", and using a minimum dual armed tractor, the arms must have sufficient material strength to deliver the high pulling force needed to pull the CT to target depth in extended reach wells. This proved to be a major constraint, as the necessary expansion ratio from 2.125" up to 7.4" could not provide sufficient strength in the arms to meet the desired pulling force.

The relationship between the expansion ratio and the maximum pulling force is directly correlated. As the expansion ratio increases, the cross-sectional area of the arm material must be increased to maintain the same level of structural strength to prevent mechanical failure. The forces or strain acting on the arms during the pulling process put the material under stress, in reaction to the load applied to the material.

The basic relationship between the load applied to the cross-sectional area of the material and the resultant stress is as follows:

$$\text{Stress} = \sigma = \frac{F}{A} \quad (1)$$

where σ = stress (lb per in²), F = applied force (lb), and A = cross-sectional area (in²).

Therefore, an increase in the cross-sectional area of the load bearing structure will result in a stress reduction. A secondary constraint on the design is that the materials not only need to be high strength and durable, they must also be able to perform in hostile conditions with exposure to high concentration levels of hydrogen sulfide (H_2S), 15% hydrochloric (HCl) acid, high temperature, and pressure. The main components of the tractor are constructed from inconel/beryllium copper and are well equipped to withstand the toughest of downhole environments.

A review of the simulations for the most challenging extended reach wells in the field determined that a pull force of 3,500 lb was needed to pull the CT to target depth. The challenge was to find an alternative solution to the standard tractor construction, to satisfy all the criteria and meet the project objectives. To increase the pull force, a novel solution was found. Instead of a centralized dual or tri-arm tractor, the main body of the tractor itself is effectively used as one of the arms, allowing for a larger, heavy-duty arm to grip the other side of the hole, Fig. 5.

This solution proved a breakthrough for the innovative tractor design, along with several other key features described later. A prototype was built successfully proving the concept, followed by the manufacturing of three tractors for field trials. A rigorous and lengthy testing phase was conducted on the tractor to simulate actual downhole conditions as close as possible, before release for the actual field trial.

TRACTOR OPERATIONAL ELEMENTS

The 2⅛" CT tractor is powered by the differential pressure from the bore of the CT to the wellbore annulus. The actual operation of the tool from the surface is very simple, and only requires a pre-set pump rate limit to be met for the tractor to be activated. The tractor can be turned off at any time by reducing the pump rate below the pre-set level.

To reactivate the tractor, the pump rate is first set to zero, then increased to the pre-set level to restart the tractor.

Fig. 5. A 2⅛" hydraulically powered CT tractor — the eccentric link gripper (ELG) section.

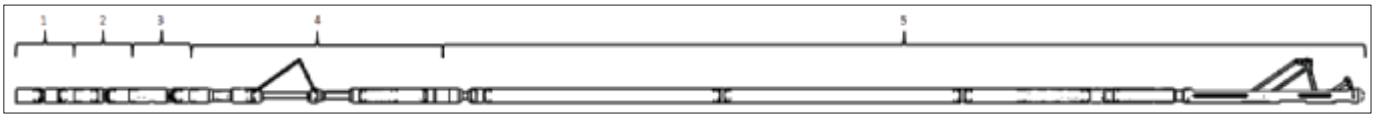

1	Relief Valve Sub (RVS)
2	Bottom-hole assembly (BHA) Isolating Circulation Sub (BICS)
3	Filter Nozzle Sub (FNS)
4	Static Gripper
5	Tractor and Gripper Assembly

Fig. 6. A 2⅛" CT tractor with dual ELG actuated.

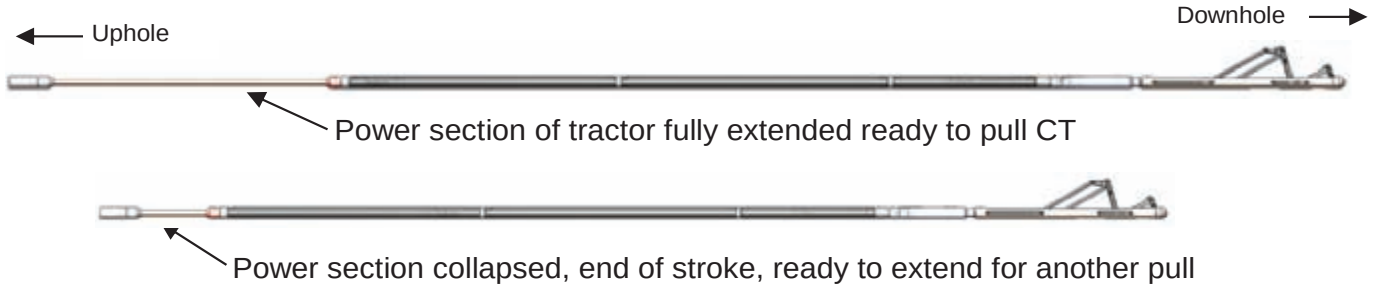

Fig. 7. Operation mode of the 2⅛" CT tractor.

Intervention fluid, usually diesel or water, delivers pressurized fluid to the power section and the eccentric link gripper (ELG) in a synchronized manner via a piston control assembly. When the tractor is walking, fluid pumped though the tractor exits through the front ELG assembly. This constant flushing maintains a debris free environment necessary for the optimum tool operation. The 2⅛" CT tractor "walks" in an accordion-like motion; with the ELG collapsed and sitting at the bottom of the hole, the power section pushes and extends the gripper assembly downhole.

Next, the ELG is powered, thereby engaging the gripper on the roof of the hole, away from any debris. The ELG is designed to orient the gripping elements to the top of the wellbore regardless of initial positioning. The self-righting feature of the ELG involves three aspects of the design. First, the gripper assembly is free to rotate relative to the tractor body and CT. Second, the gripper body naturally sits at the bottom of the wellbore. Third, as the gripper links extend from the bottom of the hole and contact the wellbore, it applies a normal force with both a radial and circumferential component. The radial component provides the traction for the tractor. The circumferential component puts a moment that twists the freely rotating gripper body until the links reach the top of the hole, where there is only normal radial force, and the gripper is centered. Importantly, this process is empirically verified every time the tractor functions. With the ELG gripping the roof of the wellbore, the power section is energized, pulling the CT downhole. Figure 6 illustrates the typical configuration of the 2⅛" CT tractor. Figure 7 demonstrates the CT tractor in operation mode.

For the 2⅛" CT tractor to operate in both a cased and open hole, the ELG is equipped with two gripping elements — a smaller gripper for the cased hole and a large gripper for an open hole. The open hole gripper has a larger gripping element to accommodate irregular hole shapes. With the potential for retrieval difficulties after completion of an intervention, the ELG is equipped with an automatic gripper collapse by depressurization of the system. In addition, two fail-safe systems can be activated hydraulically or mechanically. Extensive empirical verification of forced reset retraction for both the mechanical and hydraulic fail-safe were performed.

Fig. 8. Assembly of 2⅛" tractor subs.

Figure 8 shows an external view of the filter nozzle sub (FNS), which filters intervention fluid to power the tractor; the relief valve sub (RVS) maintains optimum tractor operating pressure; a BHA isolating circulation sub (BICS) isolates the tractor during acidization or allows pressurized fluid to activate the tractor by cycling the surface pumps. The 2⅛" tractor is 100% hydraulic and requires no electrical power.

KEY DESIGN FEATURES

The 2⅛" CT tractor has several key design features to provide a reliable and safe deployment:

- Dual ELG: A specially designed, small diameter, high capacity gripper that engages the top of the wellbore,

away from any debris at the bottom of the hole. It is designed to operate in various open and cased hole diameters.

- Hydraulically actuated secondary fail-safe mechanism (hSFM): A feature that forcefully disengages the gripper from the wellbore via hydraulic pressure.
- Mechanical secondary fail-safe mechanism: The same forced deactivation of the tractor gripper as the above hSFM, but activated via shear pins and POOH over pull forces on the tractor.
- Forced reset: The forced reset system unloads the gripper from the wellbore and facilitates complete gripper collapse. The function is activated once the CT center line pressure drops below the forced reset setting.
- Static gripper: A low capacity anchoring mechanism with an inherent fail-safe system that provides a platform for the 2⅛" tractor to operate.
- Compact design: The overall length of the tool is 29 ft; the relatively short tool length can be accommodated for most onshore and offshore applications.
- All operation and controls are hydraulic — no E-line required — so they deliver increased reliability during extended in-well service.
- A debris tolerant design provides continuous traction in a wide range of open hole or cased hole wellbore sizes without damaging the casing or formation.
- Compatible with almost all intervention fluids.
- A tough nonmagnetic, acid-resistant Inconel®/beryllium copper construction, which can withstand harsh downhole environments.
- The tractor's gripper provides continuous traction with a pulling force of up to 3,500 lb.

SIMULATION MODEL

The subject well was selected for stimulation based on the well's performance post-rig operations. After the well was hooked up to the flow line, it was unable to flow naturally or with the aid of an ESP artificial lift — suffering repetitive ESP trips due to high motor temperature. Several troubleshooting procedures were conducted without success. The conclusion for the well being unable to flow was attributed to wellbore damage from the rig activity. One of the first requirements when preparing the acid stimulation program is to run a simulation to estimate the CT reach along the extended reach well — this simulation is a critical element in the decision making process. It is therefore important that the simulations are as close to reality as possible. Several parameters are included in the simulation: equipment weight, well geometry, buoyancy, and frictional forces — all of these forces are included to model the helical buckling and eventual lockup.

Most of the inputs for the model are known with some accuracy, as the single factor that can vary from well to well is the friction coefficient. Historical data can be used and an average friction coefficient applied, but this may be too high or too low for the actual well conditions. The recent addition of high-pressure jetting from 60° deviation to the end of the cased horizontal section has become the preferred option, leading to a more consistent friction coefficient across all wells, by lowering the friction in the wellbore to the lower end of the range. This provides more confidence in that the friction coefficient applied in the simulation will result in more accurate lockup depths before the tractor is activated, and also when the expected lockup with the tractor is activated.

Figure 9 plots the simulated data with the depth expected for the CT lockup, and also for reaching target depth with the tractor activated. The simulated depths accurately predicted the actual lockup depths.

ACID STIMULATION PRE-JOB

As part of the stimulation planning, a full review is completed of the well to ensure the suitability of the candidate and to highlight any additional challenges that could be experienced during the well intervention. The open hole caliper log and wellbore surveys are studied to check for any complex well trajectory, irregular hole size, and any washouts. Once the review has been completed, a detailed job program is constructed and issued for job execution.

Prior to deployment of the CT unit, a wireline retrieves a mechanical plug ESP bypass set below item 25 in Fig. 2 — removing the plug allows the CT to access the open hole. A wireline was deployed, but was unable to latch the mechanical plug — the wireline tools returned covered in tar. The CT unit

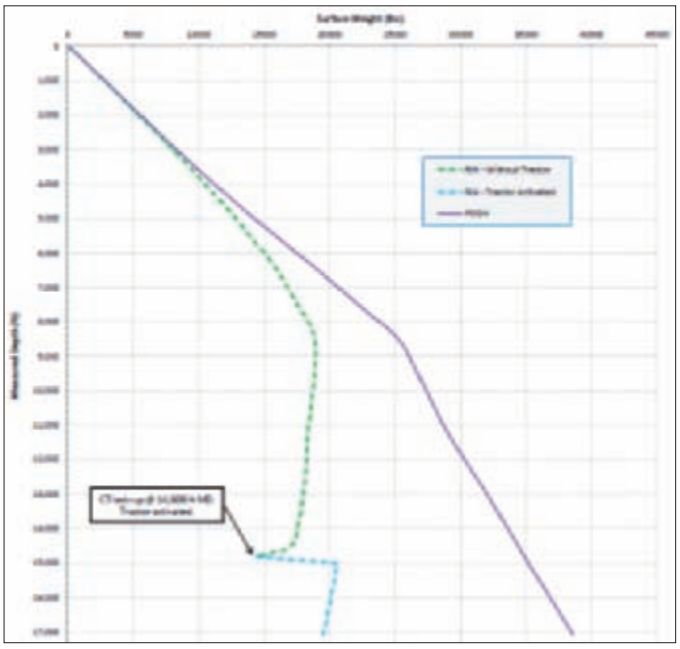

Fig. 9. Plot of simulated depth reached vs. surface weight.

was rigged up and ran in the hole to a position above the plug, where an effective tar dissolving solvent was spotted on top of the plug and left to soak. After a few hours, the plug was successfully latched by the CT and POOH to the surface. The liner section was then cleaned by using high-pressure jet blasting and a solvent to reduce the friction coefficient for the well.

ACTUAL CASE: ACID STIMULATION JOB

The tractor was connected to the CT and went through a full function test on the surface. Once all checks were successfully completed, the tractor was installed in the surface pressure control risers and pressure tested. The tractor was RIH to approximately 8,000 ft in the 4½" tubing for a second function test. The tractor was activated and a pull test was conducted to check the pull force on the downhole tension compression sub. On completion of the successful pull test, the tractor was deactivated and continued to RIH. At the start of the open hole section, the CT commenced pumping a pre-flush of mutual solvent to prepare and condition the wellbore for the acid stimulation. The solvent used was ethylene glycol monobutyl ether, which can help remove any heavy carbon deposits from the rock face.

The CT continued to RIH until lockup at 14,600 ft. The CT was picked up 50 ft to take the slack, and the tractor was started by setting the pumping at a tractor activation rate of 1.2 barrels per minute. The tractor continued to pull the CT in the hole at an average speed of 15 ft per minute, eventually reaching the target depth of 17,100 ft. A 0.25" ball was dropped through the CT to isolate the tractor and activate the circulation valve in preparation for the acid treatment. At target depth, the fiber optic distributed temperature sensing (DTS) was initiated, and the warm back of the formation was monitored over 4 hours. The objective of the DTS is to identify any high intake zones.

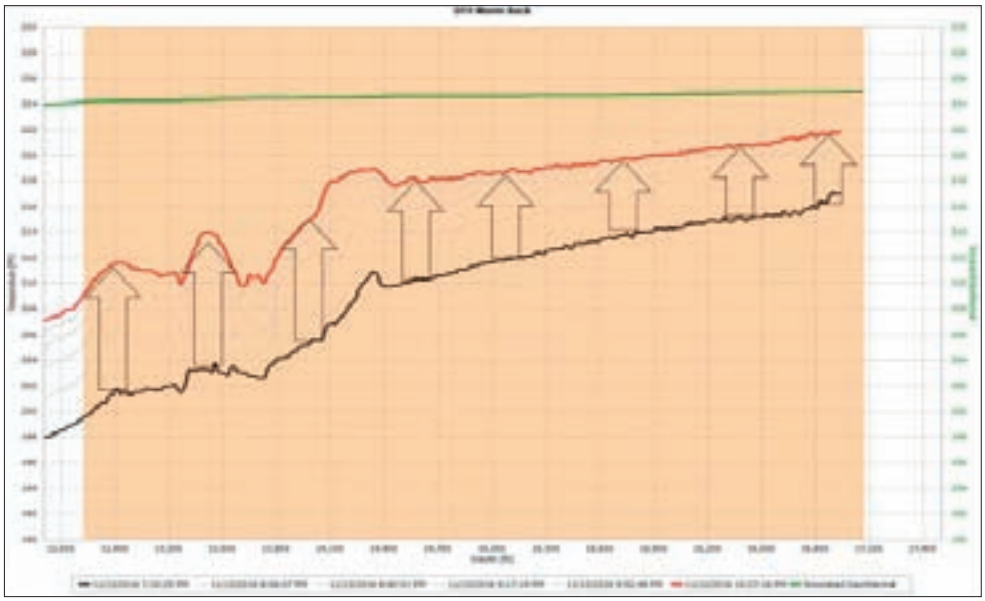

Fig. 10. DTS results.

Figure 10 shows the temperature profiles. The black line represents the hole's continuous temperature profile at the beginning of the survey, where the formation has been cooled down during the pumping of the pre-flush fluids. The red line represents the hole's temperature profile 3 hours later, once the well has started to warm back to geothermal temperature represented by the green line. The two profiles are compared and analyzed, and the zones where the warming is progressing more slowly are identified as high intake zones — a result of larger volumes of cooler fluids entering these zones.

The 10-stage acid pumping schedule is adjusted to account for the high intake zones and the treatment is diverted away from these zones to the more damaged zones. The acid recipe is designed to remove any near wellbore formation damage from the reservoir that happened during drilling operations.

The matrix acid stimulation treatment is comprised of a couple main stages, which include a 15% HCl acid spearhead pumped at 10 gallons per foot, followed by 15% HCl emulsified acid at 10 gallons per foot. The emulsified acid is a mix of HCl acid with diesel. This mixture acts to retard the acid, and to allow enough time for the acid to penetrate deeper into the reservoir before it starts to react. Once the main stages have been pumped, a post-flush mutual solvent treatment is pumped to push the acid treatment deeper into the reservoir for greater penetration.

The CT and BHA are then POOH to the surface. On recovery of the tractor to the surface, it was function tested and was found to be still in good working condition, despite being exposed to the hostile conditions of HCl acid and H_2S for over 3 days while in the hole. A full break down and inspection of the tool showed the tractor to be in relatively good condition overall, with some wear on a few of the seals. The CT was again RIH to lift the well with nitrogen. The well was flowed via the surface flow back package, including a solids filtration unit, and then diverted back to the production flow line.

An estimated volume of 4,000 bbl of spent acid and oil was recovered during the cleanup flow. Around 40 lb of solids were recovered from the filtration unit — this was later identified as drilling by-products. After all equipment was rigged down and moved off-site, the well was put back in production, with the ESP directed to a multiphase flow meter. The well sustained a flow of over 7,000 barrels of oil per day over a 24-hour test period with zero water cut.

RESULTS

The original lockup before activating the tractor only covered around

50% of the open hole. The hydraulic tractor was activated from this depth and performed as per the simulation, pulling the CT to target depth on the first attempt. The 10-stage HCl acid stimulation treatment was pumped over the entire open hole interval, providing 100% zonal coverage. After a cleanup flow had been completed, the well was successfully tested via a multiphase flow meter for 24 hours. A combination of creative thinking, robust design, rigorous testing of the equipment prior to deployment, and careful execution of the planned operation were all key to the eventual successful outcome of this trial.

CONCLUSIONS

The journey of CT tractor technologies for extended reach wells has involved multiple teams to create and incrementally improve the technology, to achieve consistent performances to meet the main objective of reaching the target depth. The latest design of a hydraulically powered tractor has come a long way to meeting these goals. Although the previous slim CT tractor designs were successful in their own right, they were still falling short in terms of delivering the consistent and required pull force to reach the target depth for the more challenging extended reach wells.

To overcome these deficiencies, a new approach was taken by effectively going back to the drawing board, to design a tool that could deliver nearly double the previous pull force and to provide more effective gripping on the open hole carbonate formation. This resulted in a transformation in design to bring this innovative technology to field trial.

The new compact slim CT tractor design is less than one-half the length of the previous wheel-based slim CT tractors, bringing major benefits to the surface rig up and producing nearly double the pulling force, thereby significantly improving the reach capability. The field trial demonstrated the viability of the technology in aiding the CT to reach the target depth of the well. This in turn allowed the successful matrix acid stimulation of the well. This successful field trial represents an important milestone in overcoming the challenges associated with rigless stimulation and intervention in ESP Y-Tool completion extended reach wells, and will lead to improved operational cost efficiency and increased well productivity.

The trial phase is continuing to test the tractor in ever more applicable wells, and development of new generations are ongoing to allow real-time production logging and an increased expansion ratio for larger open hole sizes.

ACKNOWLEDGMENTS

The authors would like to thank the management of Saudi Aramco and WWT International for their support and permission to publish this article.

This article was presented at the Abu Dhabi International Petroleum Exhibition and Conference, Abu Dhabi, UAE, November 13-16, 2017.

REFERENCES

1. Beheiri, F.I., Al-Mubairik, A.J., Al-Mulhim, A.K., Al-Meshal, F.M., et al.: "Optimization of Coiled Tubing Interventions on Extended Reach Open Hole Completions in a Field in Saudi Arabia," SPE paper 116845, presented at the Russian Oil and Gas Technical Conference, Moscow, Russia, October 28-30, 2008.
2. Al-Najim, A., Zahedi, A., Al-Khonaini, T., Al-Sharqawi, A., et al.: "A New Methodology for Stimulation of a High Water Cut Horizontal Oil Well through the Combination of a Smart Chemical System with Real-Time Temperature Sensing: A Case Study of South Umm Gudair Field, PZ Kuwait," SPE paper 154387, presented at the SPE/ICoTA Coiled Tubing and Well Intervention Conference and Exhibition, The Woodlands, Texas, March 27-28, 2012.
3. Arukhe, J.O., Duthie, L.S., Al-Ghamdi, S., Hanbzazah, S., et al.: "World's First Tandem 2.125" Coiled Tubing Tractor for ESP Open Hole Completions," IPTC paper 17386, presented at the International Petroleum Technology Conference, Doha, Qatar, January 19-22, 2014.
4. Arukhe, J.O., Hanbzazah, S., Ahmari, A., Al-Ghamdi, S., et al.: "Saudi Arabia's Manifa Giant Offshore Field Development: The Role of Technology," OTC paper 25119, presented at the Offshore Technology Conference, Houston, Texas, May 5-8, 2014.

BIOGRAPHIES

Laurie S. Duthie is a Production Engineer with Saudi Aramco and part of a team focused on the development of the Manifa field increment. He has more than 27 years of experience in oil and gas exploration and production operations, management, and petroleum engineering consulting. Laurie started his career in 1986 on offshore installations in the U.K. North Sea as a Field Engineer in well testing and wireline operations. He gained extensive operational experience in diverse remote locations — onshore and offshore — across Africa, Central Asia, the former Soviet Union and the Asia Pacific, with the last few years in the Middle East region.

Laurie received his M.S. degree in Petroleum Engineering in 2005 from the University of New South Wales, Sydney, Australia.

Abubaker S. Saeed joined Saudi Aramco in 2011 as a Petroleum Engineer, working in the sensing and intervention focus area of the Production Technology Team in the Exploration and Petroleum Engineering Center – Advanced Research Center (EXPEC ARC). He has published eight patents and several technical and journal papers, and he has led the successful field deployment of several new intervention technologies.

Abubaker has been a recipient of several international awards, including the 2015 Best Young Oil and Gas Professional of the Year award as well as the prestigious 2015 Young ADIPEC Engineer of the Year award. His project work in the area of downhole sensing and intervention was awarded the ICoTA Intervention Technology Award in 2014, as well as being nominated as a finalist for the World Oil Awards 2014 — Best Production Technology.

Abubaker received his B.S. degree in Systems Engineering from King Fahd University of Petroleum and Minerals (KFUPM), Dhahran, Saudi Arabia. He received his M.S. degree in Mechanical Engineering from King Abdullah University of Science and Technology (KAUST), Thuwal, Saudi Arabia.

Saud A. Shaheen joined Saudi Aramco in 2014 as a Petroleum Engineer, and is currently working in the Manifa Production Engineering Unit. His experience includes working as a Reservoir Engineer at the Berri field, where Saud oversaw the field's reservoirs' development and performance monitoring. He also worked as an Operation Engineer in the Abu Ali plant, handling the plant and the field downstream facilities.

In 2014, Saud received his B.S. degree in Petroleum Engineering (with honors) from Texas A&M University, College Station, TX.

Hussain A. Al-Saiood is a Production Engineer in the Manifa Production Engineering Division of Saudi Aramco's Northern Area Production Engineering and Well Services Department. His experience includes work as a Petroleum Engineer, a Drilling Engineer, and a Reservoir Engineer, working at several onshore fields.

Hussain received his B.S. degree in Petroleum Engineering from the University of Oklahoma, Norman, OK.

Dr. Norman B. Moore has over 30 years of experience in the oil field, during which he has held several positions, including as a Research Scientist at Christensen Diamond Products, Worldwide Technical Product Manager and Western Hemisphere Sales Manager at Vetco Offshore, Vice President at Cameron Offshore Engineering, and for 20+ years was Vice President of Engineering for WWT International Engineering Services. He has directed engineering, manufacturing and marketing teams in size from three to 95 people. Norman has managed numerous oil field development equipment projects.

During his tenure at WWT International, Norman's teams developed products that have won international awards for innovation and one product line, the coiled tubing tractor, and set multiple world records in open hole tractoring.

He is the recipient of a number of academic and industry awards. Norman has authored 14 technical papers, two commercial books, and has 58 U.S. patents granted/pending.

He received his B.S., M.S. and his Ph.D. degrees in Mechanical Engineering, all from the University of Utah, Salt Lake City, UT. Norman's graduate research included material science, fracture mechanics, and nonlinear continuum mechanics.

Ernst Krueger joined WWT International in 1997, and is currently an Engineering Manager who works with oil companies and oil field service providers to develop solutions to complex technical problems encountered in the international oil and gas business. He believes that tool designs that push conventional thinking in regards to capability and simplicity are the foundation of advancing field operations.

In 1997, Ernst received his B.S. degree in Mechanical Engineering from Colorado School of Mines, Golden, CO.

Evolution of Coiled Tubing Descaling Interventions in Saudi Arabia Depleted or Subhydrostatic Gas Wells

Ahmed N. Al-Duaij, Mohammad H. Al-Buali, Mohammad Arifin, Danish Ahmed, Rodrigo Sa, Madhurjya Dehingia, and Mohammed Y. Santali

ABSTRACT

This article describes the evolution of descaling interventions via coiled tubing (CT) performed in Saudi Arabian gas wells in the Ghawar field. Throughout these operations, the introduction of new technologies and improved surface equipment has significantly enhanced the efficiency and effectiveness.

CT is the preferred choice for descaling interventions in wells whose reservoirs are underpressured/depleted because it can accurately place fluid and deploy mechanical tools at the specific depths where scales are present. High leakoff into the formation and hydrogen sulfide (H_2S) released at the surface are two main challenges that occur in this type of well. Therefore, it is paramount to continuously monitor and control both downhole and surface parameters. The aforementioned challenges can be addressed by optimizing real-time fluid placement or by manipulating the choke size, among other parameters. A chemical plug can be pumped to isolate the reservoir before commencing descaling interventions, but this process may require stimulation or re-perforation of the reservoir system after the treatment. Therefore, it is preferable to use a system that is flexible enough to execute a wide range of operations, from reservoir isolation to descaling treatment, while maintaining the well in balanced or marginally overbalanced conditions.

Previously, CT descaling operations were executed by relying only on surface parameters. Today, new technologies are available that can provide live downhole parameters such as pressure, temperature, load, and torque, and these technologies have advanced descaling interventions. Although downhole parameters via downhole tools have been available for years, tools providing such parameters were limited with respect to pumping rate, working pressures, temperature, and ability to sustain high torque and vibration. To address these issues, a new tool was developed that can acquire downhole parameters during milling and clean out operations. The ability to monitor downhole parameters enables field personnel to act instantly to any change in downhole conditions. At the same time, the introduction of advanced surface equipment has helped in better handling of returns from the well and in maintaining a constant wellhead pressure irrespective of dynamic returns. Therefore, the treatment is executed within its defined limits and the risks of service quality events are mitigated.

This article describes the evolution of CT descaling intervention treatments and the technologies used. It details how the introduction and integration of new technologies have enhanced descaling operations in Saudi Arabia where real-time decisions were made to optimize treatment, make the operation safer, and prevent formation damage.

INTRODUCTION

The Ghawar field was discovered in 1948. Bolarinwa et al. (2012)[1] described the geology and reservoir characteristics of the pre-Khuff clastic and Khuff carbonate reservoirs and the issue of scale buildup in Khuff gas wells. The reservoir rocks are Jurassic Arab-D limestones overlying the Jurassic Hanifa formation — a marine shelf on top of the Khuff reservoirs — sealed by impermeable anhydrite. Bolarinwa et al. (2012)[1] found variable conditions in the Khuff reservoirs in terms of permeability, which ranges from 0.1 millidarcy (md) to 0.7 md, significant porosity variations, and reservoir stratification and layering. They note that the Khuff gas wells suffer from severe buildup of inorganic scale deposits, which has resulted in inaccessibility to the wellbore deeper than 5,000 ft to 6,000 ft, in addition to the gradual loss of production.

Bolarinwa et al. (2012)[1] describe the scale deposits as a mixture of iron sulfide/iron oxides — 69% to 86% — and calcium carbonate ($CaCO_3$) — 31% to 14%. In their study, the density of the collected samples ranged from 3.5 specific gravity (SG) to 4.5 SG. They estimated the amount of scale restricting the inside diameter of the 4½" tubing from 3.92" to 2½" to range from 4.9 to 6.3 tons for every 1,000 ft of tubing. The wells in which scale was found were mostly vertical and completed with 5½" and/or 4½" tubing with either a 4½" or 7" cemented and perforated liner set at 11,500 ft and 13,400 ft across the carbonate reservoirs, respectively.

The bottom-hole temperature (BHT) in the wells considered by Bolarinwa et al. (2012)[1] was approximately 300 °F, and the bottom-hole pressure (BHP) ranged from 4,000 psi to 5,000 psi. As such, the wells could not sustain a full column of water, which leads to the requirement of performing the jobs in an underbalanced condition to help prevent damaging the formation due to fluid leakoff.

COILED TUBING (CT) DESCALING INTERVENTION EVOLUTION

CT Descaling Operation Before 2009

Until 2009, various descaling jobs were performed using conventional acids. Subsequently, it was deduced that not all the wells could be cleaned using hydrochloric (HCl) acid because of differences in the composition of the scales and corrosion issues to the tubular due to high temperature and hydrogen sulfide (H_2S) content. Chemical removal methods were not satisfactory because of the problems associated with the process. First, H_2S was released during acid dissolution of acid soluble scale. In addition, the spent acid containing the dissolved iron sulfide was redepositing iron sulfide and elemental sulfur, making the flow back operation dangerous due to high H_2S concentration.

When CT was used for chemical removal methods, several cases of differential sticking were experienced, primarily due to the lack of carrying capacity of the clean out fluid, overestimation of reservoir pressure, and uncertainties in the scale type and distribution, although a viscous pill was pumped with HCl acid. Moreover, the difference in the densities of the viscous pill made it difficult to control both surface and downhole parameters. Finally, if CT was used while the well was producing, surface equipment was exposed to erosion and was unable to handle H_2S release, which in turn, led to many service quality issues.

After studying all of the complications, it was decided that the following information must be gathered before a descaling job:

1. Determine the material to be cleaned by performing the necessary X-ray diffraction analysis to specify the scale types.
2. Fine-tune the reservoir pressure decline to determine the operational conditions and necessary precautions in balanced, underbalanced, or overbalanced conditions.
3. Evaluate the cleaning tools, specifically the use of motors/vibration/oscillation tools with respective fluids.
4. Determine the surface equipment and associated surface conditions, including the use of hydrocyclone devices, filters, expandable chokes, etc.
5. Select a fluid that will provide enough viscosity to transport other wellbore fluids, avoid formation damage, maximize fluid loading/rate of penetration, allow near overbalance conditions, and have low particle settling velocities, etc.

After this information was gathered, the first descaling job using foam-based fluid was executed due to its better capabilites to carry solids to the surface and its less damaging nature. Such an operation was one of the first few implementations by the operator of a descaling method involving mechanical scale removal using 1.75" or 2" CT strings and a 2⅞" high-pressure jetting tool with or without solid blasting. The scale removal was successful, but the nitrified guar gel, which was used to enable underbalanced clean out, carried debris to the surface, and minimized losses to the reservoir, and generated high differential pressure across the choke. The latter was washed out, and H_2S gas migrated to the surface.

To avoid an adverse situation, the well was closed immediately with debris around the pipe, resulting in stuck CT pipe. Nitrified gel also proved to be a failure due to their high leakoff into the formation, leading to formation damage when used as a fluid system for a descaling operation. The wellhead pressure must be maintained at balanced or slightly overbalanced conditions, considering the well is full of foam to attain the desired slightly overbalanced condition. Such high pressures can be achieved if the choke size is kept low.

The nitrified gas, along with debris, can plug chokes if kept at a lower choke size. This can also lead to stuck pipe situations. To avoid these complications, the decision was made to perform chemical dissolution of the scales with CT. Although the solution was able to dissolve scales, a high concentration of H_2S was produced due to the reaction of HCl acid and iron sulfide scale. Multiple CT pinhole failures occurred because of long exposure — time period of treatment — of the CT to a high concentration of sour gas.

Some of the particular points that were deemed critical and needed attention:

- The extent of the scaling must be identified.
- The CT speed must be controlled, based on the simulation result, so as to not exceed solid loading in the wellbore.
- Stimulation must be performed after proving wellbore accessibility.
- There must be a provision for a detailed revision of the instantaneous volume capacity on the sand management system.
- Annular velocities must be calculated accurately.
- Detailed analysis of retrieved materials/scales must be done.
- Fluid must be stable above high temperatures, i.e., up to 325 °F.

The issues mentioned here were associated with the specific descaling job that was executed using a foam-based fluid. An in-depth study was conducted on the descaling jobs performed up to that point in time, and the following challenges were identified:

1. Use of a small CT size of 1.75" led to a limited pump rate of 2 bbl/min.

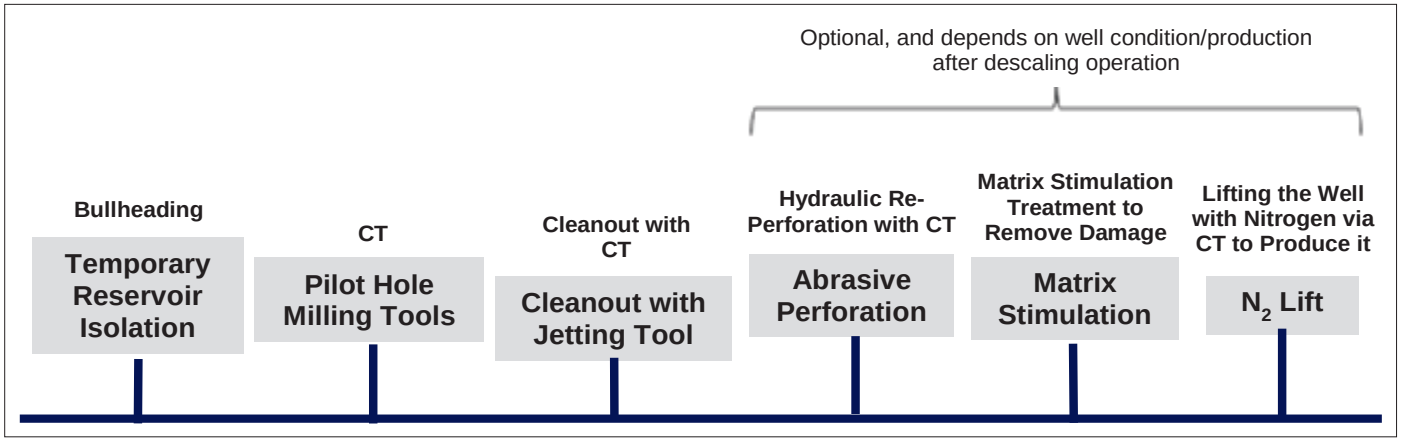

Fig. 1. Developed workflow to overcome scale removal challenges[2].

2. Real-time downhole data acquisition and control of downhole pressure were lacking. The low BHP of the reservoir during a conventional descaling job meant that fluids and gels were unable to carry debris from the wellbore.
3. The cleanout fluids had low efficiency.
4. There was an inadequate surface flow back handling system and no continuous flaring system.
5. There was a high and intermittent amount of scale deposits, accumulation, and production. The wellbores are frequently choked off by scale and there was quick choke erosion, or the scale plugs the choke and filters.
6. The composition of the scale deposits is mixed, and there is limited solubility with chemical methods — especially iron sulfide scale.
7. The scale includes hard and heavy components:
   a. Iron sulfide and sulfate scales require a specific milling and clean out assembly.
   b. The size of cuttings must be controlled to avoid plugging flow back equipment.
   c. The wellbore configuration requires high annular velocities to carry out solids to the surface.
   d. Clean out fluids that are reliable up to 320 °F are required to sustain and/or carry heavy scale — 3.5 SG to 3.6 SG — to surface.
8. H_2S content is high.

CT Descaling Operations: 2010 to 2012

In the middle of 2010, after analyzing the lessons learned and challenges, as previously mentioned, a new descaling workflow was implemented by the operator for scale removal in gas wells. In this workflow, mechanical descaling was done by using CT along with an aggressive jetting/milling to remove and circulate the scales. The main challenges faced in these operations were to maintain optimum circulation conditions and minimize losses into the formation. This workflow consisted of the steps shown in Fig. 1.

The workflow is described by Al-Buali et al. (2015)[2] as follows:

1. The first phase is reservoir isolation. Temporary isolation of the reservoir is achieved by bullheading viscoelastic fluid and $CaCO_3$ chips.
2. A pilot hole is drilled through the scaled wellbore, just above the top of the perforation. Low torque, high RPM downhole motors or turbines with mill size up to the maximum drift possible are used to cut the scale into small particles and facilitate their transport to the surface. This is to overcome the presence of hard and heavy scale components such as iron(II) sulfide and barium sulfate, which cannot be removed with conventional jetting methods, and therefore, requires a specific milling and clean out assembly. In addition, the size of cuttings must be controlled to prevent them from plugging the flow back equipment.
3. A high-pressure rotary jetting tool is used in combination with abrasive beads, and a high temperature gel are used to remove the remaining layer of scale left between the mill and the tubulars. Because this step removes the temporary zonal isolation, it is necessary to maintain slightly overbalanced conditions to minimize the risk of circulation losses or gas influx.
4. A stimulation operation commonly follows the mechanical scale removal. This is to mitigate the potential loss of original production caused by damage induced into the reservoir during the isolation stage. This intervention typically consists of matrix acidizing treatment via CT with selective placement of HCl acid and viscoelastic diverting agents, or a selective abrasive perforating operation via CT.

Such descaling operations took advantage of CT with a real-time telemetry system, which had been introduced in 2008 and consisted of the tools shown in Table 1.

The standard downhole tools recording real-time data that were deployed with CT had an outside diameter of 2⅛". The

	Sensors Package
Maximum Flow Rate	2.0 bpm
Outside Diameter	2⅛"
Ball Drop	⅝"
Pressure Rating	12,500 psi
Operating Temperature	300 °F
Measurements	BHP, BHT, GR, DTS, CCL, TC
	Fiber Optic
Outside Diameter	0.071"

Table 1. Standard CT fiber optic telemetry and downhole measurements package[3]

tools were limited to a flow rate of 2 bbl/min. This maximum pump rate value and some other limitations resulted in the following issues:

- Longer operations due to a long pumping time.
- Limited penetration of stimulation fluids leading to shallower wormholes.
- Low annular velocities of scales resulting from low pumping rates, potentially leading to CT sticking situations.
- A tendency for the low tensile strength standard fiber optics to break, if abrasive or high viscous fluids are pumped at high rates.

Despite the limitations, the workflow previously presented in Fig. 1 resulted in highly successful CT descaling interventions, and had the following benefits:

1. The CT with a real-time telemetry system provided downhole measurements, which resulted in efficient mechanical descaling and abrasive perforation operations.
2. Use of CT with a real-time telemetry system helped in:
   a. Maintaining slightly overbalanced conditions, thereby preventing risk of gas influx.
   b. Mitigating the risk of lost circulation.
   c. Achieving accurate depth control using the casing collar locator and gamma ray signals provided by the bottom-hole assembly.
   d. Optimizing downhole tool performance.

Although the workflow was a success, there was still a requirement to optimize the CT descaling interventions by expanding the tool's envelope and addressing some of the remaining limitations, which included the following:

- Performing reservoir isolation was a lengthy process.
- The fluids used for isolation could lead to formation damage.
- A high volume for the stimulation operation was needed to restore production following descaling treatment.
- Following stimulation, nitrogen (N_2) lift was sometimes required to lift the well. This also prolonged the operational time.

CT Descaling Operations: 2012 to 2014

The limitations of the conventional tools limited the efficacy of the telemetry system used for mechanical descaling operations. Table 2 shows a new system that was developed to expand the work envelope of the CT with real-time downhole parameters, as discussed next.

1. The 3¼" real-time downhole package includes:
   a. BHT gauge.
   b. BHP gauge — inside and outside of the CT.
   c. Gamma ray for accurate depth correlation and for lateral identification.
2. A high flow rate up to 8 bbl/min can be achieved through the tool. This results in deeper penetration of fluids to create deeper wormholes.
3. The tensile strength of the Inconel fiber carrier installed in the CT pipe is double that of the 2⅛" standard tool. This

	Standard System Sensors Package	New Enhanced System Sensors Package
Maximum Flow Rate	2.0 bpm	8.0 bpm
Outside Diameter	2⅛"	3¼"
Ball Drop	⅝"	1"
Pressure Rating	12,500 psi	12,500 psi
Operating Temperature	300 °F	325 °F
Measurements	BHP, BHT, GR, DTS, CCL, TC	BHP, BHT, GR, DTS
	Fiber Optic	**Fiber Optic**
Outside Diameter	0.071"	0.094"

Table 2. Comparison between standard and enhanced fiber optic telemetry and the downhole measurements package[3]

enables higher pump rates and pumping of very viscous or abrasive fluids.

4. Higher pump rate results in more efficient and faster descaling and clean out operations.
5. The CT tool performance can be monitored, based on real-time downhole parameters. In addition, it can be determined if the high pump rates deliver suitable differential pressures for optimum tool performance.

The overall workflow remained unchanged when compared to the workflow previously presented in Fig. 1. The only adjustment concerned the fact that an enhanced fiber optic telemetry and downhole measurement package was used for the job execution.

CT Descaling Operations: 2016

Further optimization of the workflow was conducted taking into account the following factors:

1. The reservoir isolation step can be removed provided the CT descaling operation is performed in balanced or slightly overbalanced conditions.
2. The following are needed to have adequate control in underbalanced and slightly overbalanced conditions:
   a. Fluid system (foamed fluid) that can carry scales to the surface continuously without causing overbalanced conditions.
   b. Downhole tools with CT real-time telemetry system during milling to record downhole parameters.
   c. An enhanced flow back system on the surface that can collect scale returns and also control pressure and flow.
3. The steps of abrasive perforations, matrix stimulation, and N_2 lift can be omitted if the reservoir isolation step is not done.

In the improved workflow, the steps related to reservoir isolation, abrasive perforations, matrix stimulation, and N_2 lift were eliminated, Fig. 2.

Although an enhanced system was readily available, it could not be used for milling operations because the tool was not resistant to shocks and vibrations, and was not suited to high temperatures and high pressure. A rugged system was therefore developed, Table 3, to overcome these limitations.

An enhanced fluid was also developed in the form of foamed fluid, Fig. 3, which can be used in low-pressure and depleted wells having cases of losses. It features the following benefits:

- Long lasting.
- Withstands oil interaction.
- Has a high solids carrying capacity.

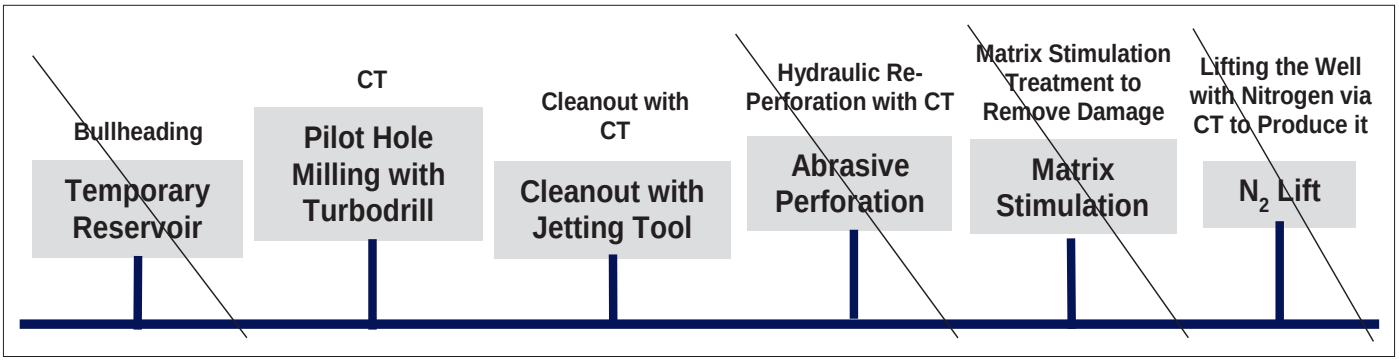

Fig. 2. Optimization of descaling workflow.

	Standard System Sensors Package	New Enhanced System Sensors Package	Rugged System Sensors Package
Maximum Flow Rate	2.0 bpm	8.0 bpm	8.0 bpm
Outside Diameter	2⅛"	3¼"	2⅞"
Ball Drop	⅝"	1"	N/A
Pressure Rating	12,500 psi	12,500 psi	17,500 psi
Operating Temperature	300 °F	325 °F	350 °F
Measurements	BHP, BHT, GR, DTS, CCL, TC	BHP, BHT, GR, DTS	BHP, BHT, GR, DTS, CCL, TC
	Fiber Optic	**Fiber Optic**	**Fiber Optic**
Outside Diameter	0.071"	0.094"	0.094"

Table 3. Comparison between standard, enhanced, and rugged fiber optic telemetry and downhole measurements[2]

Fig. 3. Enhanced foamed fluid.

Fig. 4. PFMS modular system for pressure control and solids removal.

- Is broken easily when it returns to the surface.

Further, a foam-based fluid has the unique quality that it allows solids to be carried to the surface while maintaining stable solids distribution in the annulus, thereby reducing the risk of plugging the choke. Maintaining an overbalanced condition is, however, necessary during the pumping stage because produced hydrocarbons can contaminate the foam.

Finally, a new pressure and fluid management system (PFMS), Fig. 4, provided accurate and automatic pressure control at the wellhead. This system effectively removes solids and gas from workover fluids; it also has a small footprint; finally, it is equipped with an auto-choke, mud-gas separator, shale shaker, and vacuum degasser and desilter to safely handle H_2S gas influx at the surface. The modular system can be used for operations, such as CT clean outs, which require precise pressure control and efficient removal of solids and gas from contaminated fluids. Further discussion of the system can be found in Espinosa G. et al. (2016)[3].

The pressure control section of the modular system comprises the following:

- A choke manifold, a self-cleaning dual super auto choke for precise control of well pressure, equipped with diverter line.
- A standard mud-gas separator for removal of high volumes of free gas.
- A tank outfitted with pumps, gun lines, and transfer lines.
- A Mongoose shaker that achieves high volume and solids removal efficiencies from dual motion (linear and elliptical) capability.
- A proven desilter technology for removing finer particles.
- A vacuum degasser for removing entrained gas in the fluid.

The PFMS provides a closed loop pressure control and solids separation continuous operations system to free the fluids of unwanted solids and gas to be recirculated into the well.

CONCLUSIONS

The recent introduction of the new descaling operation technique proved successful. In this technique, the phases of wellbore isolation, perforation, matrix stimulation, and N_2 lift were eliminated based on knowledge of previous descaling operations, and only the phases of pilot hole drilling and descaling operation were performed.

With the availability of a robust new generation of CT real-time telemetry tools, decisions in real-time can be made. In addition, the enhanced foamed fluid and PFMS utilization:

- Provided slight overbalanced conditions.
- Prevented loss circulation.
- Optimized downhole tool performance.
- Enabled accurate depth correlation.

ACKNOWLEDGMENTS

The authors would like to thank the management of Saudi Aramco and Schlumberger for their support and permission to publish this article. Special thanks go to the team members who participated in this operation.

REFERENCES

1. Bolarinwa, S.O., Leal, J.A., Al-Buali, M.S., Kharrat, W., et al.: "Innovative Integrated Procedure for Scale Removal in Khuff Gas Wells in Saudi Arabia," SPE paper 156021, presented at the SPE International Conference on Oil Field Scale, Aberdeen, U.K., May 30-31, 2012.
2. Al-Buali, M.H., Abulhamayel, N., Leal, J.A., Ayub, M.,

et al.: "Recent Developments in Mechanical Descaling Operations: A Case Study from Saudi Arabia," SPE paper 173662, presented at the SPE/ICoTA Coiled Tubing and Well Intervention Conference and Exhibition, The Woodlands, Texas, March 24-25, 2015.

3. Espinosa G., M.A., Leal, J.A., Driweesh, S.M., Al-Buali, M.F., et al.: "First Time Live Descaling Operation in Saudi Using Coiled Tubing Fiber Optic Real-Time Telemetry Rugged Tool, Foamed Fluid and Pressure and Fluid Management System," SPE paper 182763, presented at the SPE Kingdom of Saudi Arabia Annual Technical Symposium and Exhibition, Dammam, Saudi Arabia, April 25-28, 2016.

BIOGRAPHIES

Ahmad N. Al-Duaij joined Saudi Aramco in 2011 as a Technical Support Engineer, working in the Well Completion Engineering Support Unit of the Southern Area Well Completion Operations Department supporting gas well completion operations. He completed a one-year assignment working as a Production Engineer with the Ghawar Gas Production Engineering team handling the Ghawar gas wells, developing completion programs that include, but are not limited to, perforation programs, proppant fracturing and acid fracturing programs, among others.

Following this assignment, Ahmad was sent to Houston to work with Halliburton in their Unconventional Gas Resources Program for one year. After successfully completing this assignment, he returned to Saudi Arabia to work as an Operations Foreman executing critical rigless operations, starting from the perforation stage and progressing to the fracturing stage, utilizing state-of-the-art technologies.

Currently, Ahmad is working as an Operations Foreman for the Ghawar Gas Well Completion Engineering Support Unit.

He received his B.S. degree in Petroleum Engineering from King Fahd University of Petroleum and Minerals (KFUPM), Dhahran, Saudi Arabia.

Mohammad H. Al-Buali is now a Chemical Engineer after starting his career working as a Production Engineer for oil, water and gas wells. Since 2010, he has worked in the Gas Well Completion Operation Department, executing and supervising all rigless activities related to fracturing and stimulation, well intervention, and well testing on Saudi Aramco's onshore gas wells. Mohammad is currently a Division Head in the Southern Area Gas Well Completion Operations Department.

He is a member of the Society of Petroleum Engineers (SPE) and has participated in many SPE events as an author, presenter and delegate.

In 2002, Mohammad received his B.S. degree in Applied Chemical Engineering from King Fahd University of Petroleum and Minerals (KFUPM), Dhahran, Saudi Arabia.

Mohammad Arifin is working in Schlumberger Saudi Arabia as the Coiled Tubing Services Technical Manager for the Kingdom of Saudi Arabia and the Kingdom of Bahrain. He joined Schlumberger in March 2000 and has had several assignments, including in Coiled Tubing Services, Stimulation and Cementing Services, and other segments in the oil field involving testing, wireline and artificial lift.

Mohammad has nearly 17 years of oil field experience, which covers a broad range of operations, including assignments offshore as well as in the desert, swamp, and jungle. He also spent three years at the Schlumberger headquarters working in the Global Technical Support Group of InTouch, providing technical, operational, and safety support for the company's worldwide operations.

Mohammad has coauthored several training modules for coiled tubing (CT) operations, a number of Society of Petroleum Engineers (SPE) papers, and the documentation of InTouch Best Practices.

He is currently involved in several joint projects between Schlumberger and Saudi Aramco where he uses his expertise in CT and stimulation.

In 2000, Mohammad received his B.S. degree in Chemical Engineering from Gadjah Mada University, Yogyakarta, Indonesia.

Danish Ahmed has been working at Saudi Schlumberger since 2007. He is a Senior Intervention Optimization Engineer with Schlumberger Well Services – Coiled Tubing Services, supporting the ACTive Services Platform. Danish's experience includes working as a Field Engineer with Well Production Services (Fracturing and Pumping Services) based in 'Udhailiyah, Saudi Arabia, supporting proppant/acid fracturing and matrix acidizing jobs, followed by working as a Production Technologist with Petro Technical Services (formerly called Data and Consulting Services) in Dhahran, Saudi Arabia.

In 2007, he received his M.S. degree in Petroleum Engineering from Heriot-Watt University, Institute of Petroleum Engineering, Edinburgh, Scotland.

Rodrigo Sa works for Schlumberger Saudi Arabia Well Services – Coiled Tubing Segment. Since 2014, he has been assigned to Saudi Aramco's Gas and Production Engineering Division in 'Udhailiyah as the Coiled Tubing (CT) Technical and Sales Engineer. Rodrigo has worked as a CT Senior Field Engineer in Brazil, and in Saudi Arabia, from 2009 to 2014. His work experience involves designing, executing, and evaluating the CT interventions for offshore ultra-deepwater, high-pressure, high temperature wells, and unconventional resources. Rodrigo was the Project Leader from Schlumberger for developing and successfully implementing CT live descaling interventions for the first time in Saudi Arabia.

In 2009, he received his B.S. degree in Mechanical Engineering from Federal University of Rio Grande do Norte, Natal, Brazil.

Madhurjya Dehingia works for Schlumberger Saudi Arabia Well Services — Coiled Tubing (CT) Segment. He has been working as a CT Field Engineer in 'Udhailiyah since 2012. During this period, Madhurjya has supervised many complex CT jobs. His work experience involves designing, executing, and evaluating the CT interventions for high-pressure, high temperature wells, unconventional wells, and oil and water wells.

Madhurjya was the lead Field Engineer from Schlumberger on the project and successfully implemented CT live descaling interventions for the first time in Saudi Arabia. He was also involved in the subsequent live descaling Interventions.

In 2012, Madhurjya received his B.S. degree in Chemical Engineering from the Indian Institute of Technology, Guwahati, India.

Mohammed Y. Santali started his oil and gas career in 2008 when he joined Schlumberger Coiled Tubing Services in 'Udhailiyah, Saudi Arabia, as a Field Engineer. In September 2017, he was appointed as Schlumberger's Southern Area Rigless Business Manager. Mohammed's responsibilities are to support all of the segment's operating in SAWCOD ex. coil tubing (CT), wireline, slick line, testing, fracturing and integrated project services to achieve their objective and improve their service quality.

Prior to his current assignment, Mohammed was the CT Field Service Manager of the Southern Area, covering the Rigless and Drilling & Workover operation. He was also looking after the CT operation on the unconventional area during the start of the project.

In August 2013, Mohammed completed his GFE project (ACTive* Water Shut Off in Ghawar Field) and became a General Field Engineer. He was also an ACTive Specialist conducting a distributed temperature survey in the acid stimulation operation in the North Ghawar oil field and the Shaybah field.

In May 2008, Mohammed received his B.S. degree in Mechanical Engineering from Oklahoma State University, Stillwater, OK.

A Field Case Study of an Interwell Gas Tracer Test for Gas EOR Monitoring

Modiu L. Sanni, Dr. Mohammed A. Al-Abbad, Dr. Sunil L. Kokal, Razally M. Ali, and Ibrahim M. El-Zefzafy

ABSTRACT

Tracer technology has evolved significantly over the years and is now being increasingly used as one of the effective monitoring and surveillance (M&S) tools in the oil and gas industry. Tracer surveys, deployed as either interwell tests or single-well tests, are one of the enabling M&S technologies that can be used to investigate reservoir connectivity and flow performance, measure residual oil saturation, and determine reservoir properties that control displacement processes, particularly in improved oil recovery or enhanced oil recovery (EOR) operations.

As part of a comprehensive M&S program for a gas EOR pilot project, an interwell gas tracer test (IWGTT) was designed and implemented to provide a better understanding of gas flow paths and gas-phase connectivity between gas injector wells and producer well pairs, gas-phase breakthrough times ("time of flight"), and provide pertinent data for optimizing water-alternating-gas (WAG) field operations. Additional objectives include the detection and tracking of any inadvertent out-of-zone injection, and acquisition of relevant data for gas reactive transport modeling. Four unique tracers were injected into four individual injector wells, respectively, and their elution was monitored in four "paired" up-dip producer wells.

In addition to the reservoir connectivity and breakthrough times between the injector and producer well pairs, the results showed different trends for different areas of the reservoir. The gas-phase breakthrough times are slightly different from the water tracer breakthrough times from a previous interwell chemical tracer test (IWCTT). Residence times for the tracers indicate different trends for three of the injector and producer well pairs compared to the last well pair. These trends reflect and support conclusions regarding reservoir heterogeneities also seen from the previous IWCTT, which were not anticipated at the beginning of the gas EOR pilot.

This article reviews the design and implementation of the tracer test, field operational issues, analyses, and interpretation of the tracer results. The tracer data has been very useful in understanding well interconnectivity and dynamic fluid flow in this part of the reservoir. This has led to better reservoir description, improved dynamic simulation modeling, and optimized WAG sequence.

INTRODUCTION

The use of tracers is a versatile and generic tool suitable for a range of applications in the oil and gas industry[1]. Common to all tracer applications is that a marker — or a tracer — is added to a unit of mass, and subsequently used to identify transport of that mass to another location[2]. In the reservoir, transported mass is usually water or hydrocarbons, and tracers are used to identify and characterize movement of oil, water, or gas. The objective of most tracer applications is to identify and characterize movement of a single phase. For these applications, it is important that a tracer behave as close to the traced mass as possible. A few decades ago, this implied the use of radioactive tracers that are chemically equivalent to the traced water or hydrocarbons. Through development of chemical water tracers[3] and gas tracers[4, 5], radioactive tracers have now mostly been replaced by chemical tracers in field applications. For laboratory studies, radioactive tracers are still in use and important, e.g., as a benchmark to qualify new chemical tracers.

In some applications, the objective of tracer deployment may not be limited to identifying the movement of a single phase. Two such applications — both targeting the assessment of the remaining oil saturation (ROS) — are the partitioning interwell tracer test (PITT) and the single-well chemical tracer test (SWCTT). In these tests, at least one chemical tracer that partitions between the water and oil phases, in addition to conventional non-partitioning water tracers, are used. The degree of partitioning is determined by the partition coefficient, which is close to constant for a given oil and water composition, and can be measured in the lab. If water flows and the oil phase is stagnant, the partitioning between water and oil yields a time lag in the production curves for the partitioning vs. the non-partitioning tracer. Tracer curves from a SWCTT or a PITT yields the ROS from this time lag and the partition coefficient, through a simple relation. This information can, e.g., be used to assess the potential for enhanced oil recovery (EOR) in a field. By use of repeated testing before and after an EOR pilot flood, the effect of a given EOR methodology can be found.

For a PITT, new and stable oil-water partitioning tracers were developed[6] and the PITT has now matured into an

established methodology applicable for a wide range of reservoir conditions[6-8]. The SWCTT is a mature technology developed in the 1970s[9]. It has recently been expanded by the development of new tracers, and a recent field case study of new and improved tracers[10] demonstrated a reduction in tracer amounts from barrels to milliliters. The reduction in required tracer amounts solves several operational and logistical issues and allows for injecting a cocktail of tracers that can target a range of reservoir conditions and EOR methodologies.

In all water-alternating-gas (WAG) injections, where water and gas phases are injected in a cyclic manner, tracing each fluid type is challenging. This is also true in our case, as the injected gas is miscible with the water phase, contrary to hydrocarbon-based WAG injection. One identified possible challenge is gravity override. The injected gas will tend to rise to the top of the formation while injected water tends to slump toward the base of the reservoir, Fig. 1. The interplay of gravity override and reservoir heterogeneity may influence different fluids to follow different flow paths. As a consequence, different tracers for each fluid phase are required to diagnose the flow of oil, water, and gas in the reservoir.

Gas tracers have been used in a range of hydrocarbon gas injection projects[1], e.g., to track individual cycles during WAG injection. Gas tracers have also been used to track injected gas[11], and plans exist to use gas tracers to monitor gas flooding projects[12, 13]. Ringrose et al. (2013)[14] reported the use of gas tracers to monitor the carbon storage projects in the In Salah Carbon Capture Sequestration project where tracers were used to monitor potential transport of gas into a hydrocarbon gas reservoir. An important difference between water and gas tracers is that virtually all chemical gas tracers partition between the water and gas phases in hydrocarbon reservoirs. This fact has to be accounted for in the interpretation of the results of a gas tracer study, whenever a free gas phase is present in the reservoir.

PROJECT BACKGROUND AND OBJECTIVES

The IWGTT was deployed as part of an elaborate monitoring and surveillance (M&S) plan for a gas EOR project. There are nine producers, five injectors, and three observation wells located at the flank of the reservoir, Fig. 2. The field has been under peripheral water injection for several decades to provide necessary reservoir pressure support and voidage replacement to maximize hydrocarbon recovery.

At the early part of the project, before the commencement of gas injection, an interwell chemical tracer test (IWCTT) was conducted[8] to: (a) determine the connectivity or fluid pathways between the injector-producer well pairs; (b) assess the breakthrough times of the tracers between the injectors and producers; (c) estimate the traveling velocity of the injected fluid; (d) use the tracer data to refine static and dynamic reservoir models; and (e) conduct field qualification of some new tracers that were being developed. The gas EOR pilot

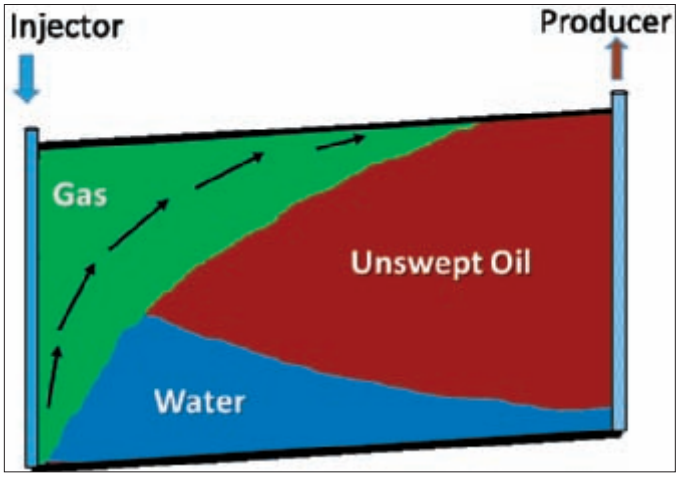

Fig. 1. Gravity override problem due to the high density contrast between gas and water.

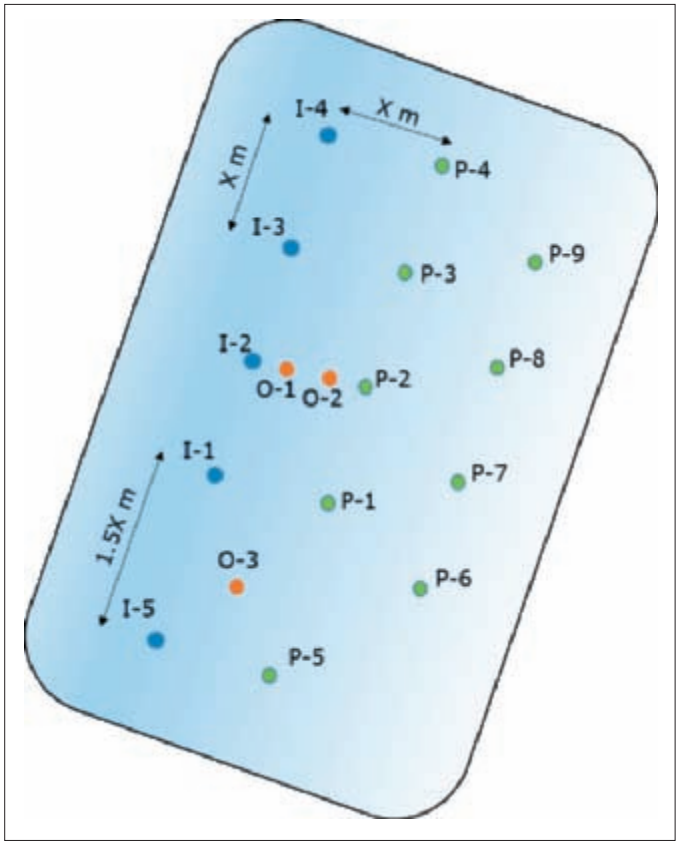

Fig. 2. Area of interest showing the producer, injector and observation wells.

project typically injects water and gas into two alternate injector wells in a WAG mode for optimal sequestration and oil recovery.

The IWGTT was implemented to provide a better understanding of gas flow paths and gas phase connectivity between the gas injector and producer well pairs, gas phase breakthrough times — time of flight — and provide pertinent data for optimizing WAG field operations. Additional objectives include the detection and tracking of any inadvertent out-of-zone gas injection, and acquisition of relevant data for gas reactive transport modeling.

Injection Well	Tracer Name	Tracer Amount (kg)	WAG Cycle
I-1	PMCP	0.85	1
I-3	PECH	0.92	1
I-2	PMCH	0.90	2 (~6 weeks later)
I-4	n-PPCH	0.95	2 (~6 weeks later)

Table 1. Selected tracers used and injected

TRACER PROJECT DESIGN

Based on the volumetric assessment of the reservoir section, the tracer amount for each well was calculated, taking into consideration the density of supercritical carbon dioxide under reservoir conditions and the detection limit of the tracers at surface condition — parts per trillion. Four different tracers were screened for the field project. These are perfluoro(methylcylopentane) (PMCP), perfluoro(ethylcyclohexane) (PECH), perfluoro(methylcyclohexane) (PMCH), and perfluoro-n-propylcylcohexane (n-PPCH). Table 1 shows the details of tracers selected and injected.

The tracer project was designed to take advantage of a chemical adsorption tube (CAT) system, combined with gas chromatography mass spectroscopy analysis[15]. The CAT sampler, Fig. 3, eliminates the need for high-pressure cylinders for sampling and eases the logistics of samples as the non-pressurized, nonflammable samples do not require any material safety data sheets or dangerous goods handling.

FIELD IMPLEMENTATION AND OPERATIONAL HIGHLIGHTS

The field deployment of the tracers was done in two tranches congruent with the WAG cycle. Two wells (Well I-1 and Well I-3) that were on gas injection mode had two different tracers — PMCP and PMCH — injected, respectively. The second tranche involved the injection of PMCH and n-PPCH into Wells I-2 and I-4, respectively, during the next WAG cycle when the wells were switched to gas injection mode. For each injection, elaborate safety protocols were followed to ensure the safety of personnel and appropriate steps were taken to avoid cross contamination of tracers.

TRACER SAMPLING PROTOCOL

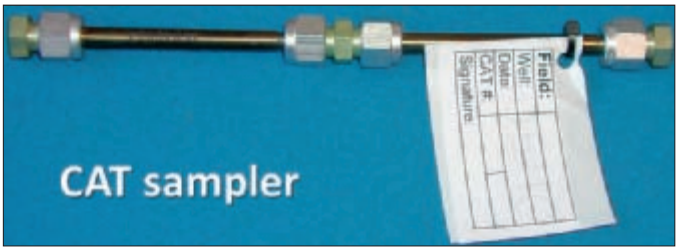

Fig. 3. Picture of a CAT sampler. The length of the sampler is around 20 cm and it weighs below 100 gram.

The tendency of gas to finger through an oil phase requires particular focus on the sampling protocol. A recommended practice is to ensure a sampling frequency in line with expected breakthrough times from a reservoir simulation, with safety margins large enough to account for any unexpected transport behavior. Additional steps taken by the project team to enhance the success of the project include the following:

- Field personnel were provided hands-on training in the specialized sampling of gas tracers using the CAT technology.
- A sampling protocol was developed for the project and routinely monitored by the project team.
- The sampling frequency was designed to ensure early breakthrough times are not missed. High frequent sampling — two samples per week — at the beginning; then weekly sampling at the middle; and more relaxed sampling — biweekly and monthly — toward the end, Table 2.
- The sampling tubes were clearly labeled with engraved ID numbers that were copied to the registration sheet along with the well's ID number and sampling date.
- Ensuring good communication between the office and field personnel to enable alignment of the objectives and priorities.

Time after Injection (T)	Sampling Frequency	Remarks
T < 1 month	Two samples per week	This is important to reduce any uncertainty about break through detection
1 month < T < 3 months	Weekly	
3 months < T < 6 months	Biweekly	
T > 6 months	Monthly	For tail end of the curve

Table 2. Sampling frequency plan

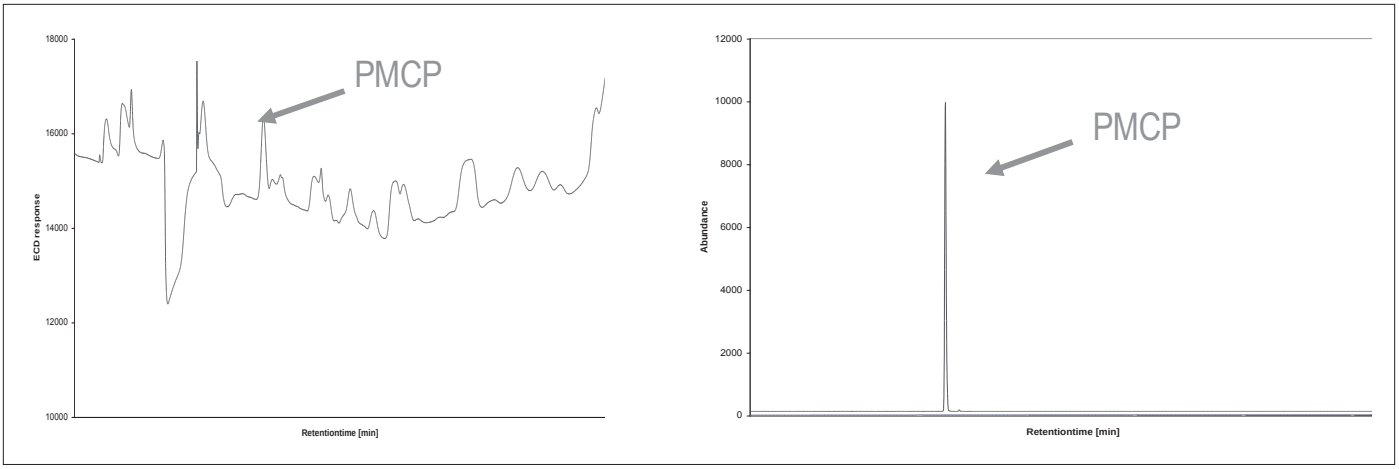

Fig. 4. Chemical analysis of a produced gas sample using the gas cylinder GC-ECD method (left), and the same sample analyzed with the CAT sampler technology (right).

TRACER ANALYSES

One of the key prerequisites for a successful tracer job is the detectability of the tracers deployed for a particular tracing job. In addition, the ease of sampling and analyses can significantly impact the success or failure of any tracer operation. When performing gas sampling using the CAT sampler, a small volume of produced gas is bled to atmospheric pressure at the sampling site before it is transferred to the CAT sampler. The sampling and transfer process takes a few minutes, allowing many wells to be sampled in a relatively short time. In addition to this, the CAT technology enables superior detection limits in the parts per trillion, 1×10^{-12} (ppt) to the parts per quadrillion, 1×10^{-15} (ppq) range, combining high sensitivity and better selectivity than the gas cylinder gas chromatography electron capture detection (GC-ECD), Fig. 4.

The left part of Fig. 4 shows chemical analysis of a produced gas sample containing ~100 ppt of the tracer PMCP using the gas cylinder GC-ECD method. In addition to the tracer signal, potentially disturbing signals from compounds naturally present in the sampled gas can be seen. The right part of the figure shows the same sample analyzed with the CAT sampler technology; no interfering compounds are visible, and a considerably better signal to noise ratio is achieved, therefore, a lower detection limit can be achieved.

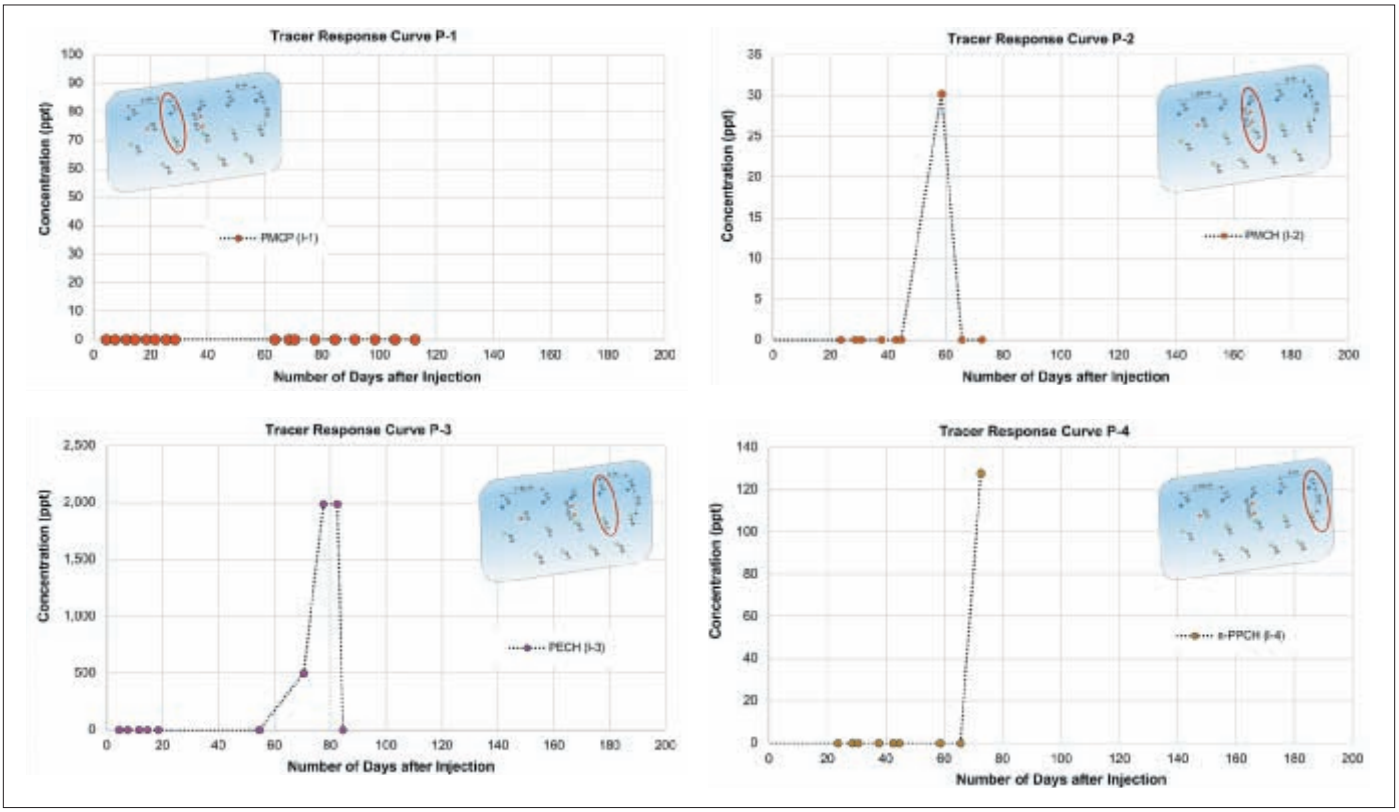

Fig. 5. Summary of the breakthrough for the gas tracers for each producer well, Wells P-1 to P-4.

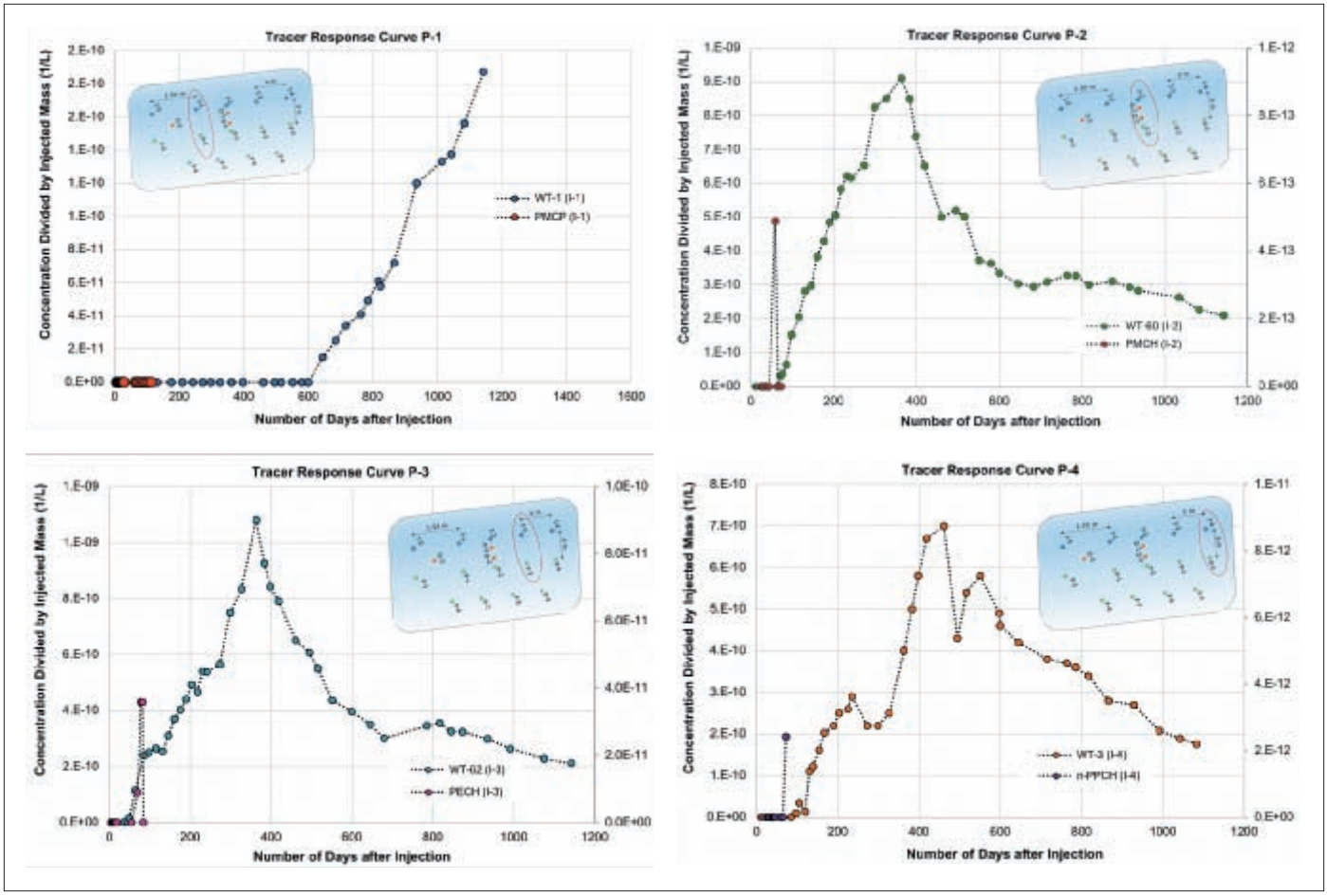

Fig. 6. Water and gas tracer concentrations normalized by the injected amount as a function of time since injection for each producer well, Wells P-1 to P-4.

RESULTS AND DISCUSSION

Figure 5 summarizes the main results of the IWGTT campaign from the data available to date. The gas tracer response curve — tracer concentrations vs. time — are plotted for each well.

A clear breakthrough of the gas tracers is seen in producer wells, Wells P-3 and P-4. A lower concentration was detected in Well P-2, but this result was not confirmed by the following sample. Whether a breakthrough has occurred in this well will have to be verified with further samples. In Well P-3, the tracer broke through between 55 and 71 days after injection. In Well P-4, the tracer broke through between 66 and 71 days after injection. No tracer breakthrough is noticed in Well P-1.

KEY OBSERVATIONS AND INTERPRETATION

The IWGTT campaign presented here is part of an extensive M&S program. At the early part of the project, before the commencement of gas injection, an IWCTT was conducted using individual water tracers in injector wells, Wells I-1 through I-4, and the results from the water tracing campaign that was conducted previously. For an easy comparison, these results are also displayed in Fig. 6.

Although the sampling period is still relatively short, as the gas tracers were injected more recently than the water tracers, a few important observations can be made at this stage. First, the results confirm that the tracers can survive in the reservoir and that they can be analyzed at the small concentrations observed. This is an important observation, as relatively few case studies have been reported where gas tracers are used to follow injected gas in hydrocarbon reservoirs. Second, the gas tracers have breakthrough times that are somewhat comparable to those found from the water tracers. For producer Well P-3, the breakthrough is almost equal to that from the water tracer — whereas for producer Well P-4, the breakthrough for the gas tracer is slightly ahead of that for water. This could indicate a gas movement that is controlled by the water movement.

The preliminary nature of the gas tracer results nevertheless calls for caution and further sampling, and observation of the tracer curves, which is needed to confirm this conclusion. The impact of the water cycle on the gas tracer also needs to be studied. For the PMCP tracer injected in Well I-1, non-zero concentrations are yet to be observed in Well P-1. This is not surprising, considering the fact that the water tracers injected in Well I-1 used significantly longer times to break through than the water tracers injected in Wells I-2, I-3, and I-4.

The results are also in agreement with the wellhead gas breakthrough trend observed for each well. Wells P-3 and P-4 had a higher concentration of gas within three months of the

gas injection, whereas Wells P-1 and P-2 had a delayed gas breakthrough at the wellhead. The gas breakthrough time for Well P-1 was about 21 months.

It is worth highlighting in Fig. 6 that the time from injection is longer for the water tracers injected about three years ago. The sampling period is significantly longer for the water tracer than for the more recently injected gas tracers. In all the subfigures, the right axis represents the gas tracers and the left axis represents the water tracers.

LESSONS LEARNED

1. The sampling protocol and hands-on training for specialized sampling of gas tracers using the CAT technology given to the field personnel were invaluable and contributed to obtaining good samples for the project.
2. Good communication between office staff and field personnel is essential to ensure alignment of objectives and priorities. For this project, it helped to eliminate sample contamination and other headaches that could have jeopardized the tracer project.
3. The use of the CAT system simplified the logistics of sample handling and transportation.
4. Previous experience gained during the IWCTT operation was useful in expediting the IWGTT field deployment and implementation. Where possible, using the same crew that are familiar with similar operations eliminated some of the stumbling blocks that might have negatively impacted the success of the IWGTT project.

CONCLUSIONS

1. The IWGTT data proves to be effective in determining gas phase connectivity between the gas injector and producer well pairs.
2. Early results showed some similarities and some differences between IWGTT and IWCTT breakthrough times observed for some of the injector and producer well pairs.
3. The interplay of gravity override, reservoir heterogeneity, and differences in mobility ratio might have contributed to the differences observed between the IWGTT and IWCTT data. Further analyses and comparison will await additional data to generate a broader concentration vs. time curve. The impact of the water cycle on the gas tracer also needs to be studied.
4. The results provided a better understanding of gas flow paths and gas phase connectivity between the gas injector and producer well pairs, gas phase breakthrough times — time of flight — and data for optimizing WAG field operations.

ACKNOWLEDGMENTS

The authors would like to thank the management of Saudi Aramco for their support and permission to publish this article. This article would not have been possible without the contributions and efforts of many colleagues. In particular, we would like to acknowledge and thank Hasan Al-Abbad, Hassan Hassan, Abdullah Ghamdi (Lafi), Bassam Al-Awami, Sabine Telle, Øyvind Dugstad, and many others for their contributions toward the project.

This article was presented at the Abu Dhabi International Petroleum Exhibition and Conference, Abu Dhabi, UAE, November 13-16, 2017.

REFERENCES

1. Dugstad, Ø.: *Well-to-Well Tracer Tests*, Chapter 6 in *Petroleum Engineering Handbook*, *Vol. 5: Reservoir Engineering and Petrophysics*, Holstein, E.D. (ed.) SPE, Richardson, Texas, 2007, 1640 p.
2. Zemel, B.: *Tracers in the Oil Field*, Elsevier Science, 1995, 486 p.
3. Galdiga, C.U. and Greibrokk, T.: "Ultra-trace Determination of Fluorinated Aromatic Carboxylic Acids in Aqueous Reservoir Fluids Using Solid-phase Extraction in Combination with Gas Chromatography Mass Spectrometry," *Journal of Chromatography A*, Vol. 793, Issue 2, January 1998, pp. 297-306.
4. Dugstad, Ø., Bjørnstad, T. and Hundere, I.A.: "Measurements and Application of Partition Coefficients of Compounds Suitable for Tracing Gas Injected into Oil Reservoirs," *Revue de l'Institut Francais du Petrole*, Vol. 47, Issue 2, March 1992, pp. 205-215.
5. Kleven, R., Høvring, O., Opdal, S.T., Bjørnstad, T., et al.: "Non-Radioactive Tracing of Injection Gas in Reservoirs," SPE paper 35651, presented at the SPE Gas Technology Symposium, Calgary, Alberta, Canada, April 28-May 1, 1996.
6. Viig, S.O., Juilla, H., Renouf, P., Kleven, R., et al.: "Application of a New Class of Chemical Tracers to Measure Oil Saturation in Partitioning Interwell Tracer Tests," SPE paper 164059, presented at the SPE International Symposium on Oil Field Chemistry, The Woodland, Texas, April 8-10, 2013.
7. Hartvig, S.K., Huseby, O., Yasin, V., Ogezi, O., et al.: "Use of a New Class of Partitioning Tracers to Assess EOR and IOR Potential in the Bockstedt Field," paper We A02, presented at the 18th European Symposium on Improved Oil Recovery, Dresden, Germany, April 14-16, 2015.
8. Sanni, M.L., Al-Abbad, M., Kokal, S.L., Dugstad, Ø., et al.: "Pushing the Envelope of Residual Oil Measurement:

A Field Case Study of a New Class of Inter-Well Chemical Tracers," SPE paper 181324, presented at the SPE Annual Technical Conference and Exhibition, Dubai, UAE, September 26-28, 2016.

9. Deans, H.A.: "Method of Determining Fluid Saturations in Reservoirs," U.S. Patent 3,623,842, 1971.
10. Al-Abbad, M., Sanni, M., Kokal, S.L., Krivokapic, A., et al.: "A Step-Change for Single Well Chemical Tracer Tests (SWCTT): Field Pilot Testing of New Sets of Novel Tracers," SPE paper 181408, presented at the SPE Annual Technical Conference and Exhibition, Dubai, UAE, September 26-28, 2016.
11. Mukherjee, J., Nguyen, Q.P., Scherlin, J., Vanderwal, P., et al.: "CO_2 Foam Pilot in Salt Creek Field, Natrona County, WY: Phase III: Analysis of Pilot Performance," SPE paper 179635, presented at the SPE Improved Oil Recovery Conference, Tulsa, Oklahoma, April 11-13, 2016.
12. Kumar, J., Draoui, E. and Takahashi, S.: "Design of CO_2 Injection Pilot in Offshore Middle East Carbonate Reservoir," SPE paper 179832, presented at the SPE EOR Conference at Oil and Gas West Asia, Muscat, Oman, March 21-23, 2016.
13. Vandeweijer, V., van der Meer, B., Hofstee, C., Mulders, F., et al.: "Monitoring the CO_2 Injection Site: K12B," *Energy Procedia*, Vol. 4, December 2011, pp. 5471-5478.
14. Ringrose, P.S., Mathieson, A.S., Wright, I.W., Selama, F., et al.: "The In Salah CO_2 Storage Project: Lessons Learned and Knowledge Transfer," *Energy Procedia*, Vol. 37, 2013, pp. 6226-6236.
15. Galdiga, C.U. and Greibrokk, T.: "Ultra-trace Detection of Perfluorocarbon Tracers in Reservoir Gases by Adsorption/Thermal Desorption in Combination with NICI-GC/MS," *Fresenius' Journal of Analytical Chemistry*, Vol. 367, Issue 1, April 2000, pp. 43-50.

BIOGRAPHIES

Modiu L. Sanni is a Senior Petroleum Engineering Consultant with the Reservoir Engineering Technology Division of Saudi Aramco's Exploration and Petroleum Engineering Center – Advanced Research Center (EXPEC ARC). He is currently leading the monitoring and surveillance program for Saudi Aramco's first carbon dioxide enhanced oil recovery (EOR) and sequestration demonstration project. Since joining Saudi Aramco in 2004, Modiu has been involved in research projects relating to improved/EOR, tracer technology, logging tool development, petrophysics and integrated reservoir description. Prior to joining Saudi Aramco, he worked for Shell for about 15 years in Africa, Europe and the Middle East in various capacities.

Modiu is a member of the Society of Petroleum Engineers (SPE) and the Society of Petrophysicists and Well Log Analysts (SPWLA). He has authored and coauthored several technical papers. He holds four patents in the area of application of nanotechnology in reservoir description.

In 1987, Modiu received his B.S. degree in Mechanical Engineering from the University of Benin, Benin City, Nigeria. In 1990, he received his M.S. degree in Mechanical Engineering from the University of Ibadan, Ibadan, Nigeria.

Dr. Mohammed A. Al-Abbad is a Senior Petroleum Engineer with the carbon dioxide (CO_2) enhanced oil recovery (EOR) team within the Reservoir Engineering Technology Division of Saudi Aramco's Exploration and Petroleum Engineering Center – Advanced Research Center (EXPEC ARC). He is leading the work on tracers and has been involved in the deployment of single well and interwell tracer tests. Mohammed has worked in various disciplines, including petrophysics, production engineering, reservoir management, reservoir simulation, and EOR.

He is a Society of Petroleum Engineers (SPE) Certified Petroleum Engineer, actively participating in local and regional events with several technical publications to his credit.

In 2002, he received his B.S. degree in Chemical Engineering from King Fahd University of Petroleum and Minerals (KFUPM), Dhahran, Saudi Arabia. Mohammed received his M.S. and Ph.D. degrees in Petroleum and Natural Gas Engineering from Pennsylvania State University, State College, PA, in 2008 and 2012, respectively.

Dr. Sunil L. Kokal is a Principal Professional and a Focus Area Champion of enhanced oil recovery (EOR) in the Reservoir Engineering Technology team of Saudi Aramco's Exploration and Petroleum Engineering Center – Advanced Research Center (EXPEC ARC). Since joining Saudi Aramco in 1993, he has been involved in applied research projects on EOR/improved oil recovery, reservoir fluids, hydrocarbon phase behavior, crude oil emulsions, and production related challenges. Currently, Sunil is leading a group of scientists, engineers and technicians to develop a program for carbon dioxide EOR and to conduct appropriate studies and field demonstration projects. Prior to joining Saudi Aramco, he worked at the Petroleum Recovery Institute, Calgary, Alberta, Canada.

Sunil is a member of the Society of Petroleum Engineers (SPE), and is a Registered Professional Engineer and a member of the Association of Professional Engineers, Geologists and Geophysicists of Alberta (Canada).

He has written over 125 technical papers. Sunil has served as the Associate Editor for the *Journal of Petroleum Science and Engineering*, and SPE's *Reservoir Evaluation and Engineering Journal*.

He is the recipient of several awards, including the SPE IOR Pioneer Award (2018), the SPE Honorary Member Award (2016), the SPE DeGolyer Distinguished Service Medal (2012), the SPE Distinguished Service Award (2011), the SPE Regional Technical award for Reservoir Description & Dynamics (2010), and the SPE Distinguished Member Award (2008) for his services to the society. Sunil also served as a SPE Distinguished Lecturer during 2007-2008.

In 1982, Sunil received his B.S. degree in Chemical Engineering from the Indian Institute of Technology, New Delhi, India, and in 1987, he received his Ph.D. degree in Chemical Engineering from the University of Calgary, Calgary, Alberta, Canada.

Razally M. Ali is a Reservoir Engineering Specialist with Saudi Aramco's Southern Area Reservoir Management Department. He has 23 years of industry experience. Prior to joining Saudi Aramco in 2006, Razally worked at various postings as a Reservoir Engineer for Petronas Malaysia, Brunei Shell, Talisman Scotland and Woodside Australia. He also spent 4 years with Schlumberger Consulting Services formulating integrated field development plans for numerous operators.

Razally is currently working with the 'Uthmaniyah Reservoir Management Unit, managing the mature northern sector. He has been involved with several reservoir assessment studies, including the Event Solutions Center. Razally is a core team member for the 'Uthmaniyah carbon dioxide enhanced oil recovery (EOR), SmartWater Flood and chemical EOR pilot projects.

In 1994, he received his M.S. degree in Petroleum Engineering from Imperial College London, London, U.K.

Razally is a member of the Society of Petroleum Engineers (SPE).

Ibrahim M. El-Zefzafy is a Senior Petroleum Engineer with Saudi Aramco's South Ghawar Production Engineering Division of the Southern Area Production Engineering Department. He has close to 22 years of experience in the oil and gas industry in rigless well intervention, oil artificial lift design, well performance and production optimization, well completion and testing, and workover interventions. Ibrahim also has comprehensive well services and production enhancement experience in onshore and offshore operations.

Since joining Saudi Aramco in 2006, he has been involved in a wide variety of technical projects and planning activities as part of oil development and enhanced oil recovery projects. Ibrahim manages a team responsible for the introduction and implementation of new technology applications, to improve productivity, in collaboration with Saudi Aramco's Exploration and Petroleum Engineering Center – Advanced Research Center (EXPEC ARC) and the Research and Development Center (R&DC).

Prior to joining Saudi Aramco, he worked as a District Production Engineer with Gulf of Suez Petroleum Company's joint venture with British Petroleum in Egypt.

Ibrahim is a registered member of the Society of Petroleum Engineers (SPE), and he has authored and coauthored numerous SPE papers.

In 1995, Ibrahim received his B.S. degree in Petroleum Engineering from Al-Azhar University, Cairo, Egypt.

Self-Healing Durable Cement; Development, Lab Testing, and Field Execution

Dr. Abdullah S. Al-Yami, Mohammad H. Alqam, Riefky Abdurrahman, and Ali U. Shafqat

ABSTRACT

Pressure and temperature changes during the life of the well — drilling and production — cause some casing-casing annulus (CCA) pressure leaks in the annulus between the 13⅜" and 9⅝" casings, and the 13⅜" and 18⅝" casings, thereby indicating that the well barriers failed to isolate all the zones, subsequently resulting in the migration of the fluid to the surface. Such failures in wellbore isolation prevent us from taking full potential of our high performance wells.

Under most failure conditions, the tensile strength of cement has a greater impact on its failure as compared to the cement's compressive strength. Consequently, increasing tensile strength of cement is a higher priority than increasing its relative compressive strength. This can be achieved by using additives such as latex, polyvinyl alcohol or fibers, or simply by increasing cement flexibility. The objective of this article is to discuss the development, testing, and field execution of a new type of cement, a self-healing durable cement, to mitigate such failures due to pressure or temperature cycling.

This new cement was developed utilizing novel components that results in a cement with a reduced Young's modulus. A lower Young's modulus makes the cement more elastic to resist pressure and temperature cycling, absorb applied stresses, and prevent cement cracks. The developed self-healing durable cement also provides an additional benefit of mechanical properties' enhancement as the included additive exhibits swelling and sealing capacity when contacted by hydrocarbon fluids. In the event cracks form in the cement, this will be a path for the fluid to trigger the swelling and self-healing mechanism.

The article includes detailed testing data for thickening time, rheology, and free water, settling at different ranges of densities. An additional test was also included to evaluate the durability of the system with time. Mechanical properties testing was performed for cement samples after 10, 20, and 30 days curing at representative targeted field conditions. Single-stage triaxial tests were performed on dry cement core plugs to measure static and dynamic properties through ultrasonic and shear velocities. These properties were determined at confining pressures and included the Young's modulus, the Poisson's ratio, and peak strength.

Offset wells cemented with conventional formulations have shown CCA pressure with slight oil flows. The developed self-healing durable cement was applied to the 13⅜" casings covering oil-bearing zones. The deployments were declared successful since negative testing, temperature, and pressure cycling did not result in any CCA pressure leaks. Ultimately, good cementing performance is always measured by having a zero psi CCA pressure.

INTRODUCTION

Cementing is used to[1]:

- Isolate zones by preventing fluid migration between formations.
- Support and bond casings.
- Protect casings from corrosive environments.
- Seal and hold back formation pressures.
- Protect casings from drilling operations such as shock loads.
- Seal loss circulation zones.

El-Marsafawi et al. (2006)[2] discussed that throughout the life of the well, the cement integrity experienced different challenges, due to:

- Opening windows for multilateral wells.
- Temperature increase in production phase.
- Pressure increase due to gas production.
- Changing of mud weight after drilling to a lighter weight or switching to lower density completion fluids.
- Changing of mud weight during drilling different formations.
- Stimulation treatment such as fracturing operations or aggressive matrix acids[3].
- Formation loading if applicable such as creep, compaction, and faulting.

In multistage cementing, the diverter valve can fail,

resulting in remedial operations such as perforations and squeeze or secondary cementing jobs. The weakest point in the casing is often the conventional low-pressure stage tool, which might comprise wellbore integrity[4].

To overcome wellbore limitations against temperature and pressure limitations, we need to consider self-healing durable types of cement. Adding elastomers to cement will reduce its Young's modulus to make it more elastic so as to resist pressure and temperature cycling[5, 6].

Elastomers can also provide an additional benefit for mechanical properties' enhancement, which is the elastomers' swelling and sealing capacity attained through contact with hydrocarbon fluids. The elastomers will volumetrically expand or swell once they are in contact with organic solvents such as hydrocarbons[7]. In case we have cracks in the cement, this will be a path for the fluid to trigger the swelling and expansion mechanism[8].

Cavanagh et al. (2007)[9] discussed using self-healing material for cementing for when high-pressure risks are anticipated. The self-healing material within the cement will provide self-preparing properties within the set cement when cracks or other flow paths are generated due to pressure or temperature cycling in the presence of hydrocarbons. The authors also mentioned that the integrity of the self-healing cement after exposure to oil for one year showed good results with no signs of deterioration. Thermal activated monomers were combined in self-healing cement where no fluid is required to trigger the swelling[10].

The cements need to be designed to prevent short-term and long-term gas migration scenarios. In the short term, the cement must prevent gas migration problems after cement placement and as cement is converted from liquid to a semi-solid. In the long term, the cement must resist pressure and temperature cycling during drilling, fracturing and production[1].

The objective of this article is to discuss the development, testing, and field execution of a new type of cement, a self-healing durable cement, to mitigate such failures due to pressure or temperature cycling.

EXPERIMENTAL STUDIES

Slurry Preparation Procedure

The slurry formulation is prepared in the lab using a standard American Petroleum Institute (API) blender. The maximum speed used during slurry preparation was 12,000 rotations per minute (rpm). The slurry was mixed in the blender for 15 seconds at 4,000 rpm and 35 seconds at 12,000 rpm, respectively[11].

Slurry Rheology

The slurry was conditioned in the atmospheric consistometer before obtaining the rheological measurements. A Fann viscometer (Model-35) was utilized to measure the slurry's apparent viscosity[11].

Thickening Time Test

The prepared slurry was then poured into an API standard high-pressure, high temperature (HPHT) consistometer slurry cup for a thickening time test, which is important for evaluating the pumpability of the cement slurry[11].

Fluid Loss Test

Dynamic fluid loss — loss of fluid from the slurry while pumping — results in an increase in slurry density, which may cause lost circulation. In addition, other properties such as rheology and thickening time may be adversely affected. Static fluid loss — loss of fluid from the slurry after placement — if not carefully controlled, will lead to a slurry volume reduction and drop pressure that can allow formation fluids to enter the slurry.

Free Water and Slurry Sedimentation Tests

When cement slurry is allowed to stand for a period of time prior to setting, water may separate from the slurry. A free water test is used to measure water separation using a 250 ml graduated cylinder set in the cement slurry for 2 hours. Settling can be measured by comparing densities of different sections of the cement column cured[11]. A cylindrical shaped cell, used to cure the cement formula for settling tests, had a diameter of 1.4" and length of 12". Sections measuring 2" long were taken from different parts of the cement column sample.

Expansion Performance Testing

To measure expansion, an annular expansion ring test is used to measure linear expansion under conditions of free access to water. Free access to water means an open system. An annular expansion mold is used to simulate the annulus of the well. The cement slurry is poured into the annular space in the mold and then the mold is placed into a water bath or pressurized curing chamber. Water will be in contact with the slurry during the entire curing process. The diameter will increase if the cement expands[11].

Curing at Downhole Conditions

The HPHT curing chamber is used for curing cement specimens at elevated temperatures and at pressures simulating conditions in the wells. The slurries were poured into cylindrical cells (1.5" × 3") and lowered into the curing chamber. The curing chamber is filled with water to expel gas. A temperature controller regulates the sample temperature. Pressures

and temperatures were maintained until shortly before the end of the curing. The temperature and pressure were reduced to ambient conditions, and then the test specimens were removed from the curing chamber after 10, 20, and 30 days.

Mechanical Properties Testing

Single-stage triaxial tests were performed on dry cement core plugs with lengths ranging between 2.997" and 3.020" and diameters ranging between 1.490" and 1.510" to measure static and dynamic properties through ultrasonic and shear velocities. These properties were determined at a confining pressure of one MPa (1 MPa = 145.038 psi) and included the Young's modulus, the Poisson's ratio, and the peak strength.

During each test performed, a series of ultrasonic measurements and dynamic moduli were computed. The final dynamic moduli of a plug were taken as the average of the moduli computed at each ultrasonic velocity measurement.

Sample Preparation: Sample preparation includes the following steps:

- Cement plug preparation.
- Surface grinding of the parallel end faces until they become flat to within 0.001".
- Jacketing of the plug and positioning of two end caps equipped with velocity transducers on the ends of the sample, while a coupling medium is set between the plug's flat surfaces and the transducer.

Sample Loading: After completing the sample preparation, the plug is equipped and loaded onto the testing frame as follows:

1. The jacket is clamped to the transducers from both ends to allow for the hydrostatic application of confining pressure around the sample, Fig. 1.
2. Radial and axial linear variable differential transformers (LVDTs) are positioned around and along the sample to measure the radial and axial displacements, respectively.
3. Confining pressure is applied hydrostatically around the sample. The confining pressures are selected to approximately simulate the stress conditions in the wellbore.

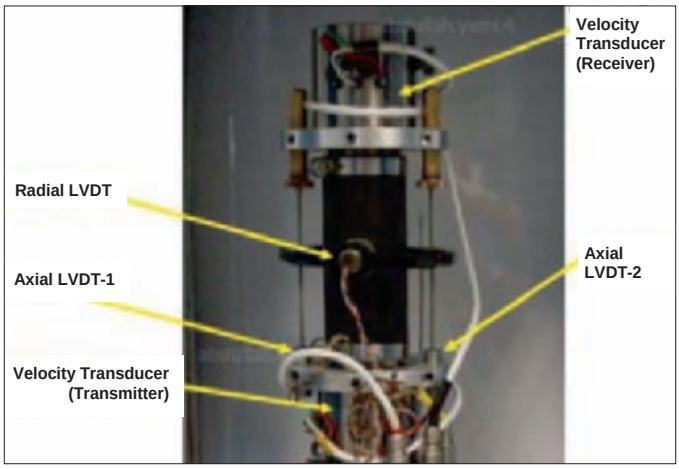

Fig. 1. Loading of the cured cement sample.

Sample Testing

Multistage and/or single-stage loading are performed on selective samples, which involve loading the cement sample at a given confining pressure to failure (single stage) or near failure (multistage); then a new sample is tested or a new loading cycle is applied on the same sample using a different confining pressure. A Mohr-Coulomb failure envelope may then be constructed if three to four tested samples or three to four loading cycles are available.

For multistage loading, a sample is hydrostatically loaded to a given confining pressure and the differential axial stress is increased slowly until a nonlinear radial strain is observed, upon which the sample is unloaded and a new confining pressure is applied to go through the next loading stage. Multistage loading is applied when it is determined that the sample is a good candidate for such a testing methodology. It must be emphasized that the sample must not be loaded beyond the initiation of a plastic deformation (Yield Point).

For this project, single-stage triaxial tests at low confining pressures were performed. A Mohr-Coulomb failure envelope is not constructed as the cement plugs for each formulation are tested only at a single confining pressure.

The dynamic elastic properties are determined simultaneously with the static properties using ultrasonic measurements. The static properties are required for many petroleum engineering applications, although dynamic data are often collected in the field and therefore the necessary calibration must be obtained.

To perform dynamic measurements — ultrasonic velocity measurements — the end caps of the core sample are equipped with two ultrasonic transducers and receivers, which can generate and detect both compressional and shear waves. One transducer is a transmitter, which is excited to induce an ultrasonic wave at a frequency of 700 kHz, and the other one is a receiver. In this report, the velocities of these waves are used to compute the dynamic Young's modulus and Poisson's ratio.

MECHANICAL PROPERTIES SIMULATION

The primary reason for performing stress analysis is to provide an upfront easy method to allow the field to determine whether a durable self-healing cement system is needed in a well, and to provide suitable analysis and reports to show that there is a need to implement a durable cement or a self-healing cement. Many different scenarios arise when there is a

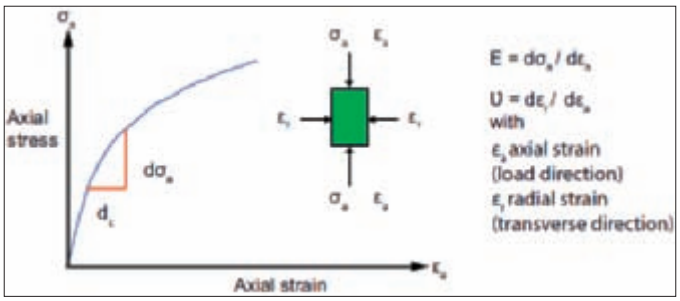

Fig. 2. Young's modulus and Poisson's ratio definition.

well event, e.g., pressure testing, fluid change out during the completion phase, where the cement sheath is suspected to be compromised in one way or another. This software allows a very easy and fast way in determining if the integrity of the cement sheath is compromised.

A cemented well is a combination of three structures in interaction with each other, involving at least a thin cement sheath confined between a metallic casing and a rock formation. To evaluate the integrity of such a system, it is necessary to understand and analyze the mechanical behavior of the whole set, considering the specificities of each substructure.

Young's modulus E characterizes the material's longitudinal deformation under uniaxial loading, i.e., along an axis when opposing forces are applied. Transverse deformation is quantified with the Poisson's ratio, υ, which is the ratio between transverse and axial deformation, Fig. 2. A Poisson's ratio equal to 0.5 means the material is incompressible. Conventional cements have a Poisson's ratio of approximately 0.15.

For isotropic materials, Young's modulus and Poisson's ratio are independent of direction. They are generally measured during uniaxial compression or tensile tests, with constant — or zero — stress on the transverse surfaces. In the case of cement characterization tests, samples must be saturated with water, and the strain rate must be chosen appropriately to prevent the generation of capillary pressure and excessive pore pressure, which would change the sample response. Measurements are often made at different pressures to determine the influence of confining pressure on elastic response.

FAILURE MECHANISMS OF THE CEMENT SHEATH

Three major failure modes have been identified, Fig. 3. Their initiation depends on the stress state generated by a change in downhole conditions:

- Shear failure: Crushing of the cement matrix due to severe compressive stresses.
- Tensile failure: Radial cracks due to high tensile stresses.
- Creation of a microannulus: Debonding between cement and either the casing or the formation.

Shear failure — also called compression failure — in the cement sheath is caused by high compressive stresses exceeding the rupture compressive strength. Shear failure is typical for wellbore pressure and/or temperature increases, when the formation is rigid — high Young's modulus — or when the cement sheath is between two casings. Due to the pressure increase inside the wellbore, the casing will be pushed outwards. In a confined configuration, when the surrounding medium is hard, the rock — or the external casing — is rigid enough to contain the push, so the cement sheath becomes squeezed between the casing and the formation — or between two casings. In these circumstances, the push creates compressive stresses in the cement. If the compressive stresses exceed the cement rupture strength, a shear failure occurs.

Rupture compressive strength is different from the compressive strength. The compressive strength is the maximum compressive stress attained at the end of a crush test in which the cement is free to expand laterally during the loading. It is also called the unconfined compressive strength. The rupture strength is the maximum compressive stress that the cement would support when not allowed to expand laterally, or if lateral compressive stresses are applied. The rupture strength is greater than the compressive strength. Temperature increases will also produce the effect of pushing the casing outwards, due to thermal dilation. Similar to the case of the pressure increase, in a confined configuration this push may lead to cement shear failure.

Cement fails in traction because of high tensile stresses exceeding the tensile strength. Tensile failure is typical for wellbore pressure or temperature increases, when the formation is soft — low Young's modulus — and/or the cement is rigid — high Young's modulus. A pressure increase inside the wellbore has the effect of pushing the casing outwards. In a nonconfined configuration, when the surrounding medium is soft, the rock is not rigid enough to contain the push, and therefore the casing and cement sheath expand outward. This expansion involves a deformation of the cement sheath as it increases in diameter. Such deformation would stretch the cement creating tangential stresses. Portland cement has a much higher resistance to shear failure than in tensile failure. In these

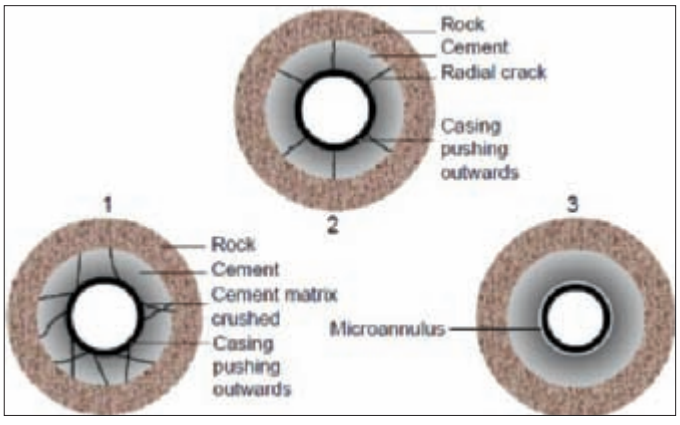

Fig. 3. The three major failure modes: (1) Shear failure, (2) tensile failure, and (3) microannulus.

circumstances, the cement frequently fails under the tensile stress, showing radial cracks that extend vertically along the wellbore. Temperature increases will also produce an outward expansion of the casing due to thermal dilation. Similar to the case of an increase in pressure in a nonconfined configuration, this expansion may create tensile cracks in the cement.

Even a temperature decrease in the wellbore may lead to cement cracking, especially when the interface between the casing and the cement is de-bonded, and the interface between the cement and the formation is fully bonded. In this case, the cement sheath would have a tendency to retract and become smaller in diameter. The bond to the rock may prevent the

RPM	Ramp Up (measurement)	Ramp Down (measurement)	Average
300	150	150	150
200	115	114	114.5
100	75	74	74.5
60	56	56	56
30	40	39	39.5
6	22	20	21
3	16	16	16

Table 1. Rheology at 80 °F of the self-healing cement at 106 pcf

RPM	Ramp Up (measurement)	Ramp Down (measurement)	Average
300	107	107	107
200	81	75	78
100	46	42	44
60	32	29	30.5
30	20	19	19.5
6	9	8	8.5
3	7	6	6.5

Table 2. Rheology conditioned at 271 °F and run at 190 °F for the self-healing cement at 106 pcf

Thickening Time	
Consistency	**Time**
100 Bearden consistency	7:03 hours
Free Fluid	
250 ml in 2 hours, 80 °F, 0° inclination	0 ml
Fluid Loss	
API fluid loss, 30 min, 271 °F, and 1,000 psi	22 ml

Table 3. Additional testing results of the self-healing cement at a density of 106 pcf

Duration (days)	Sample Type	Young's Modulus – Static (psi)	Poisson's Ratio – Static (psi)	Peak Strength (psi)
10	Conventional	2.748 × 10^6	0.378	7,733.90
20	Conventional	2.453 × 10^6	0.323	7,468.10
30	Conventional	1.787 × 10^6	0.081	11,077.20
10	Self-Healing Durable Cement	7.758 × 10^5	0.389	2,841.30
20	Self-Healing Durable Cement	5.939 × 10^5	0.347	3,207.10
30	Self-Healing Durable Cement	7.224 × 10^5	0.208	3,545.60

Table 4. Mechanical properties of the self-healing cement at a density of 106 pcf

RPM	Ramp Up (measurement)	Ramp Down (measurement)	Average
300	65	65	65
200	51	47	49
100	31	25	28
60	23	17	20
30	14	9	11.5
6	7	5	6
3	5	3.0	4

Table 5. Rheology at 80 °F of the self-healing cement at 118 pcf

RPM	Ramp Up (measurement)	Ramp Down (measurement)	Average
300	75	75	75
200	68	55	61.5
100	40	35	37.5
60	30	27	28.5
30	21	19	20
6	12	12	12
3	9	9	9

Table 6. Rheology at 110 °F of the self-healing cement at 118 pcf

Thickening Time	
Consistency	**Time**
100 Bearden consistency	3:53 hours
Free Fluid	
250 ml in 2 hours, 80 °F, 0° inclination	0 ml
Fluid Loss	
API fluid loss, 30 min, 110 °F, and 1,000 psi	18 ml

Table 7. Additional testing results of the self-healing cement at 118 pcf

Duration (days)	Sample Type	Young's Modulus – Static (psi)	Poisson's Ratio – Static (psi)	Peak Strength (psi)
10	Conventional	9.41 × 10^5	0.111	4,729.52
20	Conventional	1.31 × 10^6	0.236	5,282.33
30	Conventional	1.65 × 10^6	0.260	7,213.94
10	Self-Healing Durable Cement	7.16 × 10^5	0.185	2,998.11
20	Self-Healing Durable Cement	5.83 × 10^5	0.367	3,160.01
30	Self-Healing Durable Cement	4.24 × 10^5	0.454	3,032.58

Table 8. Mechanical properties of the self-healing cement at a density of 118 pcf (cement cores samples set #1)

cement sheath contraction. Therefore, the cement sheath could develop tensile stresses that may lead to cracking.

A microannulus occurs when the cement sheath loses its bond with the casing and/or the formation. A microannulus typically occurs when there is a pressure or temperature decrease in the wellbore. A pressure or temperature decrease inside the wellbore has the effect of contracting the casing inwards. If the bond at the casing/cement interface is weak, the casing detaches from the cement, creating a gap.

Duration (days)	Sample Type	Young's Modulus – Static (psi)	Poisson's Ratio – Static (psi)	Peak Strength (psi)
10	Conventional	1.38 × 10^6	0.323	6,251.43
20	Conventional	1.18 × 10^6	0.257	6,347.54
30	Conventional	1.59 × 10^6	0.227	7,016.56
10	Self-Healing Durable Cement	8.31 × 10^5	0.183	2,939.63
20	Self-Healing Durable Cement	7.48 × 10^5	0.264	3,246.22
30	Self-Healing Durable Cement	2.08 × 10^6	0.301	3,607.08

Table 9. Mechanical properties of the self-healing cement at a density of 118 pcf (cement cores samples set #2)

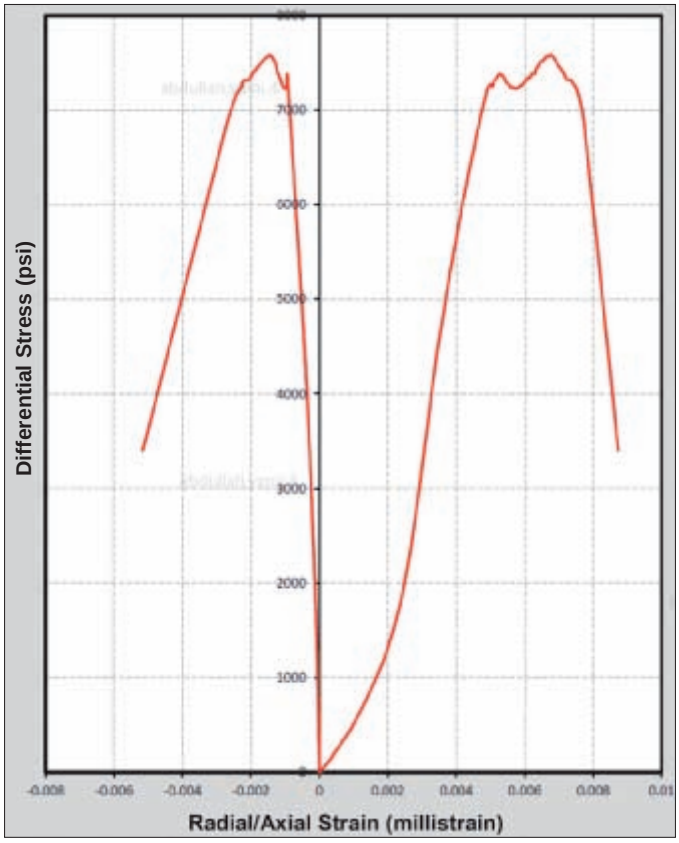

Fig. 4. Mechanical properties of conventional cement after curing for 10 days.

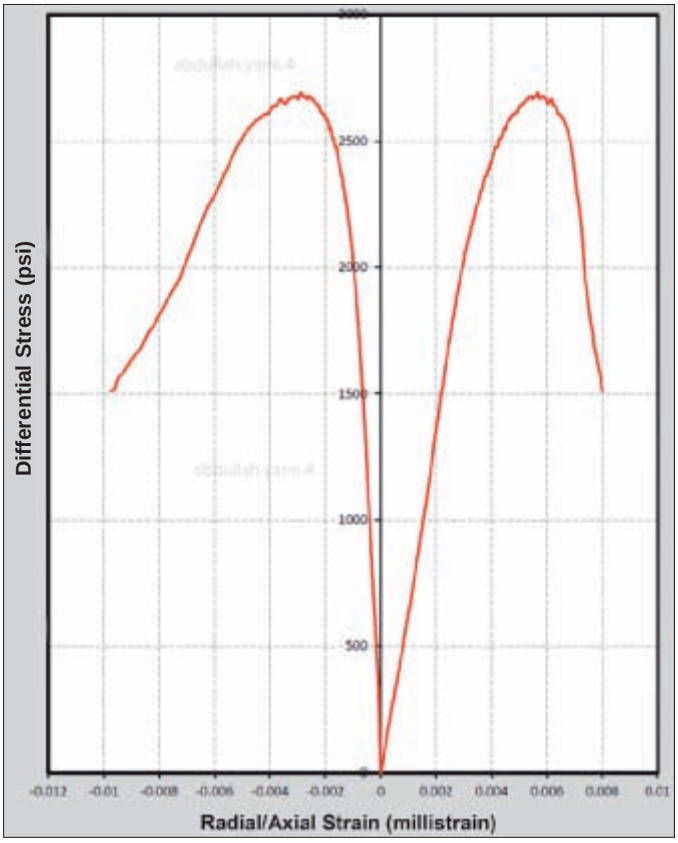

Fig. 5. Mechanical properties of self-healing cement after curing for 10 days.

RESULTS AND DISCUSSION

The cement slurry was tested for rheology, thickening time, fluid loss, free water, sedimentation, expansion performance, and mechanical properties, to evaluate the performance of cement slurry. Tables 1 to 4 show properties of the self-healing cement at a density of 106 pounds per cubic foot (pcf). Tables 5 to 9 show properties of the self-healing cement at a density of 118 pcf.

Figure 4 shows the test results of the mechanical properties of conventional cement, and Fig. 5 shows the test results of the mechanical properties of the self-healing cement.

MECHANICAL PROPERTIES SIMULATION RUNS FOR CONVENTIONAL VS. DEVELOPED DURABLE SELF-HEALING CEMENT

The simulation was run utilizing lab data from Table 4. The assumed condition changes in the well after cementing, as the completion and fracturing are represented in Fig. 6. The pressure represented in the Y axis and time in minutes is represented in the X axis. Initially, the pressure dropped due to changes in mud weight followed by the pressure test to 2,000 psi and then to 5,000 psi. The last part of the pressure chart shows the pressure increase during the fracturing operation to 8,000 psi. The pressure changes in the well have affected the cement sheath. As per the software simulations — cement

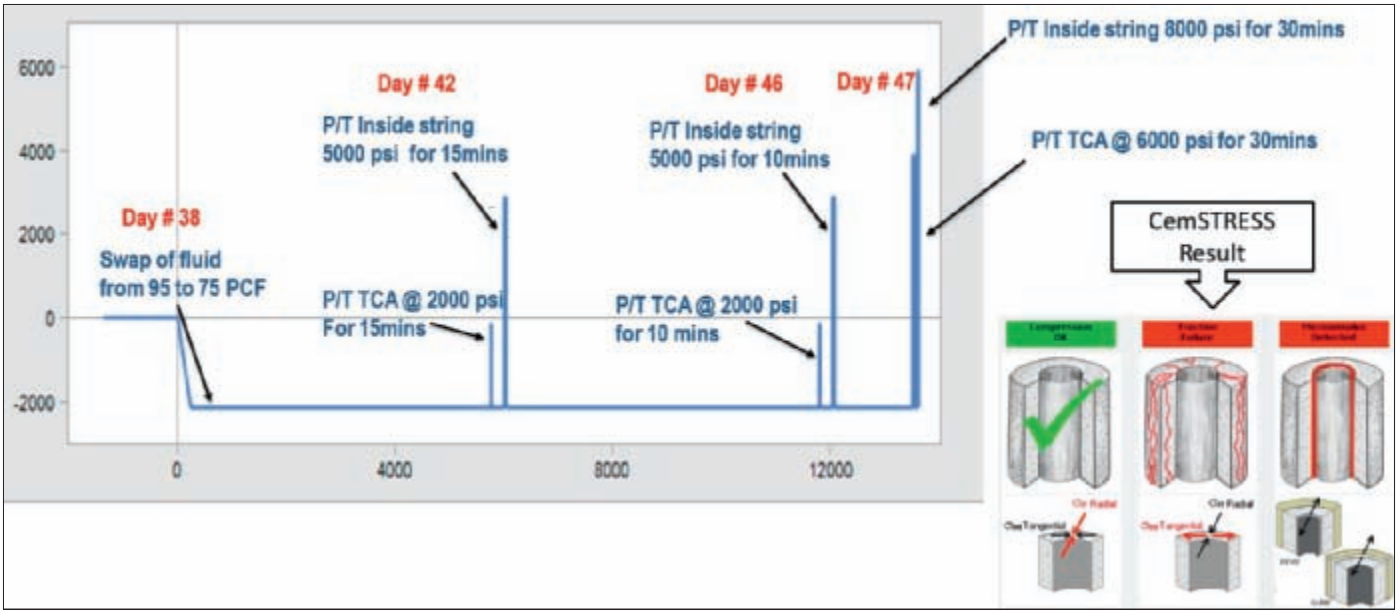

Fig. 6. Pressure changes in the well after the cement was set until the fracturing operation was performed.

sheath stress analysis software — the cement will initially fail in traction at the inner casing-cement boundary.

Due to the changes in well condition, the cement sheath was exposed to tangential tensile stress, which is higher than the tensile strength of the cement. Also, the Young's modulus of the cement used is high — 2.5 Mpsi — indicating that the cement is rigid, and this resulted in the cement sheath failing in traction. At the same time, a microannulus was detected between the cement and formation, and the cement and casing.

Both traction failure and microannulus development resulted in fluid migration through the cement column and may potentially result in casing-to-casing annular pressure leaks. Figure 7 shows the simulation output, indicating the failure in cement traction and the microannulus development.

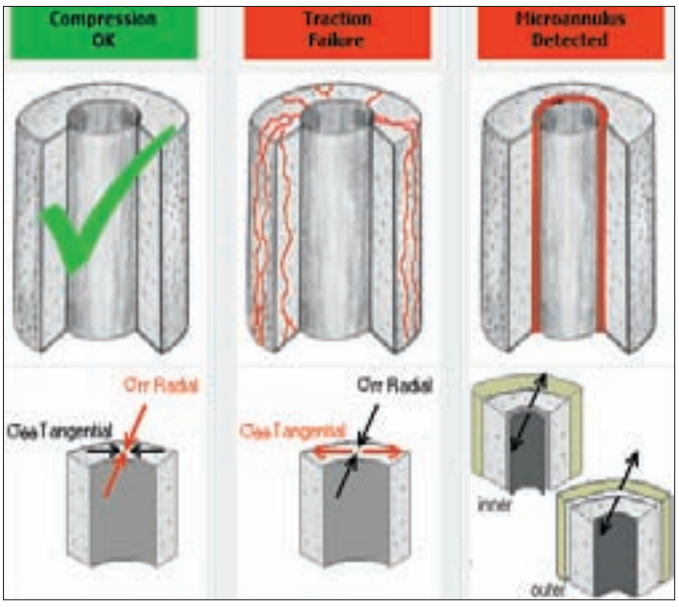

Fig. 7. Failure in traction and microannulus development utilizing the conventional cement.

The same well condition was applied on the durable self-healing cement system showing better mechanical properties. The significant drop in the Young's modulus value of the self-healing durable cement system, compared to the conventional cement system, indicates that it is less rigid than the conventional cements.

Figure 8 shows the software output based on the changes in well condition and utilizes the durable self-healing cement system instead of the conventional cement system. The simulation indicates no failure in traction or compression, however, a microannulus is detected. To overcome the microannulus development, expansion additives need to be added to allow for set cement expansion, and to close the microannulus. The durable cement system has been developed with an expanding agent.

FIELD DEPLOYMENT

A few offset wells cemented with conventional cement have shown pressure with little oil flowing to the surface in a 13⅜" and 18⅝" annulus. The challenges of such zonal isolations are:

- Post-job hydraulic evaluation such as a high-pressure casing test and formation integrity test to 155 pcf equivalent mud weight.
- Well displacement to lighter fluid resulting in cement de-bonding.
- Challenge with annulus pressure before, having hydrocarbon (oil) migration.

Prior to applying the developed self-healing cement job, an additional simulation run was performed on the self-healing cement at a density of 118 pcf. Mechanical properties were measured after curing for 1 month at simulated field

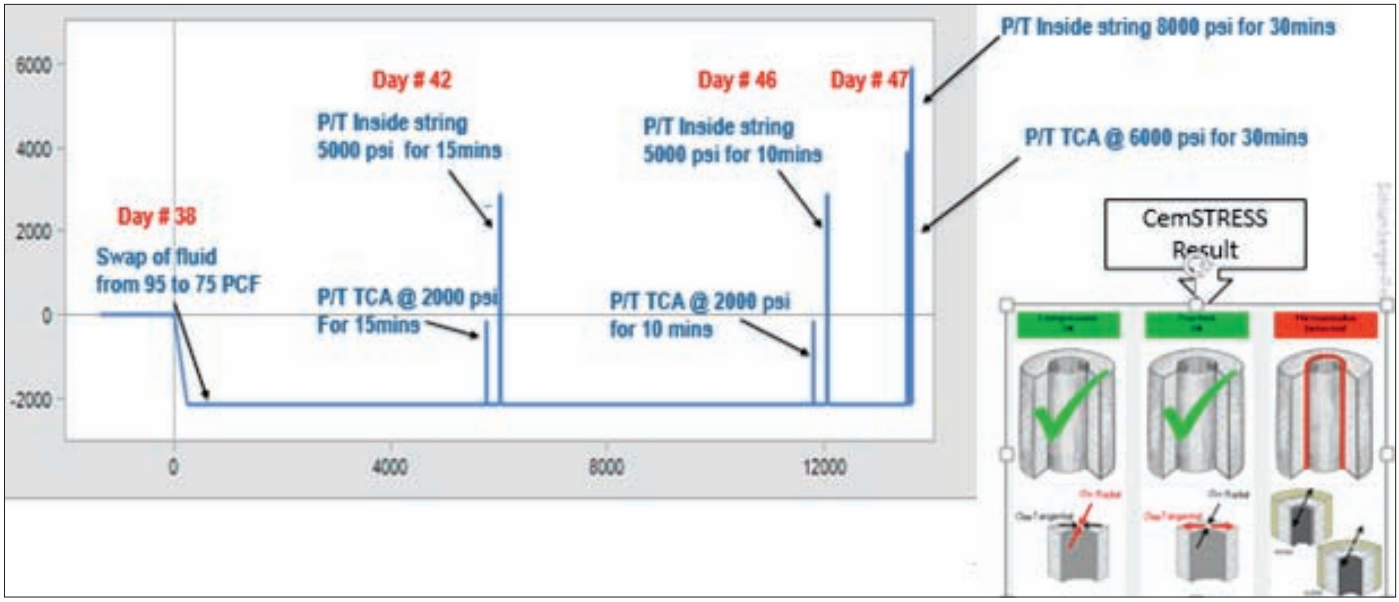

Fig. 8. No failure in traction or compression, with the simulation indicating microannulus development.

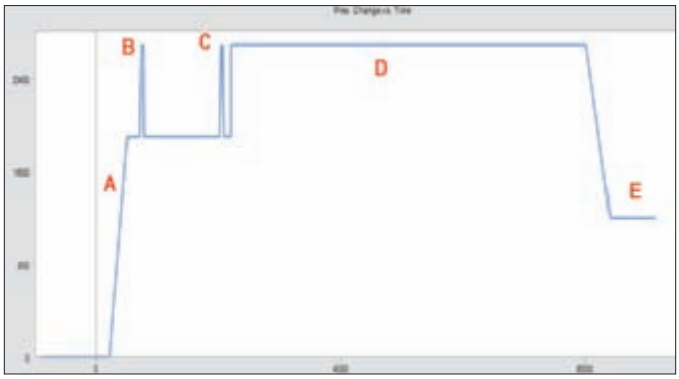

Fig. 9. Stress analysis at the diverter valve depth.

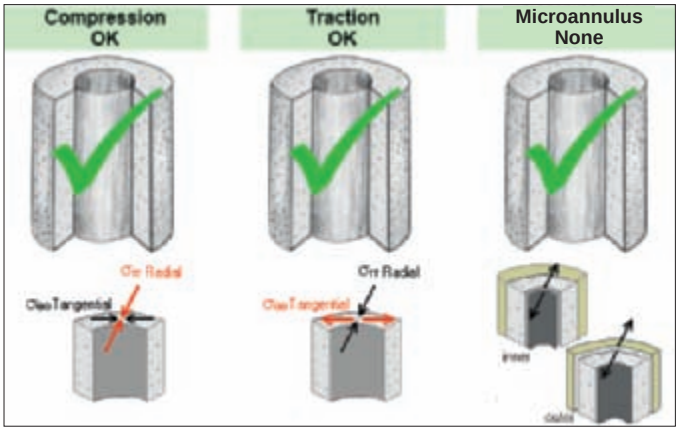

Fig. 10. No failure is found in the traction and compression simulation, which also indicates that there is no microannulus development.

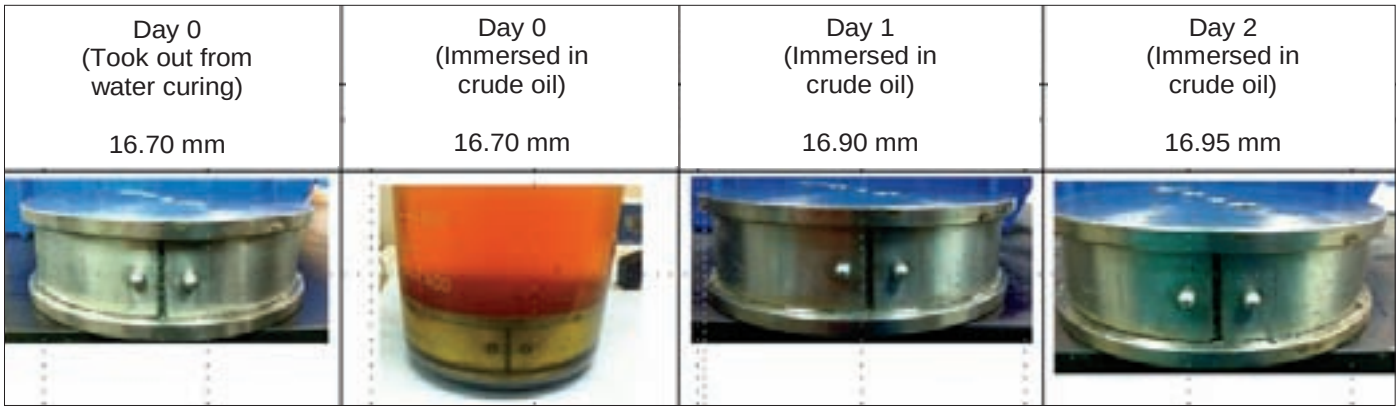

Fig. 11. The self-healing cement swelling capability after reacting with hydrocarbons.

conditions, Table 8. Figure 9 shows the stress analysis at the diverter valve depth, which included the following:

- Displacement of the well from 85 pcf of mud to 145 pcf of mud.
- 155 pcf casing pressure test with 145 pcf mud in the well.
- 155 pcf FIT with 145 pcf mud in the well.
- Drill the next section with 145 pcf of mud with an average equivalent circulating density of 155 pcf managed pressure drilling.
- Displacement of the well from 155 pcf of mud to 105 pcf of mud after a 9⅝" liner is placed.

The simulation outcome showed that the self-healing cement will resist pressure and temperature stresses and all changes above, Fig. 10.

Expanding additive is added in the slurry to overcome the microannulus development after the well is subject to pressure cycles. The developed self-healing durable cement also provides an additional benefit to mechanical properties' enhancement, which is swelling and sealing capacity when contacted by hydrocarbon fluids. In case we have cracks in the cement, this will be a path for the fluid to trigger the swelling and self-healing mechanism. Figure 11 demonstrates the self-healing cement swelling capability after reacting with hydrocarbons. Durable self-healing cement will react with hydrocarbon to close the gap and maintain the isolation to provide assurance for well integrity.

So far, the self-healing cement was successfully applied in the field. Typically, for the 13⅜" casing, the self-healing cement is applied at 118 pcf in the second-stage tail section at 1,200 ft, Fig. 12. Figure 13 shows typical playback data of the 13⅜" casing second-stage cementing. So far, these wells cemented with self-healing cement did not show any signs of casing-casing annular (CCA) pressure leaks, even after aggressive pressure testing.

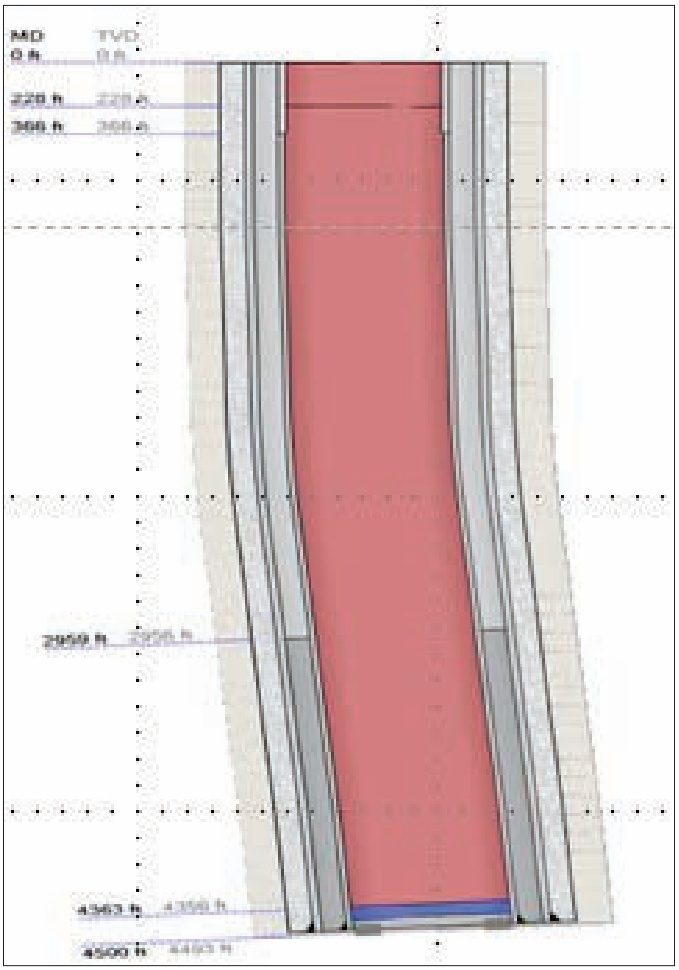

Fig. 12. The self-healing cement is applied at 118 pcf in the second-stage tail section.

CONCLUSIONS

1. Due to pressure and temperature changes during the life of the well (from drilling to production); globally many CCA pressure leaks are observed in the annuli between surface and intermediate casings.
2. A new approach to well cementing had to be developed, and advanced cement technologies considered, taking into account both short- and long-term design parameters.
3. The new approach consists of performing finite elements stress modeling during the well planning phase to custom design cement systems that will withstand the anticipated loads.
4. A new self-healing system was designed to prevent CCA issues.
5. The self-healing durable system has mechanical properties that withstand temperature and pressure cycling, and

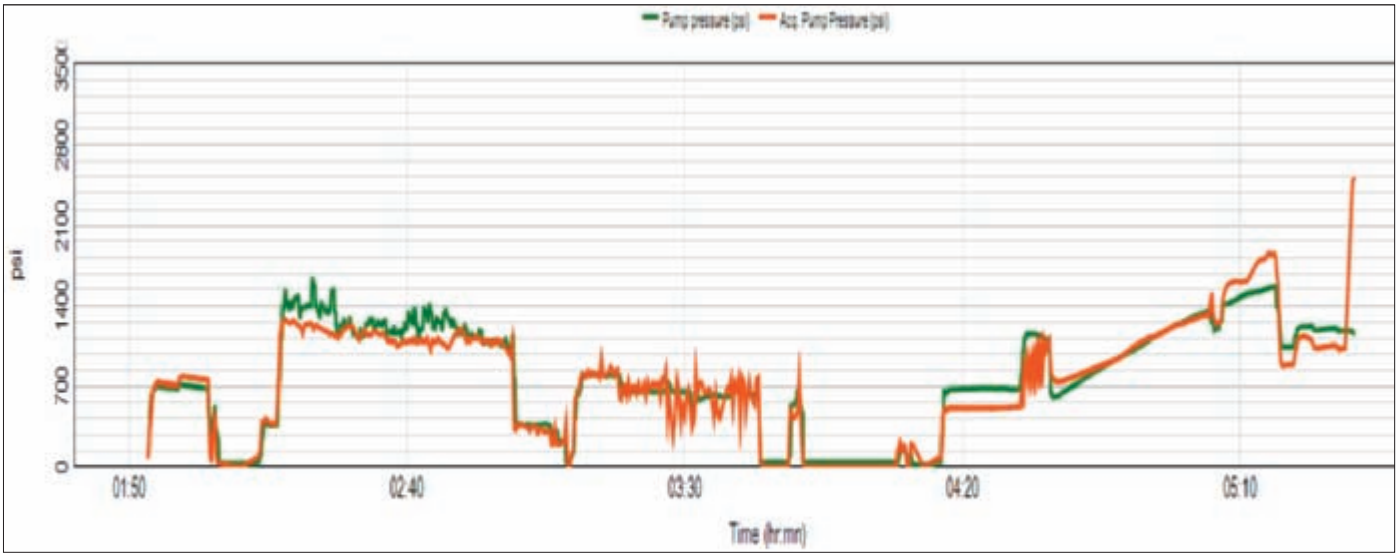

Fig. 13. Playback data of the 13⅜" casing second-stage cementing.

also can swell in the presence of hydrocarbon in case of microcracks or wellbore integrity issues.

6. Self-healing cement were deployed as a tail slurry on the 13⅜" tie-back casing to provide 1,200 ft of long-term hydraulic isolation in the cased annulus to seal the high-pressure oil-bearing formation.
7. The wells were later drilled to total depth, completed, fractured and delivered to production without CCA pressure leaks at the wellhead.

ACKNOWLEDGMENTS

The authors would like to thank the management of Saudi Aramco for their support and permission to publish this article.

This article was presented at the SPE/IADC Middle East Drilling Technology Conference and Exhibition, Abu Dhabi, UAE, January 29-31, 2018.

REFERENCES

1. Al-Yami, A.S., Wagle, V.B., Abdurrahman, R. and Taoutaou, S.: "Engineered Fit-for-Purpose Cement System to Withstand Life-of-the-Well Pressure and Temperature Cycling," SPE paper 188488, presented at the Abu Dhabi International Petroleum Exhibition and Conference, Abu Dhabi, UAE, November 13-16, 2017.
2. El-Marsafawi, Y.A., Al-Yami, A.S., Nasr-El-Din, H.A., Al-Jeffri, A.M., et al.: "A New Cementing Approach to Improve and Provide Long-Term Zonal Isolation," SPE paper 100558, presented at the SPE Asia Pacific Oil and Gas Conference and Exhibition, Adelaide, Australia, September 11-13, 2006.
3. Nasr-El-Din, H.A., El-Marsafawi, Y.A. and Al-Yami, A.S.: "A Study of Acid Cement Reactions Using the Rotating Disk Apparatus," SPE paper 106443, presented at the International Symposium on Oil Field Chemistry, Houston, Texas, February 28-March 2, 2007.
4. Al-Yami, A.S., Nasr-El-Din, H.A., Al-Saleh, S.H., Al-Humaidi, A., et al.: "Long-Term Evaluation of Low-Density Cement: Laboratory Studies and Field Application," SPE paper 105340, presented at the Middle East Oil and Gas Show and Conference, Kingdom of Bahrain, March 11-14, 2007.
5. Darbe, R., Gordon, C., and Morgan, R.: "Slurry Design Considerations for Mechanically Enhanced Cement Systems," AADE paper 08-DF-HO-06, presented at the AADE Fluids Conference and Exhibition, Houston, Texas, April 8-9, 2008.
6. Wray, B.L., Beford, D.R., Leotaud, L. and Hunter, W.J.: "The Application of High-Density Elastic Cements to Solve HPHT Challenges in South Texas: The Success Story," SPE paper 122762, presented at the SPE Annual Technical Conference and Exhibition, New Orleans, Louisiana, October 4-7, 2009.
7. Billmeyer Jr., F.W.: *Textbook of Polymer Science,* New York: John Wiley & Son, 1984, 578 p.
8. Browing, R., Duffy, M.A., Gaugler, D. and Jones, P.: "Effectiveness of Self-Healing Cement Additives based on Test Methodology Using Simulated Cement Sheath Cracks," SPE paper 161028, presented at the SPE Eastern Regional Meeting, Lexington, Kentucky, October 3-5, 2012.
9. Cavanagh, P.H., Johnson, C.R., Le Roy-Delage, S., DeBruijn, G.G., et al.: "Self-Healing Cement — Novel Technology to Achieve Leak-Free Wells," SPE paper 105781, presented at the SPE/IADC Drilling Conference, Amsterdam, The Netherlands, February 20-22, 2007.
10. Reddy, B.R., Liang, F. and Fitzgerald, R.: "Self-Healing Cements That Heat without Dependence on Fluid Contact: A Laboratory Study," *SPE Drilling & Completion*, September 2010, pp. 309-313.
11. Nelson, E.B.: *Well Cementing*, *Vol. 28 of Developments in Petroleum Science*, Elsevier Science Publishers B.V., the Netherlands, 1990, 1515 p.

BIOGRAPHIES

Dr. Abdullah S. Al-Yami is a Petroleum Engineer with Saudi Aramco's Drilling Technology Team at the Exploration and Petroleum Engineering Center – Advanced Research Center (EXPEC ARC). He has 18 years of experience with Saudi Aramco and previously worked in different positions, including as a Lab Scientist and Drilling Engineer, conducting research related to drilling engineering.

Abdullah has received several awards during his career, including Saudi Aramco's Research and Development Center (R&DC) Innovation Award and its Successful Field Application Award for his research work. He also received Saudi Aramco's EXPEC ARC Effective Publications Award. A member of the Society of Petroleum of Engineers (SPE), Abdullah was awarded the 2009 SPE Outstanding Technical Editor Award for his work on the SPE *Drilling and Completion Journal*. He also received the 2014 SPE Regional (Middle East, North Africa and South Asia) Drilling Engineering Award and the 2015 CEO Saudi Aramco Excellence Award. In 2016, Abdullah received Oil & Gas Middle East Award "highly commended" recognition in the category of internal control valve (ICV) Strategy of the Year for his efforts in developing drilling products utilizing a local resources strategy.

He is a coauthor of the textbook *Underbalanced Drilling: Limits and Extremes*; has 13 granted U.S. patents and more than 30 filed patents; and has more than 60 publications to his credit, all in the area of drilling and completions.

Abdullah received his B.S. degree in Chemistry from Florida Institute of Technology, Melbourne, FL; his M.S. degree in Petroleum Engineering from King Fahd University of Petroleum and Minerals (KFUPM), Dhahran, Saudi Arabia; and his Ph.D. degree in Petroleum Engineering from Texas A&M University, College Station, TX.

Mohammad H. Alqam is currently a Scientist Specialist in the Rock Mechanics Lab in the Advanced Technical Services Division in Saudi Aramco's Exploration and Petroleum Engineering Center – Advanced Research Center (EXPEC ARC). He has more than 35 years of experience with Saudi Aramco and has been involved in an emulsion study, formation damage, hydraulic fracturing studies and rock mechanics studies.

In 1991, Mohammad received his B.S. degree in Chemistry from California State University, Fresno, CA, and in 1997, he received his M.S. degree in Chemistry from King Fahd University of Petroleum and Minerals (KFUPM), Dhahran, Saudi Arabia. Mohammad is currently working on his Ph.D. degree in Petroleum Engineering at KFUPM.

Riefky Abdurrahman joined Schlumberger as a Field Engineer in 2003. He was assigned to Azerbaijan, and involved in cementing projects in the offshore Caspian Sea field. Riefky receive well integrity training at the Schlumberger U.K. Training Center in 2003 and 2004.

His second assignment was in Indonesia as the Cementing Field Service Manager working on the Duri Steam Flood project. Upon completion, Riefky moved to Saudi Arabia to work as the District Technical Manager for the Southern Area.

After spending four years in Saudi Arabia, he then moved to Russia to be the Senior Instructor at the Schlumberger Siberia Training Center. Riefky delivered courses for cementing engineers, and as guest instructor for other segments.

In 2014, he moved back to Saudi Arabia to be the Cementing Manager in al-Khobar. Then, in 2016, Riefky was moved to his current position, the Cementing Domain Manager for Saudi Arabia and Bahrain.

He received his B.S. degree in Environmental Engineering from Bandung Institute of Technology, Bandung, Indonesia, in 2002.

Ali U. Shafqat is a Technical Manager of Well Integrity Technologies at Schlumberger Saudi Arabia and Bahrain. After joining Schlumberger in 2005, he has worked in various locations and in different roles to acquire extensive knowledge in well integrity technologies and techniques.

Based on Ali's technical expertise and cementing knowledge, he was assigned in 2012 to complete complex projects in the Gulf of Mexico for deep-water cementing. After this assignment, Ali was transferred to work as the Well Integrity Senior Instructor in Schlumberger's training facility in Abu Dhabi, UAE, a position he held for more than two years.

Ali has authored or coauthored more than six technical publications related to well integrity solutions and has been an active member of the Society of Petroleum Engineers (SPE) since 2004.

In 2004, he received his B.S. degree in Petroleum Engineering from the University of Tulsa, Tulsa, OK.

Characterizing the Effects of High Power Laser Performance on Carbonate Rocks

Dr. Damian P. San-Roman-Alerigi, Clemens P. van Dijk, Vinicius Lube, and Prof. Gilles Lubineau

ABSTRACT

Perforation is essential to provide channels for hydrocarbons to flow from reservoirs into wells. High-power laser (HPL) radiation has shown great potential to provide an alternative means for drilling and perforation. The HPL is a contactless and waterless technology that can improve conductivity and reduce general damage to the rock formation. The dynamics in this application are involved and intense; yet, they can be controlled to achieve different applications in subsurface environments.

In our work we develop a comprehensive characterization protocol to determine the effect of laser radiation on rocks. Here we present the elements of a comprehensive characterization of laser perforated rocks; introduce the principles of laser-rock interaction; describe the physical effects through advanced characterization results; and discuss future developments. Since a significant proportion of Middle East reservoirs are carbonates, the first experiments were done on carbonate samples from U.S. quarries.

The characterization process takes advantage of advanced tools and qualitative petrology to describe the physical and chemical changes in the laser perforated samples. We use micro-computed tomography (CT) to measure the changes in porosity, connectivity, and general structure of the samples; thin-section, and X-ray diffraction (XRD) to analyze chemical and mineralogical changes.

The results, coupled with real-time observations of the process, provide an in-depth view of the physical dynamics. It shows how lasers can alter the inner structure of the rocks, change their porosity, and affect the pore connectivity. This insight is critical to understand the effects, optimize the subsurface photonic tools, and expand their applications.

INTRODUCTION

Laser is an acronym that stands for "light amplification by stimulated emission of radiation." The result of this process is a highly controllable beam of light that is monochromatic, bright, unidirectional, and coherent. The amplification process can produce continuous beams of high intensity, with commercial high-power lasers (HPLs) reaching up to several hundred kilowatts.

Figure 1 depicts the governing dynamics of energy coupling and key electro-thermal geomechanical properties[1]. When the HPL beam illuminates a rock, a portion of the incident — electromagnetic (EM) — energy is absorbed and transformed into thermal energy. The — thermal — energy feeds a thermo-mechanical process that may spallate, dissociate, melt, or vaporize the rock, and in some cases, the fluids within it. This rapid and localized surge in temperature induced by the laser irradiation is highly dependent on the transient and spatial distribution of the beam, the rock properties, and the EM thermal coupling[1-3].

Earlier results showed that HPL can be a contactless and waterless alternative to perforate any type of rock, improve

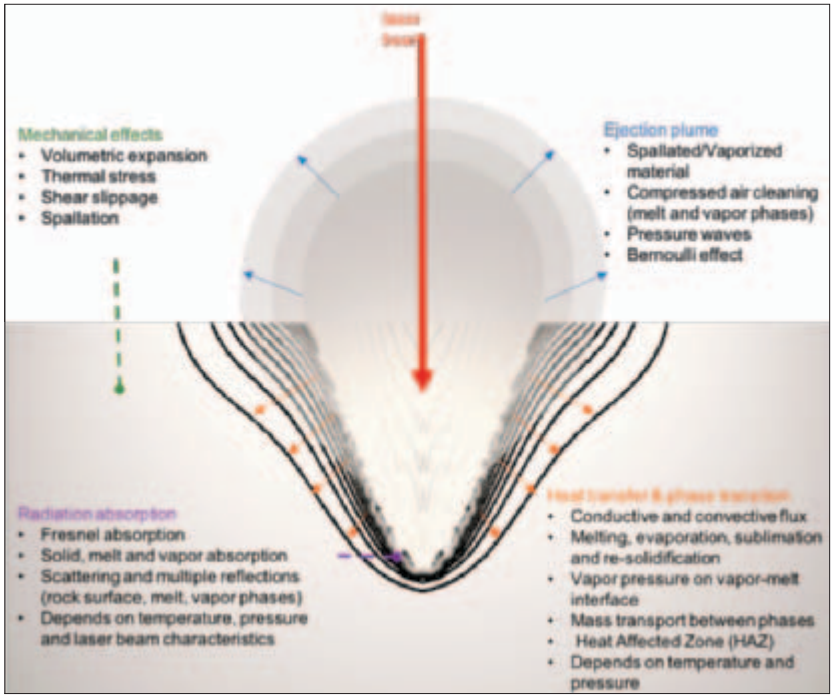

Fig. 1. Outline of HPL rock interaction. Note that the ensuing dynamics depends on the EM, thermal and elastic properties of the material. These, in turn, are a function of the local temperature and pressure, with optical properties also related to the EM field intensity, polarization, and frequency[1].

their permeability, and reduce damage to the neighboring formation[4]. Therefore, it is critical to characterize the properties of the materials, analyze the laser-rock interaction, and create models that enable prediction and optimization[5].

This work summarizes the elements of a comprehensive characterization protocol to determine the effect of laser radiation on rocks. It leverages on different technologies to characterize key properties before and after laser exposure; e.g., pore structure, inter-pore connectivity, mineral distribution, and petrology.

The experiment focuses on carbonate rocks of four different types: Indiana Limestone (IL), Yellow limestone (YL) and Desert Pink limestone (DP), and Edwards Brown dolomite (EB). Carbonates were chosen because they are an important component of worldwide hydrocarbon systems. Moreover, the expected behavior during laser ablation differs from that of sandstones and shales widely reported in previous studies[5]. This publication discusses the results for two rock types, including YL and EB dolomite.

METHODS

The experimental setup uses triplicate samples of each rock type: (1) one reference sample (labeled R), and (2) two samples for experimental batches 1 and 2. Each sample was described macroscopically to evaluate the presence of lamination, and its orientation with respect to the plug axis. Table 1 summarizes the laser and purging parameters used for each batch. Before and after exposure each experimental sample was characterized to determine its macro and micro structure, morphology, and petrology. Table 2 is a list of the characterization techniques and corresponding measurements reported in this article.

For thin section preparation, each sample was vacuum impregnated with blue-dye resin to allow porosity identification; one longitudinal and four radial thin sections were prepared from the plugs. These were half stained with alizarin red-S to differentiate between calcite and dolomite. The thin sections from the lased samples were prepared a few weeks after the experiments. The experimental samples were completely impregnated prior to thin section preparation. Samples for X-ray diffraction (XRD) analysis were ground, back pressed in sample holders, and scanned using CuKα radiation from 4° to 75°2θ.

RESULTS

Rock Types

The YL reference sample (YL-R), shows a predominance of grain mouldic porosity, Fig. 2a. Most of the original inter-particle porosity is filled with calcite cement, which results in very poor pore connectivity. It contains characteristic grain-cement configurations — grains outlined by very fine crystalline calcite cement rims and dissolved grain cortices — which were helpful when identifying features produced as a result of laser ablation in the alteration rim.

The EB dolomite reference sample (EB-R) is predominantly composed of very fine to fine crystalline dolomite, typically forming microporous rhombic fabrics. The sample shows an intergranular texture, the dolomite outlining abundant grain-mouldic pores with a typical size range between 200 µm

	Parameter	Value	
		Batch 1	Batch 2
Laser Beam	Power	10 kW	2.5 kW
	Irradiation Time	3 s	12 s
	Beam Diameter (at sample top)	10.68 mm	
	Wavelength	1,060 nm	
Purging	Fluid/Gas	Air	
	Pressure	120 psi	
	Distance (from sample top)	2.5 cm	
	Geometry	Coaxial	

Table 1. Laser and purging parameters

Technique	Measurement	Batch
Nuclear magnetic resonance (NMR)	Pore structure and inter-pore connectivity (permeability)	1
Dual energy X-ray micro-CT	Pore structure, morphology, and spatial mineralogy	2
Thin section petrography	Texture, mineralogy and porosity	1
XRD	Mineral and chemical composition	1

Table 2. The characterization techniques and corresponding measurements used in this study

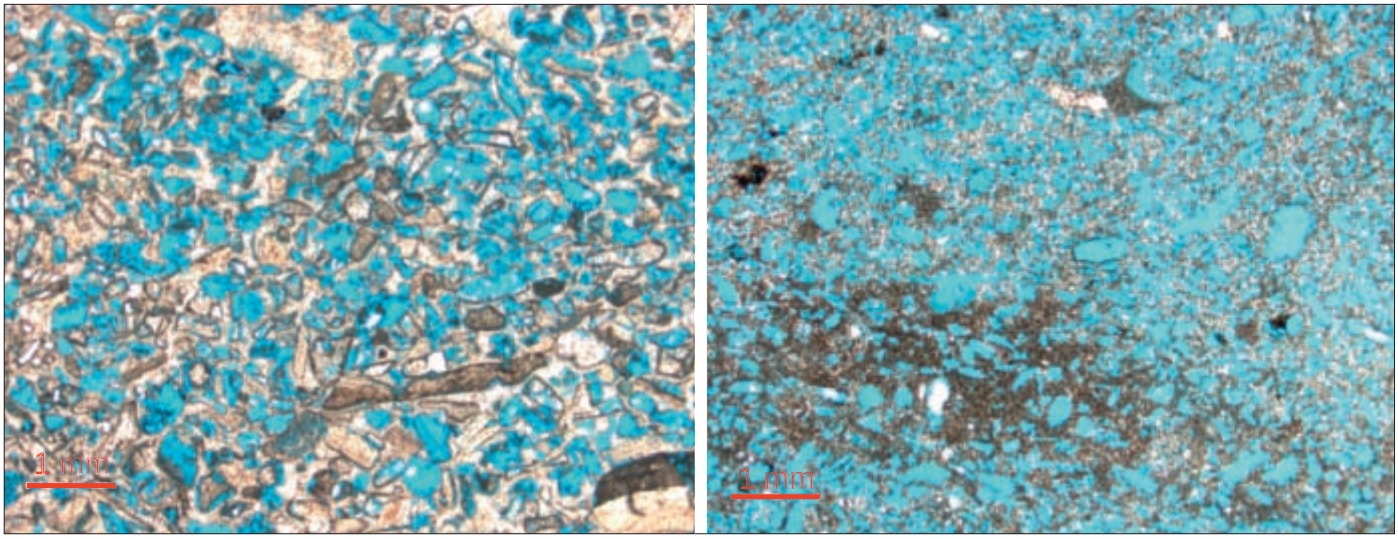

Fig. 2. Photomicrographs showing texture and porosity of the reference samples: (left) YL (YL-R), and (right) EB dolomite (EB-R).

Grains (%)	Clays (%)				Carbonate (%)			Porosity (%)		
Quartz grains	Glauconite	Clay aggregates	Clay between dolomite rhombs	Clay lining vug	Calcite	Dolomite	Dolomite silt in vugs	Inter-crystalline pores	Vugs	Intra-crystalline pores
1.23	0.62	0.31	2.77	1.85	2.46	62.15	0.31	11.69	15.38	1.23

Table 3. Point counted composition of the EB dolomite reference sample (EB-R) — 325 points were counted

to 600 µm, Fig. 2b. The rock also contains a small amount of coarse crystalline calcite and clay, and very rare quartz sand grains. Table 3 shows the point-counted composition of the dolomite sample.

Macroscopic Sample Description after Lasing

Macroscopic examination showed the development of a deep, circular perforation after lasing of the samples — YL-1 and EB-1 — in batch 1, Figs. 3a and 3b. There is a marked difference, however, between the perforations in the limestone compared to the dolomite sample. The limestone samples have a perforation showing a smooth, shiny light yellow surface. This glass-like layer extends well above the upper surface of the plugs, forming a ring-shaped protrusion with a height of a few mm and about 1 mm thickness. On the upper plug surface, a narrow, concentric light grey to white alteration zone was visible in the rock immediately around the glass-like layer, but its downward extent could not be seen. About two weeks after the experiment, however, the glassy protrusion and material covering the laser hole had almost completely disintegrated. This allowed examination of the inner structure of the material around the laser perforation down to a level of several mm below the upper plug surface, Fig. 3c. It appeared that

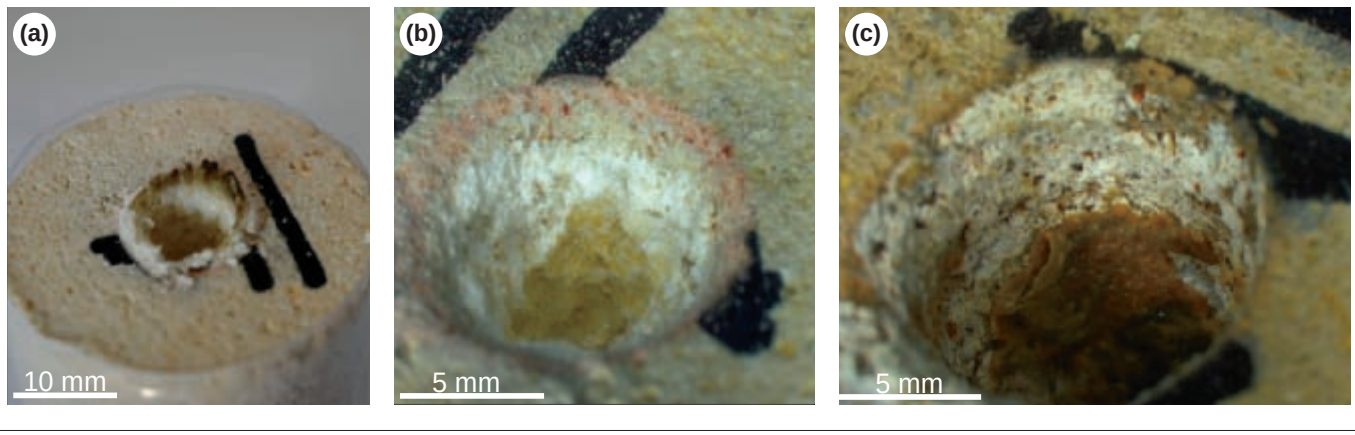

Fig. 3. Macroscopic features of laser perforation in batch 1 samples: (a) Macrophoto laser perforation in YL-1, 8 days after the experiment, (b) Stereoscope image of laser perforation in the same sample 15 days after the experiment, and (c) Stereoscope image of laser perforation in EB-1 dolomite 15 days after the experiment.

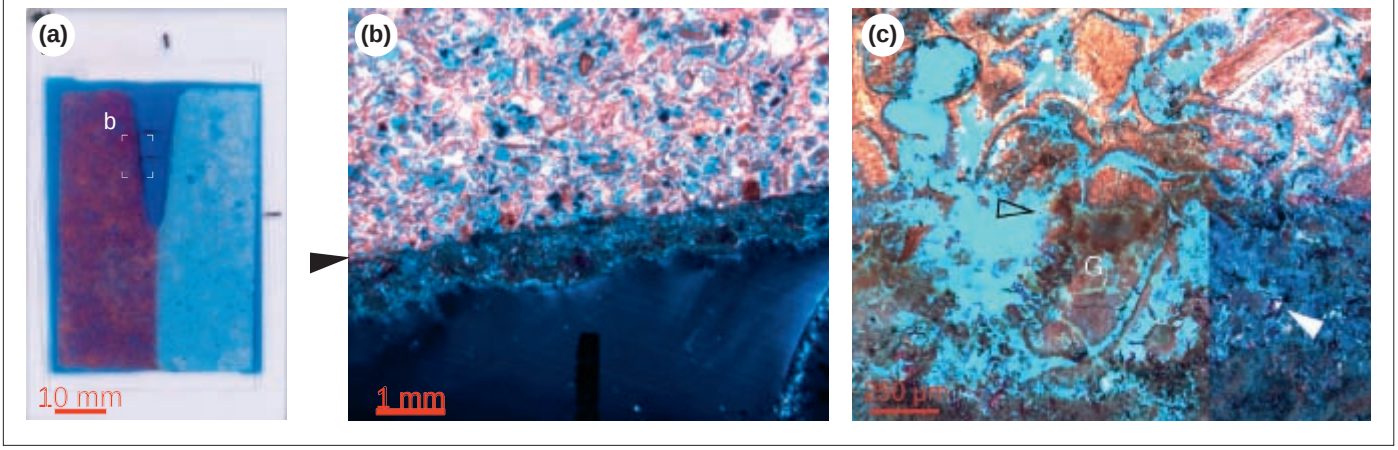

Fig. 4. Petrographic features of laser ablation in YL-1. (a) Thin section scan showing geometry of laser perforation. (b) Crossed polarizers view showing sharp transition from host rock to alteration rim. The black arrows marks the boundary between unaltered host rock above and alteration rim below. (c) Plane/crossed polarized light view of a partially calcined grain (G) at the boundary between alteration rim and unaltered limestone. The faithful preservation of a grain-cement fabric commonly seen in the host rock attests to in situ calcination of limestone. Note the portlandite crystals in the microcrystalline alteration rim (white arrow). In Fig. 4a, "b" marks the location of the photomicrographs.

the laser perforation is surrounded by a thick alteration rim of very fine grained white material — at least ½ mm thick — with the light yellow material forming a very thin, dense layer covering the white layer.

The perforation in the dolomite is extensively lined with an irregular layer of moderately shiny, brown glass. The glass forms several sinuous bands, which incompletely cover the perforation and are oriented approximately parallel to the hole axis. Small spherical and larger elongate bubbles are locally seen within the glassy layer where it is broken. The laser hole shows white color in a thin zone immediately underneath the glassy layer, visible between bands of glass. High magnification stereoscope examination in places revealed the presence of white rhombs, apparently representing in situ replacement of the dolomite host rock. In other parts of the laser hole wall, the white material forms a dense white paste. The white color of this alteration zone contrasts with the light brown original color of the dolomite rock. Small glass droplets extensively cover the outer part of the upper plug surface.

The limestone and dolomite samples exhibit radial fractures in the upper part of the plug, extending from the laser hole to the plug side. These fractures reach down to varying depths below the upper plug surface, but have occasionally penetrated the entire plug length. The inner perimeter of the perforation measured 7.5 mm in YL-1 and 11.5 mm in EB-1.

Microscopic Thin Section Description after Lasing

The laser perforations in YL-1 and EB-1 show an approximate parabolic shape in the longitudinal thin sections, Figs. 4a and 5a. In thin section, the inner part of the laser hole consists of microcrystalline material, forming a layer with a thickness of several hundreds of µm. The outer surface of this layer is commonly somewhat irregular, which is thought to reflect later disintegration. The microcrystalline layer shows a sharp transition to rock lacking any visible signs of chemical

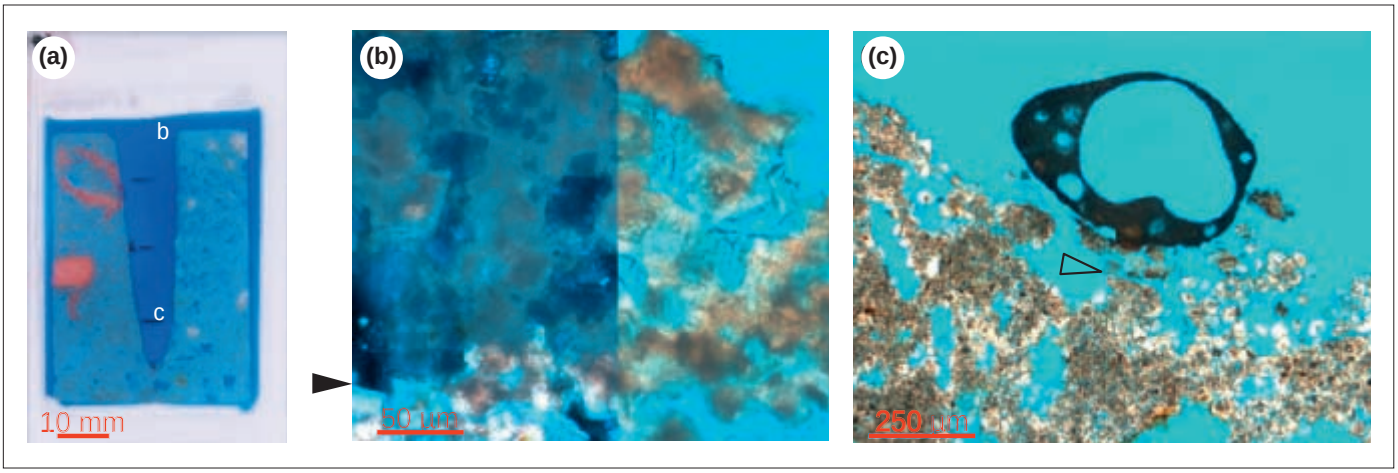

Fig. 5. Petrographic features of laser ablation in EB-1. (a) Thin section scan illustrating rock texture and laser hole geometry. The red particles (in the stained left half of thin section) are recrystallized fossil fragments. Here, "b" and "c" mark the areas of photomicrographs. (b) Crossed/plane polarized light view showing microcrystalline calcine and the preservation of the original microporous rhombic dolomite fabric, attesting to in situ calcination of rock during laser exposure. (c) Plane-polarized light view of glass particle covering the laser hole characterized by the presence of smaller and larger spherical bubbles. The black arrows mark the boundary between the unaltered host rock below and the alteration rim above.

alteration. The transition between unaltered rock and the microcrystalline layer forms a very regular and almost smooth surface, Fig. 4b. The limestone and dolomite host rock regularly shows a few small cracks in grains and cement near the laser hole, which are oriented roughly parallel to the host rock surface. Figure 5c shows the glass lining the laser hole in the dolomite sample. XRD analysis of the alteration rim from YL-1 indicates a predominance of portlandite [calcium hydroxide ($Ca(OH)_2$)], moderate amounts of calcite [calcium carbonate ($CaCO_3$)] and a small amount of lime [calcium oxide (CaO)] (3%).

Both samples show clear evidence for in situ formation of the microcrystalline layer. YL-1 shows the rare presence of grain-cement ghost structures within the inner part of the microcrystalline layer — near the host rock — which closely mimic grain-cement textures regularly observed in unaltered host rock, Fig. 4c. These are not observed in the outermost part of the microcrystalline layer, where the microcrystalline layer commonly has a much denser appearance. In EB-1, porous clusters of rhomb-shaped microcrystalline material are locally observed within the microcrystalline layer. These rhombs have a similar size to dolomite rhombs in the host

Sample	Sample Length (cm)	Sample Diameter (cm)	He Porosity (% BV)	Grain Density (g/cc)	NMR Porosity (% BV)		
					Before	After	Difference (%)
YL-1	5.23	3.88	29.90	2.66	28.10	28.80	2.49
EB-1	5.09	3.82	43.70	2.78	38.00	40.50	6.58

Table 4. Characterization of the porosity for both samples in batch 1. Permeability was measured under a confining stress at 400 psi

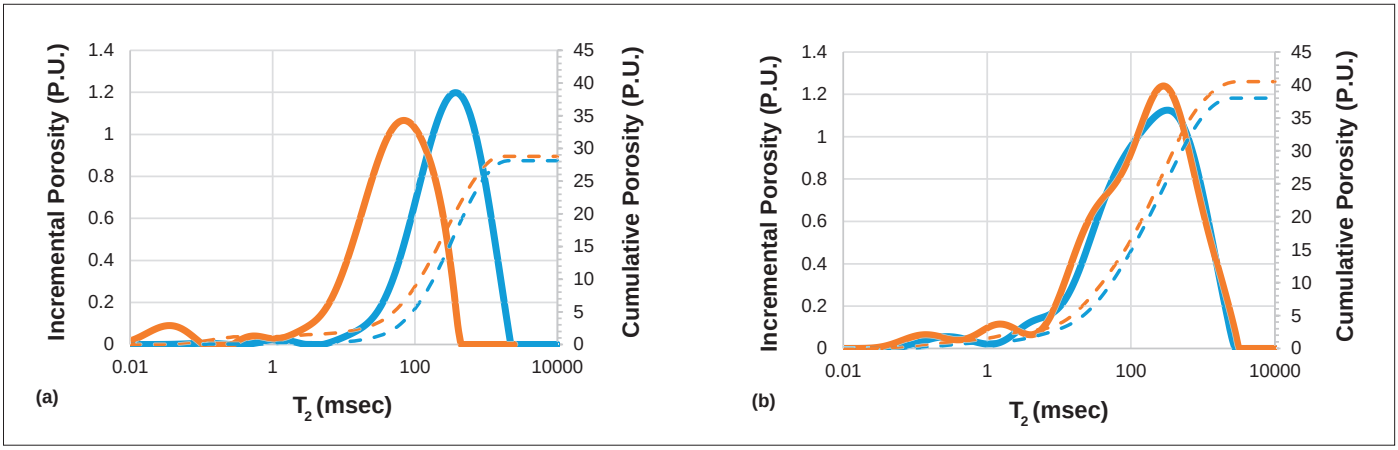

Fig. 6. Cumulative (dashed) and incremental (solid) T_2 distributions before (blue) and after (red) lasing: (a) YL-1, and (b) EB-1.

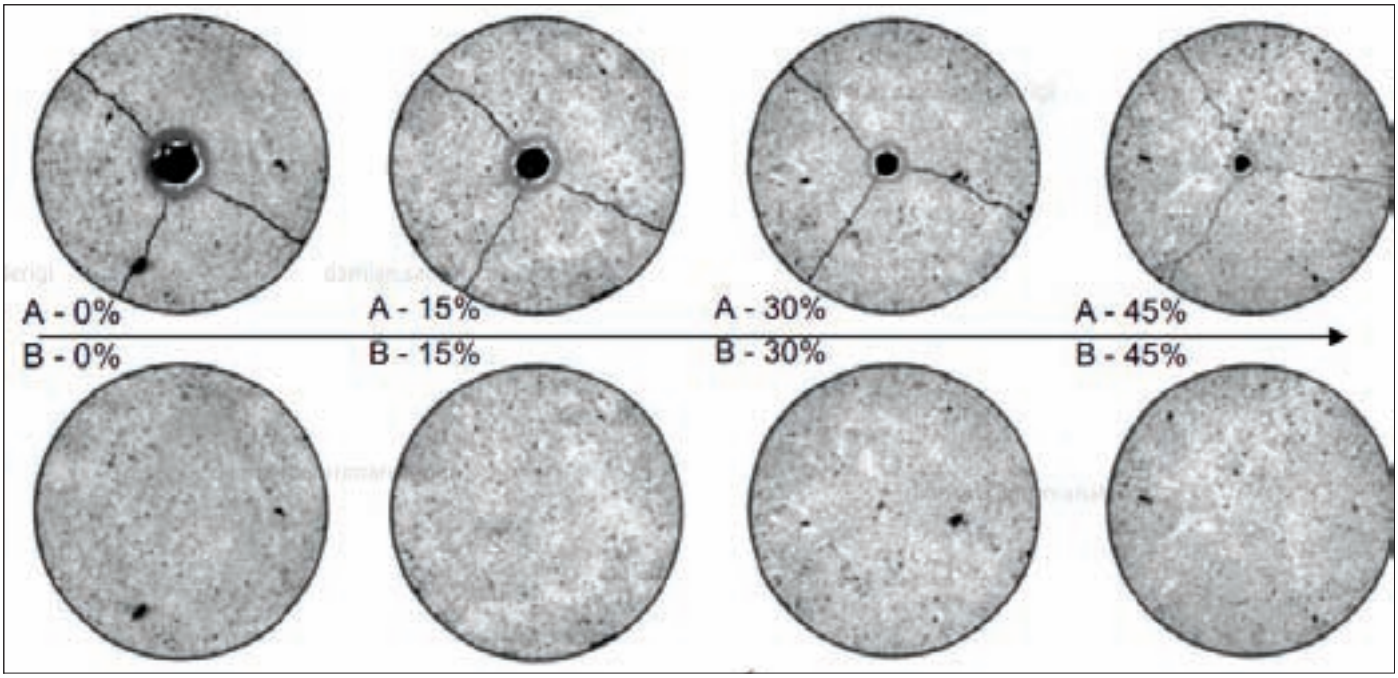

Fig. 7. Top to bottom cross-section images of YL-2 before (bottom) and after (top) lasing at 0%, 15%, 30%, and 45% levels, respectively.

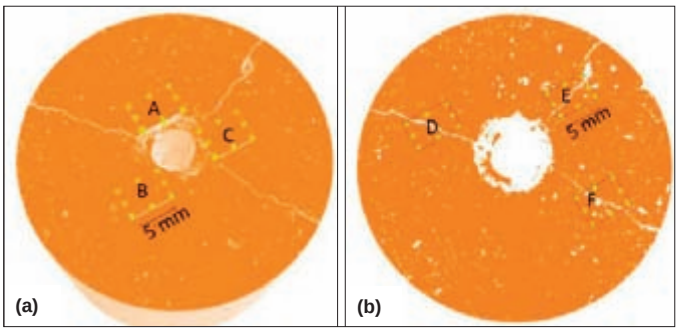

Fig. 8. Two reconstructed 3D views of the core plug with localization of sub-volumes for porosity calculation. (a) Around the perforation and alteration rim, and (b) Along the fractures. Scale bar is 5 mm. Sub-volumes extend along the full length of YL-2.

rock, while the fabric of the porous clusters mimics the microporous rhombic dolomite fabric observed in adjacent unaltered rock, Fig. 5b.

NUCLEAR MAGNETIC RESONANCE (NMR)

Table 4 and Fig. 6 summarize the NMR measurements for YL-1 and EB-1. The results agree with the petrographic analysis, which revealed laser-induced changes in the pore structure of the samples. Data for YL-1 shows a left-shift and broadening in the T_2 distribution, typically related to changes in the micropore structure. The porosity change can be explained by the creation of microporosity in the alteration rim, and radial and circumspherical fractures around the perforation.

Sub-volume	Calculated Porosity (% B-SV)			
	Before	After	Difference	Average
A	1.0659	1.7573	64.865	63.04
B	0.6277	0.9611	53.115	
C	0.8590	1.4701	71.141	
D	1.1960	3.3366	178.980	133.17
E	1.5060	2.9718	97.330	
F	0.9730	2.1718	123.210	

Table 5. Calculated porosity for the sub-volumes defined in Fig. 8 for a voxel resolution of 22 µm

Micro-CT

Dual energy X-ray micro-computed tomography (micro-CT) was carried out on the samples of batch 2. The voxel size was set to 22 µm. Figure 7 displays the cross-section images before and after lasing of YL-2 at 0%, 15%, 30%, and 45% levels, respectively.

Sub-volume porosity (% B-SV) can be calculated using the micro-CT scan data. The results provide an insight about the distribution of porosity and features before and after laser exposure, and above the scanning resolution, 22 µm.

Figure 8 depicts the six sub-volumes selected for the localized calculation of porosity. The results are summarized in Table 5. The calculation shows that the porosity at 22 µm resolution around the alteration rim increased an average absolute of 0.55% B-SV. In the fractured region the porosity increased

Sample	Height (cm)	Diameter (cm)	He Porosity (% BV)			Weight (g)		
			Before	After	Difference (%)	Before	After	Difference (%)
YL-2	5.49	3.85	29.49	30.25	2.6	119.92	118.62	-1.08
EB-2	5.34	3.81	38.36	39.87	3.9	104.47	101.91	-2.45

Table 6. Core analysis porosity of samples in batch 2

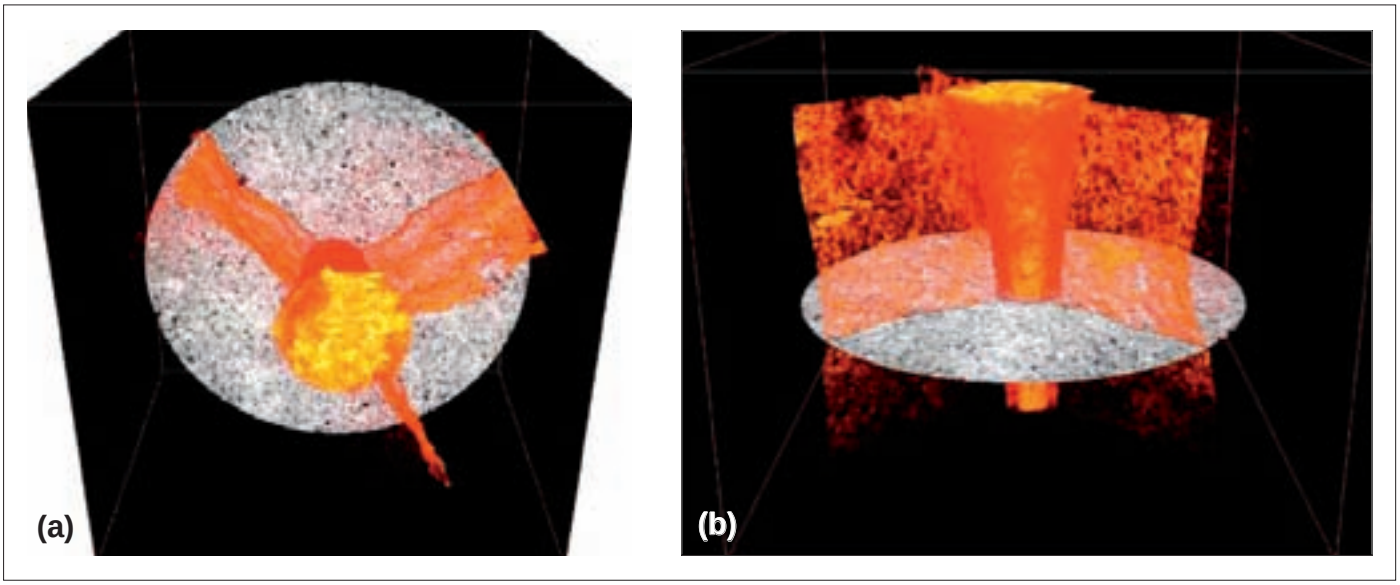

Fig. 9. Rendering of perforation and fractures (orange) in YL-2: (a) Top view, and (b) Side view.

an average absolute increase of 1.6% B-SV. The porosity change in the fractured region can be explained by the creation of fracture porosity. In the case of the reaction rim, the increase in porosity could be due to the effect of circumspherical cracks within the alteration rim, also observed in batch 1. For comparison, Table 6 summarizes the core analysis porosity for YL-2 and EB-2.

Figure 9 displays the rendering of the perforation and fractures. The images show the geometry of the perforated hole across the entire length of the YL-2 plug. The perforation resembles a funnel in the upper half of the plug, and becomes straight in the bottom half. The shape is the result of the thermal mechanical coupling in the laser-rock interaction, the carbon dioxide (CO_2) gas ejected from the calcination reaction, and the purging gas flow[1, 5].

PROCESSES AND ENERGY BUDGET

The macroscopic and microscopic features provide information on the processes and conditions within the perforation during laser ablation. This can be used to calculate the energy budget of ablated rock during the laser experiment.

The energy consumed by the process must be balanced:

$$E_{in} = E_{thermal\ loss} + E_{absorbed} + E_{reflected}, \quad (1)$$

where the input energy, E_{in}, includes the contribution of the HPL beam and purging fluids. The right side of Eqn. 1 encompasses the portion of energy reflected by the material, the energy absorbed, and the thermal energy dissipated to the environment. The amount of energy absorbed will depend on the efficiency of the EM thermal coupling between the laser and the rock; this energy in turn drives the transport phenomena that changes the host rock, and creates the alteration rim and the perforation itself. Therefore, the energy absorbed is divided into the energy used in: (a) thermal processes, and (b) chemical reactions.

The balance in Eqn. 1 also provides a first approximation of the temperature change induced by the laser. If the system is thermodynamically insulated, then the only thermal loss is due to blackbody radiation:

$$E_{in} = A\epsilon\sigma_B(T_{rock}^4 - T_{amb}^4) + E_{reflected} \quad (2)$$

where E is the emissivity, σ_B is Boltzmann constant, A is the area of the beam, and T the temperature; therefore:

$$T_{rock} = \left(\frac{\alpha E_{laser}}{A\epsilon\sigma_B} + T_{amb}^4\right)^{1/4} \quad (3)$$

where α is the EM absorption coefficient of the rock. Assuming a HPL energy of 10 kW, then the temperature range expected in carbonate rocks is in the range between 1,000 °C to 3,500 °C.

The calcium oxide, which was identified in XRD, presently forms a minor constituent of the alteration rim, but is thought to have originally dominated the alteration rim. It would have been gradually transformed to calcium hydroxide after the experiment by absorbing water vapor, and possibly $CaCO_3$ following a reaction with atmospheric CO_2. The latter reaction — carbonation — could have occurred either at a lower temperature during cooling of the samples[6] or later at room temperature. The presence of CaO in the alteration rims analyzed from the limestone samples indicates that the calcite was thermally decomposed. The dolomite sample would have undergone a similar process of dolomite decomposing to CaO and magnesium oxide (MgO).

Thermal decomposition of carbonate to oxides is known as calcination, which also liberates CO_2 as a gas. The process of calcination can be described in two steps: (1) rock heating to calcination temperature, and (2) calcination. The energy required for calcination of the rock within the laser perforations can be calculated, provided the volume of each laser perforation and the temperature conditions inside the perforation are known.

Digital thin section scans provide the 2D geometry of the laser perforations of the batch 1 samples, which were converted to 3D volumes using a modified elliptic cylinder model to account for asymmetric hole shape. The large volumes of CO_2 generated during the calcination reaction compared to the volume of the laser hole suggests that calcination of limestone and dolomite took place in a CO_2 atmosphere. Laboratory experiments suggest that calcination of calcite in a CO_2 atmosphere occurs above 943 °C[7]. Calcination of dolomite occurs in two steps. In a CO_2 atmosphere, dolomite decomposes to $CaCO_3$ and MgO between 550 °C to 765 °C followed by calcite decomposition to CaO between 900 °C and 960 °C[8]. Robie and Hemingway (1995)[9] provide data on heat capacity and formation enthalpy of calcite, dolomite, and oxides within the temperature interval reconstructed from the petrographic observations.

Table 7 shows the reconstructed solid rock volume of the laser perforations, assuming a pure dolomite composition of

Rock Type	Perforation Length (mm)	Perforation Top-Diameter (mm)	Calculated Volume (cm^3)	Solid Rock Mass (g)	Evolved CO_2 (g)	Evolved CO_2 at Calcination Temperature (cm^3)
YL-1	25.5	7.5	0.85	1.64	0.72	1,675
EB-1	43.5	11.5	2.50	4.19	2.00	4,652

Table 7. Perforation length and reconstructed volume and mass of laser hole and evolved CO_2 of batch 1 samples

Rock Type	Calcination Temperature (°C)	Rock Heating Energy (kJ/mol)	Calcination Energy (kJ/mol)	Calcine and CO_2 Heating Energy (kJ/mol)	Rock Heating Energy (kJ)	Calcination Energy (kJ)	Calcine and CO_2 Heating Energy (kJ)
YL-1	943	102.6	168.6	66.18	1.68	2.76	0.94
EB-1	960	177.5	279.7	94.52	4.03	6.35	2.52

Table 8. Preliminary energy budget of laser ablation for reconstructed laser hole volume of YL-1 and EB-1. Energy budget of rock from 25 °C to calcination temperature, of calcine and CO_2 from calcination temperature to 1,527 °C

EB-1. The calculated heating and calcination energy for the reconstructed laser hole volumes at calcination temperature is 4.44 kJ for the limestone and 10.38 kJ for the dolomite sample, Table 8.

Following calcination, the material at the hole wall was probably heated to higher temperatures, but the exact temperature conditions within the laser hole are unknown. The formation of glass in the dolomite sample, however, suggests that the hole's wall could have reached temperatures well above calcination temperature. Heating of the solid and gaseous reaction products to 1,527 °C would add 0.94 kJ heating energy for the limestone and some 2.52 kJ for the dolomite sample. The total amount of energy emitted by the laser beam is 30 kW, of which a calculated 62.2% would have reached the inner perimeter of the laser hole in YL-1 and 77.5% in EB-1, based on the observed laser hole diameters.

CONCLUSIONS

The energy budget depicts the complex dynamics in these processes, which are governed by the efficiency of EM thermal coupling and the transport phenomena in the host rock, alteration rim, and the perforation itself. These phenomena encompass mineral dissociation, chemical reactions, phase change, and convective flow. The experiments and characterizations detailed in this work provide a comprehensive insight about these physico-chemical dynamics. The petrographic and petrophysical analyses show to what extent HPLs can alter the inner structure of the rocks, change their porosity, and affect the inter-pore connectivity. Furthermore, this information is critical for the development of future subsurface applications.

ACKNOWLEDGMENTS

The authors would like to thank the management of Saudi Aramco and KAUST for their support and permission to publish this article. We would also like to thank Sameeh I. Batarseh from the EXPEC Advanced Research Center, Saudi Aramco, for his support and guidance; Shouwen Shen from the Advanced Analysis Unit/Technical Services Division, Saudi Aramco, for the XRD analysis; Hyung Kwak from the EXPEC Advanced Research Center, Saudi Aramco, for the NMR analysis; and TPS Enterprises for thin section preparation.

This article was presented at the 13th Middle East Geosciences Conference and Exhibition, Manama, Bahrain, March 5-8, 2018.

REFERENCES

1. San-Roman-Alerigi, D.P., Batarseh, S.I. and Han, Y.: "Numerical Modeling of Thermal and Mechanical Effects in Laser-Rock Interaction — An Overview," ARMA paper 2016-142, presented at the 50th U.S. Rock Mechanics/Geomechanics Symposium, Houston, Texas, June 26-29, 2016.
2. Gahan, B.C., Parker, R.A., Graves, R., Batarseh, S.I., et al.: "Laser Drilling: Drilling with the Power of Light Phase 1: Feasibility Study," Technical report, U.S. Department of Energy, September 2001, 107 p.
3. Batarseh, S.I., Gahan, B.C., Graves, R.M. and Parker, R.A.: "Well Perforation Using High-Power Lasers," SPE paper 84418, presented at the SPE Annual Technical Conference and Exhibition, Denver, Colorado, October 5-8, 2003.
4. Batarseh, S.I., Abass, H.H., Al-Mulhem, A.A. and Habib, N.S.: "High Power Laser Application in Open Hole Multiple Fracturing with an Overview of Laser Research; Past, Present, and Future," SPE paper 160836, presented at the SPE Saudi Arabia Section Technical Symposium and Exhibition, al-Khobar, Saudi Arabia, April 8-11, 2012.
5. Batarseh, S.I., Graves, R., San-Roman-Alerigi, D.P. and Chand, K.: "Laser Perforation: Lab to the Field," SPE paper 188729, presented at the Abu Dhabi International Petroleum Exhibition and Conference, Abu Dhabi, UAE, November 13-16, 2017.
6. Stanmore, B.R. and Gilot, P.: "Review — Calcination and Carbonation of Limestone during Thermal Cycling for CO_2 Sequestration," *Fuel Processing Technology*, Vol. 86, Issue 16, November 2005, pp. 1707-1743.
7. Escardino, A., García-Ten, J., Feliu, C., Saburit, A., et al.: "Kinetic Study of the Thermal Decomposition Process of Calcite Particles in Air and CO_2 Atmosphere," *Journal of Industrial and Engineering Chemistry*, Vol. 19, Issue 3, May 2013, pp. 886-897.
8. Engler, P., Santana, M.W., Mittleman, M.L. and Balazs,

D.: "Non-isothermal in Situ XRD Analysis of Dolomite Decomposition," *Thermochimica Acta*, Vol. 140, March 1989, pp. 67-76.

9. Robie, R.A. and Hemingway, B.S.: "Thermodynamic Properties of Minerals and Related Substances at 298.15 K and 1 Bar (105 Pascals) Pressure and at Higher Temperatures," *U.S. Geological Survey Bulletin 2131*, 1995, 461 p.

BIOGRAPHIES

Dr. Damian San-Roman-Alerigi is a Petroleum Scientist working with the Production Technology Team of Saudi Aramco's Exploration and Petroleum Engineering Center – Advanced Research Center (EXPEC ARC). His focus is on developing the next generation of subsurface photonic and electromagnetic tools.

Damian's previous research focused on the interaction of waves with complex media and its application to subsurface technologies. His work encompasses different areas of science and engineering, from oil and gas to applied mathematics; he has published papers in various international journals and conferences around the world.

Damian received his B.S. degree in Physics from the National Autonomous University of Mexico, Mexico City, Mexico. In 2008, he enrolled in King Abdullah University of Science and Technology (KAUST) as a founding class student where he completed his M.S. degree in 2010, and his Ph.D. degree in 2014, both in Electrical Engineering.

Clemens P. van Dijk is a Geologist in Saudi Aramco's Exploration and Petroleum Engineering Center – Advanced Research Center (EXPEC ARC). He is currently involved in research on evaluating the effects of laser ablation on carbonate rocks, and reservoir quality prediction of Paleozoic sandstones in Saudi Arabia. Clemons' research interests include clay mineralogy, diagenetic modeling, and the application of stable isotope and fluid inclusion analyses for understanding sandstone diagenesis and fluid migration.

Prior to joining Saudi Aramco, Clemens worked as a Consultant for Scott Pickford in London, U.K., and later for PanTerra Geoconsultants in the Netherlands, where he conducted integrated sedimentological and diagenetic studies aimed at understanding controls on reservoir and seal quality, as well as compaction behavior of a variety of clastic and carbonate reservoirs in the North Sea, the Middle East, West Africa, China and Peru.

Clemens has published several technical papers on sandstone diagenesis and compaction, and numerous in-house technical documents. He is a member of the International Association of Sedimentologists, Society for Sedimentary Geology, and the Royal Geological and Mining Society of the Netherlands.

Clemens received his M.S. degree in Sedimentology from Utrecht University, Utrecht, the Netherlands.

Vinicius Lube is an internationally experienced Industrial Engineer with a materials science background. He has experience in composites testing and nondestructive damage analysis using X-ray micro-computed tomography.

Vinicius came to Saudi Arabia in 2017 and joined King Abdullah University of Science and Technology (KAUST) as a visiting scholar to carry out research on morphological characterization of rocks at the Composite and Heterogeneous Material Analysis and Simulation Laboratory (COHMAS) under the supervision of Professor Dr. Gilles Lubineau, in partnership with Saudi Aramco's Exploration and Petroleum Engineering Center – Advanced Research Center (EXPEC ARC).

Earlier this year, he was accepted in KAUST for a Ph.D. program. Vinicius will now be working on a joint project involving the two divisions of Physical Science and Engineering and the Biological Science and Environmental Sciences and Engineering, addressing a research area that deals with biological materials from a mechanical engineering point of view using visualization techniques.

He received his B.S. degree in Industrial Engineering at the Federal University of Espirito Santo, Vitória, Brazil. In 2017, Vinicius received an M.S. degree in Forestry from the University of British Columbia, Vancouver, British Columbia, Canada.

Professor Gilles Lubineau is a Professor in Mechanical Engineering and the principal investigator of the Composite and Heterogeneous Materials Analysis and Simulation Laboratory (COHMAS), an integrated environment for composite engineering that he created in 2009 after joining King Abdullah University of Science and Technology (KAUST). Giles is also Faculty chair of the Faculty of Mechanical Engineering in the division of Physical Science and Engineering at KAUST.

Before joining KAUST, he was a faculty member at the École Normale Supérieure of Cachan, France. Giles also served as a visiting researcher at UC-Berkeley, and as an external faculty member at the École Polytechnique. Over his career, he has worked on both fundamental and applied research with many companies related to nonmetallic materials.

Giles has written more than 140 peer review papers ranging from applied mathematics to theoretical mechanics, composite engineering and material science, some of which have been published in: *Journal of the Mechanics of Physics and Solids*, *Advanced Materials*, *Advanced Functional Materials*, *Scientific Reports*, *Langmuir*, *Carbon*, *Composite Science and Technology*, etc.

He received his Ph.D. degree in Mechanical Engineering from École Normale Supérieure de Cachan, Cachan, France, and was granted his research habilitation in Mechanics in 2008.

Giles received the Daniel Valentin Award for best innovative works related to the field of composite materials in 2004. He is member of various editorial boards, including the *International Journal of Damage Mechanics*.

Self-Assembling Nanoparticles: A Unique Method for Downhole Sand Consolidation

Dr. Rajendra A. Kalgaonkar and Dr. Fakuen F. Chang

ABSTRACT

When the formation is unconsolidated, sand particles can be produced into the wellbore. Such production of sand particles is undesirable as it lowers the permeability of the producing zone, and erodes both surface and downhole equipment. Costly intervention may be required to mitigate the damage to the well's integrity and the reservoir deliverability. The most common methods of controlling this unwanted sand production involve: (1) Filter produced fluids through a gravel pack retained by a screen, or (2) Use of consolidating fluids such as resin — a curing agent — along with other chemicals to create a conducive environment for the resin curing reaction to occur. The gravel packing completion requires special tools and equipment, therefore the cost is increased. In the case of sand control by chemical consolidation, the resinous material tends to have relatively uncontrollable setting times, strength, placement, and regained permeability, leading to unsuccessful treatment. With both cost and treatment effectiveness in mind, it is desirable to develop an improved material and method to mitigate sand production by consolidating the formation sand without impairing well productivity or injectivity.

This article describes the development of a unique chemistry for sand control in unconsolidated formations. This chemistry involves using positive charge modified nanoparticles that can self-assemble over the unconsolidated formation sand particles to form a layer of consolidating material, thereby preventing any unwanted sand production. The new consolidation treatment material consists of colloidal nanoparticles modified using a cationic modifier and ionic strength modifier (ISM) that can be placed downhole as a single pill. The pill has high affinity to the solid surface, therefore, it is less prone to build up in the pore space. Once cured at reservoir temperature, it forms a thin layer of hard gel around the surface of the sand particles, thereby cementing the sand grains together at the same time maintaining open porosity to ensure easy flow of produced hydrocarbons or injected water.

The newly developed sand consolidation formulation was studied for its ability to consolidate loose sand and at the same time maintain good permeability. The effect of various ionic modifiers on consolidation properties was studied. The ability of the cationic modified nanoparticles to self-assemble around unconsolidated sand and eventually cure to form a consolidated sand pack was investigated. Studies showed good regain permeability of the consolidated sand pack. Furthermore, this article describes the concentration effect of the cationic modifier on the regain permeability. Finally, it shows that the new product provides a controllable curing time, thereby avoiding any premature setting of the nanoparticles in the wellbore.

INTRODUCTION

Some subterranean formations are not sufficiently competent to prevent erosion of the formation by the flow of the hydrocarbons through the formation. Such formations, often referred to as unconsolidated or incompetent formations, contain uncemented or loosely consolidated grains of sand, clay or rock, e.g., sandstone, limestone, quartz, zeolites, siltstone, shale or gravel. When the hydrocarbons or water flows through the formation, the loose materials, in particular, grains of sand, move along with the fluid causing erosion and disintegration of the formation. The loose sand can accumulate in the formation near the wellbore or in the wellbore. Such an accumulation can cause clogging and the reduced flow of the recoverable fluid, leading to productivity and injectivity decline[1].

These entrained particles of sand can also cause erosion of the underground equipment — e.g., strainers, liners, valves, and pumps — reduce pressure and restrict flow of the fluid[2-4]. Loose sand can be carried by fluid flow to the surface causing erosion to the surface equipment. If a sufficient amount of the sand is carried away from the producing formation, the formation may collapse causing significant damage to the well. Further, when sand piles up in the bottom holes, they need to be cleaned out to resume the normal production and injection operations, adding to well maintenance cost.

Many technologies have been used to prevent sanding in the wells. They are generally categorized into mechanical, cement packing, gravel packing and chemical methods[5, 6]. The mechanical sand control methods are broadly used and they include screens, gravel pack, and frac and pack[7, 8]. When these mechanical means are used for sanding prevention, they need to be designed and implemented during the well completion phase. The chemical methods require pumping a chemical that

keeps the sand grains bonded together so that they do not produce with the fluids[9, 10]. The chemicals commonly used include various resins[11] such as furan resins or epoxy resins[12, 13]. Various researchers have also proposed the use of polymers, i.e., polyacrylamides, for sand consolidation[14-17].

Resin consolidation can be used for mitigation or prevention of sanding in the wells, therefore it provides a more cost-effective process than mechanical sand control techniques. Parlar et al. (1998)[18] summarized many benefits of resin consolidation compared to other sand control methods. These chemical treatments can be performed on the fly, and no additional rigging is necessary. This technique of treating the unconsolidated formation with a resin that can cure to consolidate the loose sand can be applied as a remediation technique in mature production wells or to treat open hole wells or stand-alone screen wells[19].

The drawbacks of chemical sand consolidation methods are: (1) The resulted consolidated sand pack could lack in compressive strength, therefore the sanding issue could reoccur soon after the treatment; (2) The resin could severely impair the formation permeability; and (3) Some chemistries could be sensitive to formation sand and fluid type, making the effectiveness of sand consolidation success a hit and miss, and (4) Proper placement of the resin into the right zone could be difficult. Kalgaonkar et al. (2017)[20] proposed the use of a permeability enhancement additive with resin treatment to improve the regain permeability without the loss of compressive strength. Various studies have also been carried out using non-polymeric materials like sodium silicate to consolidate sand in oil and gas producing wells[21].

Sand control by chemical consolidation involves injecting chemicals into the unconsolidated formation to provide grain-to-grain cementation. These conventional methods of sand consolidation by chemical reagents tend to have relatively uncontrollable setting times. A setting time that is too long can result in the fluids flowing into areas with lower permeability rock, which leads to formation damage. A setting time that is too short can lead to premature curing of the resin, which leads to an unsuccessful treatment.

This article describes a method of sand control in unconsolidated formations using positively charged modified nanoparticles that can assemble over the sand particles of the unconsolidated formation. The positive charge modified nanoparticles form a thin layer of consolidating material across the unconsolidated formation to provide sand control with desired permeability characteristics. The main advantage of this treatment method is that the entire treatment can be placed downhole in a single step operation — the pill is initially a low viscosity fluid. In the presence of an ionic strength modifier (ISM), the cationic nanoparticles eventually hardens to cement the sand grains together and at the same time ensures that permeability is retained through the treatment material to facilitate production of hydrocarbons. When mixed with field sand, the cationic nanoparticles form a strong bond among the grains. Moreover, the consolidated cationic nanoparticles exhibit good permeability. The concentration of cationic nanoparticles has been optimized to produce a desirable balance between the permeability and the consolidation strength.

CATIONIC NANOPARTICLES FOR SAND CONTROL

The surface of the unconsolidated sand grains has a net negative charge. The positively charged nanoparticles modified with the cationic species can self-assemble over the unconsolidated formation sand particles due to electrostatic attraction, to form a layer of consolidating material. Initially, the cationic nanoparticles exist as a low viscosity solution. In the presence of an activator, these cationic nanoparticles gel up to form a hard composition.

Upon hardening of the composition, a thin layer of a hard gel is formed around the unconsolidated sand grains. This hard gel can cement the sand grains together while also maintaining a desired porosity through the treated consolidated material to facilitate the production of hydrocarbons. The positive charge of the cationic nanoparticles leads to repulsion between these nanoparticles, which helps to maintain the low viscosity of the composition and prevent the premature hardening of the composition, while being delivered downhole to the target zone. The charge repulsion between positively charged nanoparticles prevents any unwanted agglomeration of the nanoparticles.

Furthermore, the similar repulsive charge force ensures a monolayer coating of the surface of the sand grains in the unconsolidated formation. The positively charged nanoparticles, having an affinity for the negatively charged sand grains in the formation, produce a thin coating layer on the surface of the negatively charged grains of the unconsolidated formation.

Figures 1 and 2 show the scanning electron microscope analysis of an untreated pristine sand sample, and a treated sand sample with cationic nanoparticles, respectively. It clearly shows that there is a thin coating layer of the cationic

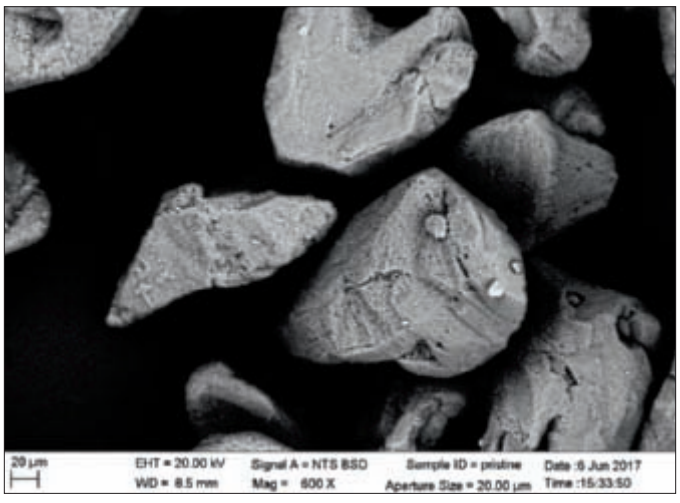

Fig. 1. A scanning electron microscope micrograph for the untreated pristine sand particles.

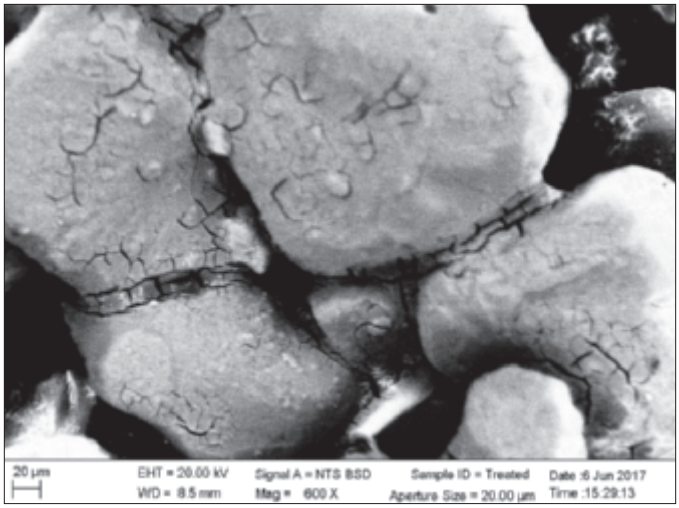

Fig. 2. A scanning electron microscope micrograph for sand treated with a cationic nanoparticle-based sand control pill.

nanoparticles around the sand particles. Moreover, the treated sand particles are cemented together due to the gelling up of the cationic nanoparticles coating. It can also be seen that the gelled up nanoparticles are able to maintain an interstitial void space for hydrocarbon production. The cationic nanoparticles create anionic bonding between the negatively charged unconsolidated formation sand grains and cationically modified nanoparticles. This eventually leads to modifying the relative permeability of the formation.

LABORATORY PROCEDURES

Evaluation of Gelation Time

The gelation time defines the amount of time available to the operator before the pumping pressure of the gel system significantly increases, once applied in the field. A reasonable gelation time must be known to allow safe pumping of the consolidation fluid through the tubular and into the near wellbore zone. Two methods were used in this study to measure gelation time: (1) The dynamic viscosity method using a Model 50 type rheometer, and (2) The sealed tube method.

Dynamic Viscosity Method

The gelation time of the gel system was determined using a Model 50 type high-pressure, high temperature (HPHT) rheometer. A #05X bob was used with a speed of 3 rev/min. Approximately 44 mL of the fluid system were measured and placed in the HPHT viscometer cup. The cup was mounted with pressure and heated using a thermostatically controlled electric heating bath. The viscosity changes were monitored as a function of time. This method defines the gelation time as the time required to begin building viscosity. The time when the viscosity begins to build can be defined as "gel time."

Inverted Sealed Tube Method

The fluid system comprising of the cationically modified nanoparticles and the activator were filled in a test tube with a cap to approximately one-third of its volume. The test tubes were placed in a preheated oven set at the test temperature and periodically taken out for observation. This method defines the gelation time as the time required for a system to reach specified gel strength and relies on the visual evaluation of the researcher. Gel time measurements were performed using this method for testing temperatures from 200 °F to 300 °F.

Batch Screening Tests

Batch tests were conducted to visualize and estimate the effectiveness of the cationically modified nanoparticles in consolidating the loose sand while maintaining the high permeability. Many different ratios of the cationically modified nanoparticles to the activator were tested to select the optimum concentrations. The procedure to conduct this type of screening test is as follows:

1. Mix formation sand with brine in a beaker. The amount of brine is sufficient to saturate the sand pack to make a slurry, but not overly abundant such that a free water layer exists above the sand pack.
2. Load the sand slurry into a syringe.
3. Squeeze a pre-flush fluid through the sand pack in the syringe. The preferred pre-flush fluid is a brine such as sodium chloride (NaCl).
4. Inject the mixture containing cationically modified nanoparticles and activator until the mixture breaks through from the outlet of the sand pack.
5. Inject post-flush fluid. A preferred post-flush fluid is also NaCl brine.
6. Set the temperature at 90 °C for 48 hours.

Retrieve the consolidated sand to check strength and permeability.

Coreflooding

The coreflooding experiment is conducted in a similar procedure to that of the batch screening tests, but at reservoir pressure condition.

1. Loose sand grains are packed in a rubber sleeve fitted inside a core holder. The initial brine permeability of the sand pack is first measured with 6% NaCl.
2. Pre-flush with NaCl for 1 pore volume (PV).
3. Inject 1 PV of the fluid system comprising cationically

Sample No.	ISM	Concentration (gpt)	SG of ISM	Result of Mixing Positive Surface Charge
1	ISM1	100	1.520	Precipitation
2	ISM1	200	1.265	Precipitation
3	ISM1	200	1.245	Precipitation
4	ISM1	100	1.200	Precipitation
5	ISM1	50	1.200	Precipitation
6	ISM1	150	1.038	Slightly Opaque
7	ISM1	100	1.038	Slightly Opaque
8	ISM2	100	1.041	Clear Solution
9	ISM2	300	1.044	Clear Solution
10	ISM3	100	1.041	Clear Solution
11	ISM4	100	1.044	Clear Solution
12	ISM4	125	1.044	Clear Solution
13	ISM4	150	1.044	Clear Solution
14	ISM4	175	1.044	Clear Solution
15	ISM4	200	1.044	Clear Solution
16	ISM4	100	1.08	Clear Solution
17	ISM4	200	1.08	Clear Solution
18	ISM4	100	1.188	Clear Solution
19	ISM4	200	1.188	Clear Solution

Table 1. Compatibility of the cationic nanoparticles with the ISMs

modified nanoparticles and an activator.

4. Shut-in the core under reservoir temperature — 140 °F — for 48 hours.
5. Measure the regained permeability to brine using 6% NaCl.

RESULTS AND DISCUSSION

Effect of Activators on Gelation Time

Inorganic activators or ISMs were investigated to study the effect on the gelation properties of cationic nanoparticles. To study this effect, the cationic nanoparticles solution was mixed with different ISMs of varying specific gravities (SGs). Clear solutions were obtained by varying the SGs of ISMs. A variety of ISMs were used for the study. Table 1 summarizes the experimental observations for the compatibility study of these activators. It was observed that most of the activators studied herein formed clear solutions when mixed with the cationically modified nanoparticles, except for ISM 1. ISM 2 through ISM 4 were investigated further as gelation activators for cationic nanoparticles.

To select an optimum activator for the cationically modified nanoparticles, the samples that gave clear solutions were kept in an air circulating oven to monitor the static gelation under reasonable time frames. Table 2 summarizes the performance of selected ISMs to gel up the nanoparticles at 90 °C. To be applicable downhole as a sand control pill, the system needs to show the preferred gelation time of 12 to 72 hours. Based on this argument, it was observed that ISM 4 gave the best gel times that would avoid any premature gelling of the sand control pill while it's being pumped downhole.

As ISM 2 and ISM 3 did not gel up even after 72 hours, they cannot be used or applied in field conditions for lack of timely gel up. When ISM 4 was used in a lower concentration

Sample No.	ISM	Gelation Time
8	ISM2	No gelation after 4 days (test aborted)
9	ISM2	No gelation after 4 days (test aborted)
10	ISM3	No gelation after 4 days (test aborted)
11	ISM4	No gelation after 4 days (test aborted)
15	ISM4	No gelation after 4 days (test aborted)
16	ISM4	72 hours
17	ISM4	< 15 hours
18	ISM4	7.5 hours
19	ISM4	4 hours

Table 2. Selected ISM performance as an activator to gel up the cationic nanoparticles at 90 °C

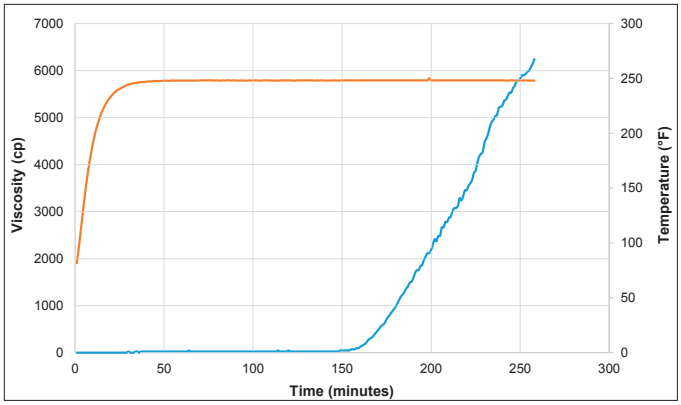

Fig. 3. Dynamic gelation of cationic nanoparticles with a composition ratio of 1:0.15 nanoparticle:activator at 250 °F.

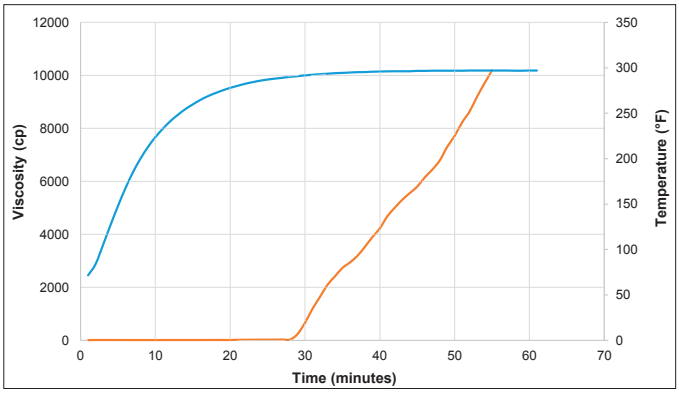

Fig. 4. Dynamic gelation of cationic nanoparticles with a composition ratio of 1:0.15 nanoparticle:activator at 300 °F.

it also did not show any gel up after 72 hours at 90 °C. ISM 4 with SG values of 1.08 and 1.188 — designated as sample numbers 16, 17, 18, and 19, in Tables 1 and 2 — showed the most controlled gelation. ISM 4 with a SG of 1.188 — sample number 18 from Tables 1 and 2 — was selected for further investigation.

Effect of Composition and Temperature on Gelation Time

Dynamic Viscosity Method: To verify the effect of sudden thermal shock on the cationically modified nanoparticle solution and the activator, two approaches were investigated: (1) The samples were conditioned at the test temperature, before mixing with each other, and (2) The nanoparticle solution and activator were added to a preheated sample cup. Any change in the appearance of the sand control pill or instantaneous change in viscosity was carefully monitored. It was observed that in both of the situations, there was no marked change in the appearance of the pill — neither showed any immediate viscosification.

This test proves the robustness of the pill under high temperature conditions and provides the operator with confidence that the pill will not prematurely gel up while pumping or before being placed in the target zone. As there was no sudden gel up of the pill, further tests were conducted by loading the sample in the test cup at room temperature and gradually heating up to the test temperature. The effect of the activator composition and temperature on the dynamic gelation time is shown in Figs. 3 and 4 at 250 °F and 300 °F, respectively. The pill exhibited low viscosity initially and over a period of time the viscosity started to build up. This is a typical representation of liquid to solid transition. The point where the viscosity starts to increase was taken as the gel time for the sample.

Inverted Sealed Tube Tests: To understand the effect of the composition of an activator as a function of temperature on the gelation time of the cationically modified nanoparticles, inversion tests were performed. The samples were subjected to a range of temperatures from 80 °C to 150 °C in static condition using an air circulatory oven. A representative inverted sealed tube test is depicted in Fig. 5. All the test samples were observed for 24 hours for this set of tests. Any samples that did not gel up in 24 hours were not monitored further.

Fig. 5. Representation of the inverted sealed tube test demonstrating gelation under static conditions.

Figure 6 summarizes the results of inverted sealed tube tests. The gelation of these cationic nanoparticles

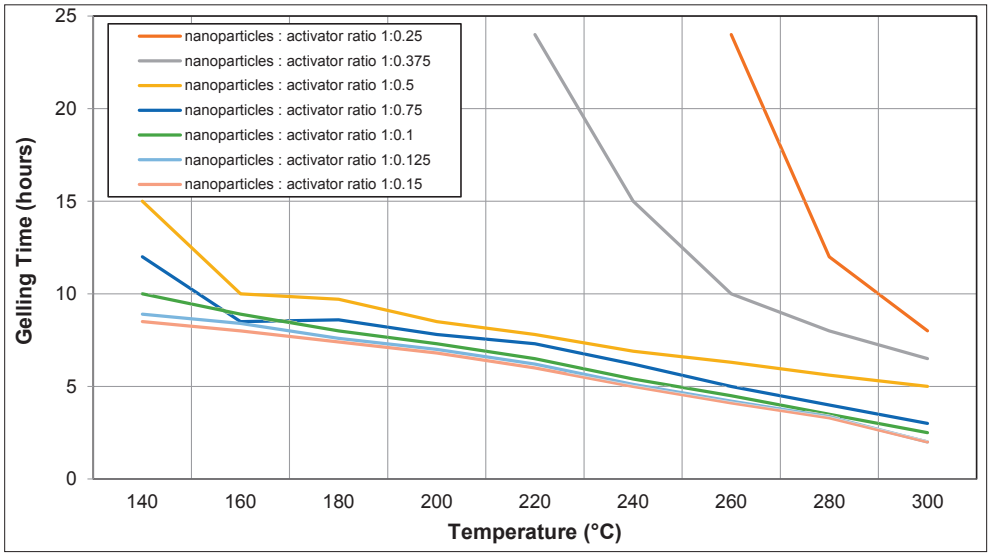

Fig. 6. Static gel time as a function of temperature and activator concentration of the inverted sealed tube tests.

required longer times at a lower temperature and low concentrations of activators. Therefore, the temperature and concentration of the activator showed a linear relationship to the decreasing gelation times. By optimizing the concentration of activators at a higher temperature, one can easily achieve longer gelation time. The strength of the gel is a function of the activator concentration. At some point, the activator concentration would be too low to provide a usable gel.

Moving to higher temperatures also makes the gelation time harder to control. A difference of a few degrees between the estimated and actual temperature will produce a much larger deviation in gelation times at high temperatures. Furthermore, it should also be noted that with higher concentrations of the activator, such as more than a nanoparticle to activator composition ratio of 1:0.35 of nanoparticles, the solution gelled instantly before the activator could uniformly disperse through the solution. Such instantaneous gelation could be avoided with a controlled drop by drop addition of the activator to the nanoparticles' solution under continuous agitation. Subsequently, the sample still gelled in less than a minute even under ambient temperature conditions. This implies the necessity to optimize the concentration of the activator to avoid any premature gelling of the sand control pill before it is placed in the target zone.

It should be noted from the static and dynamic gelation time tests that the cationic nanoparticles gel up in shorter time frames under dynamic conditions as compared to those under static conditions. This is expected because the solution to gel transition time established as the onset of viscosity increase in dynamic experiments represents the onset of gelation, which always takes place before the gelant becomes a rigid gel. Although it could be argued that the gelation time obtained from the static inverted testing tube method is a more accurate measure of the available pumping time through the tubing until the sand control pill hardens into a crystalline solid. It is recommended to design the pumping sequence based on gelation time determined using the dynamic viscosity method. It is a more conservative approach and it will give a safety control point to avoid any premature gelling up of the pill before it is placed in the target zone.

Regained Permeability

A qualitative permeability measure was conducted to demonstrate the permeable nature of the consolidated sand pack using cationic nanoparticles' treatment fluid. The permeability of the consolidated sand pack increases with the decreasing treatment fluid concentration, without sacrificing much compressive strength. Consequently, as the treatment fluid concentration is reduced, the time taken to consolidate the sand pack increases.

In some cases this consolidation time can extend from a few days to weeks. This is impractical when applying the treatment fluid as a sand control pill. A quicker turnaround in putting the well on production is what is desirable. Considering this, only those concentrations of the cationic nanoparticle treatment fluid that consolidate sand — in a 24 hour period — were chosen for further testing.

Figure 7 shows the representative sand pack consolidated by the cationic nanoparticle treatment fluid. A simple qualitative indication of the high permeability can be observed by dropping water on the top of the cured cylindrical sand pack. It can be observed that the water immediately seeps through the porous medium and penetrates all the way to the other end of the cylindrical core. Continuously dropping water on top of the face of the consolidated core sample results in a continuous drip from the bottom face with merely a hydrostatic head. Such low flow resistance indicates high regained permeability of the consolidated pack.

Coreflooding experiments were conducted using a sand pack to study the performance of the new sand control pill to retain the formation permeability after consolidating the sand. The sand pack was prepared using a 1:1 mixture of 100 mesh and 20:40 mesh sand. A ratio of 1:0.15 of cationic nanoparticles to the activator was used for the regain permeability studies. A temperature of 140 °C was maintained throughout the coreflooding test. System pressure was kept at 3,500 psi to simulate reservoir conditions. The overburden stress was maintained at 500 psi above the injection pressure to prevent any flow around the sand pack. Initial permeability using 6% NaCl was measured with multiple flow rates to confirm that the pressure transducer readings are correct as the permeability remained constant at different injection rates.

The NaCl treatment also served as the pre-flush for conditioning the sand pack for the nanoparticle treatment, due to the compatibility of the new nanoparticle treatment fluid with aqueous fluids. The sand pack was then exposed to the treatment fluid. The treatment was followed by a 48-hour shut-in period at 140 °C. After the shut-in, the regain

Fig. 7. A representative sand pack consolidated by the cationic nanoparticle treatment fluid.

Sample	Type	Initial Perm	Regain Perm
Sand Pack	1:1 mix of 100 mesh and 20/40 mesh sand	800 millidarcies	50%

Table 3. Regain permeability test results

permeability was measured with the NaCl brine. Table 3 show the results of the regain permeability experiments using this system formulation. The average permeability was maintained at approximately 50% under multiple rates of brine injection. The consolidated sand pack after the regain permeability tests was found to remain intact.

Finally, the test core sample consolidated with the cationic nanoparticles was exposed to 15% hydrochloric acid to check the effect of acid on the post-treatment core. The regain permeability remained the same after exposing the consolidated core to the acid. It appeared that the consolidated core did not disintegrate on exposure to the acid.

CONCLUSIONS

The new downhole sand consolidation system comprising of cationically modified nanoparticles and an activator that initiates the consolidation has shown properties and performance in addressing the drawbacks of the currently available chemical-based sand consolidation systems. Static and dynamic gelation time experiments were performed. A controllable gelation time can be achieved by varying the concentration ration of the cationic nanoparticles to the activator. The gelation times were found to be shorter in the dynamic tests as compared to the static tests. This difference was attributed to the onset of gelation under dynamic conditions as against complete gelation in static conditions.

The dynamic gelation data should be taken into consideration when designing a field job. The regain permeability testing showed the new sand control chemical can consolidate a loose sand pack without significantly damaging the formation. The newly developed sand control system comprising of cationic nanoparticles provided 50% regain permeability.

ACKNOWLEDGMENTS

The authors thank Abdullah Abadi for the coreflood experiments.

This article was presented at the SPE Annual Technical Conference and Exhibition, San Antonio, Texas, October 9-11, 2017.

REFERENCES

1. Rahim, Z., Al-Malki, B. and Al-Kanaan, A.: "Selection of Completion Strategy for Sand Control and Optimum Production Rate — Field Examples from Saudi Arabia's Unayzah Sandstone Reservoir," SPE paper 131078, presented at the SPE Asia Pacific Oil and Gas Conference and Exhibition, Brisbane, Queensland, Australia, October 18-20, 2010.
2. Boudi, A.A.: "ESP Suffers Erosion due to Sand Production in a Mature Onshore Oil Field," SPE paper 184179, presented at the SPE Middle East Artificial Lift Conference and Exhibition, Manama, Kingdom of Bahrain, November 30-December 1, 2016.
3. Wong, C.Y., Wu, J., Zamberi, A., Solnordal, C., et al.: "Sand Erosion Modeling," SPE paper 132920, presented at the SPE Asia Pacific Oil and Gas Conference and Exhibition, Brisbane, Queensland, Australia, October 18-20, 2010.
4. Graham, L., Wong, C.Y., Lester, D. and Wu, J.: "Laboratory Modeling of Equipment Erosion by Sand Particles," SPE paper 124108, presented at the SPE Annual Technical Conference and Exhibition, New Orleans, Louisiana, October 4-7, 2009.
5. McLeod, N.J.: "Sand Control in an Ultra-Fine Sand Environment," SPE paper 38642, presented at the SPE Annual Technical Conference and Exhibition, San Antonio, Texas, October 5-8, 1997.
6. Karian, M.A., Salleh, A., Haron, J., Sura, M.A.M., et al.: "Resin Sand Consolidation in Baram Delta, Sarawak. Case Study on Resin Performance vs. Internal Gravel Packing with Acid Prepacking," SPE paper 57314, presented at SPE Asia Pacific Improved Oil Recovery Conference, Kuala Lumpur, Malaysia, October 25-26, 1999.
7. Woiceshyn, G.E., Russell, T.G. and Caulfield, I.A.: "A Unique Sand Control Screen that Enhances Productivity," SPE paper 139360, presented at the SPE Latin America and Caribbean Petroleum Engineering Conference, Lima, Peru, December 1-3, 2010.
8. Hainey, B.W. and Troncoso, J.C.: "Frac-Pack: An Innovative Stimulation and Sand Control Technique," SPE paper 23777, presented at the SPE Formation Damage Control Symposium, Lafayette, Louisiana, February 26-27, 1992.
9. Nguyen, P.D., Ingram, S.R. and Gutierrez, M.: "Maximizing Well Productivity through Water and Sand Management — A Combined Treatment," SPE paper 106592, presented at SPE Production and Operations Symposium, Oklahoma City, Oklahoma, March 31-April 3, 2007.
10. Penberthy Jr., W.L., Shaughnessy, C.M., Gruesbeck, C. and Salathiel, W.M.: "Sand Consolidation Preflush Dynamics," *Journal of Petroleum Technology*, Vol. 30, Issue 6, June 1978, pp. 845-850.
11. Nguyen, P.D. and Jaripatke, O.A.: "Controlling Solids Flow Back to Maintain Production of Hydrocarbons: A Review of Successful Chemical Technologies in the Last Decade," IPTC paper 13725, presented at the International Petroleum Technology Conference, Doha, Qatar, December 7-9, 2009.
12. Friedman, R.H. and Surles, B.W.: "Sand Consolidation

Methods," U.S. Patent 4,842,072, June 1989.

13. Friedman, R.H. and Surles, B.W.: "Treating Underground Formations," U.S. Patent 5,005,647, April 1991.
14. Syndansk, R.D.: "Acrylamide — Polymer/Chromium (III)-Carboxylate Gels for Near Wellbore Matrix Treatments," *SPE Advanced Technology Series*, Vol. 1, Issue 1, April 1993, pp. 146-152.
15. Falk, D.O.: "Process for Selectively Plugging Permeable Zones in a Subterranean Formation," U.S. Patent 4,485,875, December 1984.
16. Moradi-Araghi, A., Bjornson, G. and Doe, P.H.: "Thermally Stable Gels for Near-Wellbore Permeability Contrast Corrections," *SPE Advanced Technology Series*, Vol. 1, Issue 1, April 1993, pp. 140-145.
17. Swanson, B.L.: "Gelled Compositions and Well Treating," U.S. Patent 4,246,124, January 1981.
18. Parlar, M., Ali, S.A., Hoss, R., Wagner, D.J., et al.: "New Chemistry and Improved Placement Practices Enhance Resin Consolidation: Case Histories from the Gulf of Mexico," SPE paper 39435, presented at the SPE Formation Damage Control Conference, Lafayette, Louisiana, February 18-19, 1998.
19. Madasu, S. and Vo, L.: "An Effective Foamed Polymer Resin Diverter System for Sand Control," IPTC paper 18656, presented at the International Petroleum Technology Conference, Bangkok, Thailand, November 14-16, 2016.
20. Kalgaonkar, R., Chang, F., Abitrabi Ballan, A.N., Abadi, A., et al.: "New Advancements in Mitigating Sand Production in Unconsolidated Formations," SPE paper 188043, presented at the SPE Kingdom of Saudi Arabia Annual Technical Symposium and Exhibition, Dammam, Saudi Arabia, April 24-27, 2017.
21. Cobianco, S., Lezzi, A., Previde Massara, E. and Pitoni, E.: "Dirty Sand Consolidation Technology for Gas Wells," SPE paper 50714, presented at the SPE International Symposium on Oil Field Chemistry, Houston, Texas, February 16-19, 1999.

BIOGRAPHIES

Dr. Rajendra A. Kalgaonkar is a Petroleum Scientist in the Productivity Enhancement Focus Area of the Production Technology Team at Saudi Aramco's Exploration and Petroleum Engineering Center – Advanced Research Center (EXPEC ARC). He has over 16 years of experience in Research and Development, out of which he spent 11 years in the upstream oil and gas industry. Prior to joining Saudi Aramco in May 2015, Rajendra worked as a Technology Leader with Halliburton. He has rich experience in areas of nanotechnology; polymer blends and composites while being associated with the National Chemical Laboratory, India, and the University of Western Sydney, Australia.

Rajendra's research is focused on developing new fluids technologies for enhancing hydrocarbon production, including fracturing, sand control, conformance control and acidizing. He has successfully developed new chemistries based on nanomaterials for enhancing hydrocarbon production as well as for drilling fluids.

Rajendra has published 25 patents and patent applications, and 35 peer-reviewed articles, invited book chapters and conference proceedings. He has delivered presentations at Society of Petroleum Engineers (SPE) key advanced technology workshops and forums.

Rajendra received his B.S. degree in Chemistry, an M.S. degree in Polymer Science, and his Ph.D. degree in Polymer Chemistry and Nanotechnology, all from the University of Pune, Pune, India.

Dr. Fakuen F. "Frank" Chang is a Petroleum Engineering Consultant in the Productivity Enhancement Focus Area of the Production Technology Team at Saudi Aramco's Exploration and Petroleum Engineering Center – Advanced Research Center (EXPEC ARC). Prior to joining Saudi Aramco in September 2012, he worked at Schlumberger for 16 years, and he was at Stimlab for 4 years before his Schlumberger career. Frank has developed many products and technologies dealing with sand control, fracturing, acidizing, and perforating.

He is an inventor and recipient of 23 granted U.S. patents and the author of more than 40 Society of Petroleum Engineers (SPE) technical papers.

Frank received his B.S. degree in Mineral and Petroleum Engineering from the National Cheng Kung University, Tainan City, Taiwan; his M.S. degree in Petroleum Engineering from the University of Louisiana at Lafayette, Lafayette, LA; and his Ph.D. degree in Petroleum Engineering from the University of Oklahoma, Norman, OK.

Case Study: Safe Through-Tubing ESP Installation in Pressurized Well through Modified Killing Techniques

Mohannad Abdelaziz, Brian A. Roth, and Dr. Jinjiang Xiao

ABSTRACT

Cable deployed electric submersible pumps (CD-ESPs) are foreseen as the future of ESP installations as they eliminate the need for a full-fledge rig on location to perform an ESP change out. One of the main challenges of performing ESP installation riglessly is the lack of a mud circulation system, which is used to monitor the rate of increased fluid loss, indicate possible well kick and bring the well back to control in case of such emergencies. With the lack of this line of defense, there is a need to develop alternative methods to ensure safe rigless ESP installation, particularly when ESP components are being made-up and lowered down the well.

The first high hydrogen sulfide (H_2S) vertical well CD-ESP worldwide was trial tested in a pressurized onshore well. The candidate well had a shut-in pressure of 390 psi, H_2S concentration of 1.12%, and fluid loss rate of 18 barrels per hour (bph) to 24 bph for 71 pounds per cubic foot (pcf) of kill fluid.

Kill fluid has to be continuously supplied at a rate equivalent to the varying loss rate of the well. For this, the surface well testing equipment — required for well flow back after ESP installation — was modified to monitor and store excess kill fluid return. The new modification allows pumping of kill fluid to continue while blowout preventer (BOP) equipment is open on top of the Christmas tree. The density of the kill fluid was monitored and maintained during the whole operation.

The operation started by bullheading with one and a half wellbore volumes. The well's performance was monitored and then the kill fluid rate was increased gradually to measure the loss rate of the well. Pumping of kill fluid was highly coordinated during the main installation phases of the CD-ESP; surface makeup of the ESP assembly in sections, run in hole with cable to the target depth and the final makeup of the cable hanger.

The returns of any excess kill fluid could be measured by the modified surface testing package. The pumping rate of the kill fluid was highly correlated with the tubing casing annulus (TCA) pressure.

While the pump was inside the well, pumping of the kill fluid caused a significant increase of weight reading. The pump — 5.62" — acted like a piston inside the 6.275" internal diameter of the 7" tubing causing high weight values.

At one point during the operation, the loss rate of the well increased dramatically. This caused negative readings on pressure gauges of the wellhead — the loss rate was higher than the maximum pump supply.

This article presents novel comprehensive well killing measures for rigless CD-ESP installation. To ensure the safe conduct of future operations, the article also shows lessons learned and contingency measures for unexpected events during the operation.

INTRODUCTION

Cable Deployed ESPs

Improving the reliability and cost-effectiveness of electric submersible pumps (ESPs) has been an area of focus for the petroleum industry. One important aspect in this is to develop a more economical way to install and change out ESPs, replacing the conventional rig-based deployment method — alternative deployed ESP systems.

The alternative deployed ESP systems depends on installation of the pump through the production tubing. The most promising method for such systems depends on utilizing the ESP's power cable as a means of deployment. This method is known as the cable deployed ESP (CD-ESP). The CD-ESP offers the advantage of having a completely retrievable system, including the electrical power cable, to the surface without the need for a rig.

Such a system brings the following benefits to the development of oil fields and its operations:

1. A reduction in costs associated with ESP change out, particularly for offshore environments. This method requires less complex equipment and fewer personnel compared to a full-fledged workover rig.
2. The availability of workover rigs to be utilized for other critical operations like completion change out or sidetracks.
3. The surface equipment required to replace CD-ESP are more readily available — coiled tubing (CT) units

compared to rig. This reflects in less wait-on-rig time, and therefore, reduces deferred production from wells with failed ESPs.

4. The requirement to shut off nearby wells can now be minimized radically (faster operation) if not eliminated — no need to shut off nearby wells if no rig is in the vicinity.
5. A reduced environmental footprint, particularly for offshore environments compared rig-based operations.

World's First High H_2S CD-ESP

The cable of the ESP has to withstand the harsh flowing condition inside the tubing; therefore, the design of the cable is key to have a feasible CD-ESP system. A 10-year service life metal-jacketed power cable was designed for this purpose. The cable provides protection against the harsh conditions where it was tested to withstand up to 15% hydrogen sulfide (H_2S) and more than 150,000 ppm chloride. The cable also offers a slick outside diameter (OD) that enables gripping and sealing for safer operations.

The ESP system architecture consists of a through-tubing inverted ESP system lowered down and supported by the power cable. The bottom part of the ESP has a stinger assembly, which resides inside a permanently installed polished borehole receptacle (PBR) in the production packer at the bottom of the well. The surface end of the cable is connected to the cable hanger, which supports the pump assembly and the cable weight. The novel design of the cable hanger maintains vertical tree configuration providing electrical termination to the surface lines for power and communication while allowing passage of hydrocarbons through annular ports.

Such architecture eliminates the conventional electrical splicing and connection for normal ESP systems. Having less electrical connections reduces the number of weak points and increases system reliability.

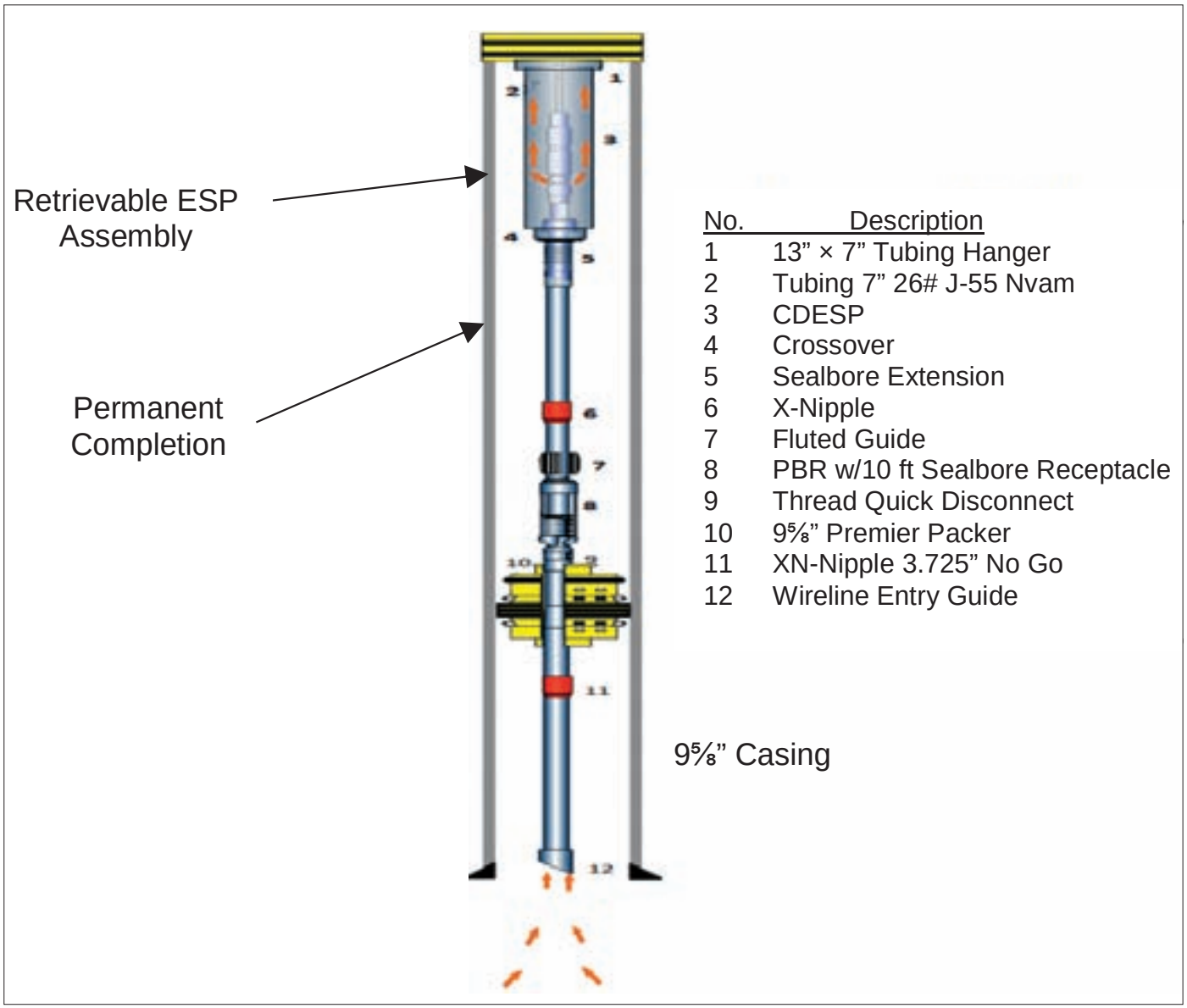

Fig. 1. Permanent completion of the well conversion[1].

THE FIRST TRIAL TEST

Well Information

A low H_2S onshore well was selected for the first CD-ESP field trial. The selection of such a benign well environment is important to build knowledge on CD-ESP rigless deployment before coming to a high H_2S and/or offshore environment. A few of the main features of the well are:

- H_2S concentration: 1.12% (dissolved gas H_2S, mole %)
- Well type: Horizontal open hole
- Bottom-hole temperature: 135 °F
- Maximum shut-in wellhead pressure (SIWHP): 390 psi
- Expected max production: 7,000 barrels of fluid per day (35% water cut)
- Planned ESP depth: 4,920 ft measured depth (~40° deviation)
- ESP type: 562 series inverted ESP

Well control for this well during rigless operation is very critical due to the following:

1. Like many wells in Saudi Aramco, the well has the ability to produce on its own, but ESPs are installed as a means to achieve higher flow rates. This means hydrocarbons will flow to the surface if no well control barriers are introduced.
2. To mitigate the need for stimulation after ESP installation, the wellbore is left with completion brine inside and after minimal filter cake formed. This is necessary to avoid pumping acid through the pump afterwards or having solids — flow back of filter cakes — produced through the pump. The cable of the CD-ESP also hinders CT accessibility after installation, preventing bottom-hole wellbore stimulation.

Permanent Completion Installation — Rig Procedure

An initial rig-based operation is required to convert the well to one that accepts CD-ESPs, Fig. 1[1]. All future ESP installations and replacements are conducted riglessly. For this, the well's permanent completion has to be changed to allow the 562 series ESP to be run through-tubing.

The workover rig completed the well with a 7" 26# production tubing crossed over to a 4½" 11.6# tubing at 4,932 ft. A 30 ft PBR seal assembly was installed as part of the tubing near the cross over. This allowed the ESP assembly to string into it once installed during the rigless operation. The permanent completion had a 9⅝" × 4½" production packer set at 5,134 ft.

Surface changes to the wellhead were also made. A new cable hanger spool was introduced on top of the tubing hanger and a larger size Christmas tree — $7^1/_{16}$" instead of 3" — were installed to allow passage of the pump size required, Fig. 2[2].

Rigless Deployment of a CD-ESP

Equipment on Location and Site Layout

The following is a list of the main pieces of equipment needed on-site:

1. The CT unit with a separate reel — spooling unit — for the ESP power cable.
2. The pressure pumping equipment includes the kill fluid storage and mixing tanks, and the filtration equipment.
3. Well testing — zero discharge — equipment connected to the zero flaring flow line. The well testing equipment was used as a means of monitoring the kill line returns and to function test the pump and measure well rates once installation is completed. Details of its use for the killing operation is presented later in this article.
4. The equipment required for tool handling include the CT tower, two cranes, and a forklift.

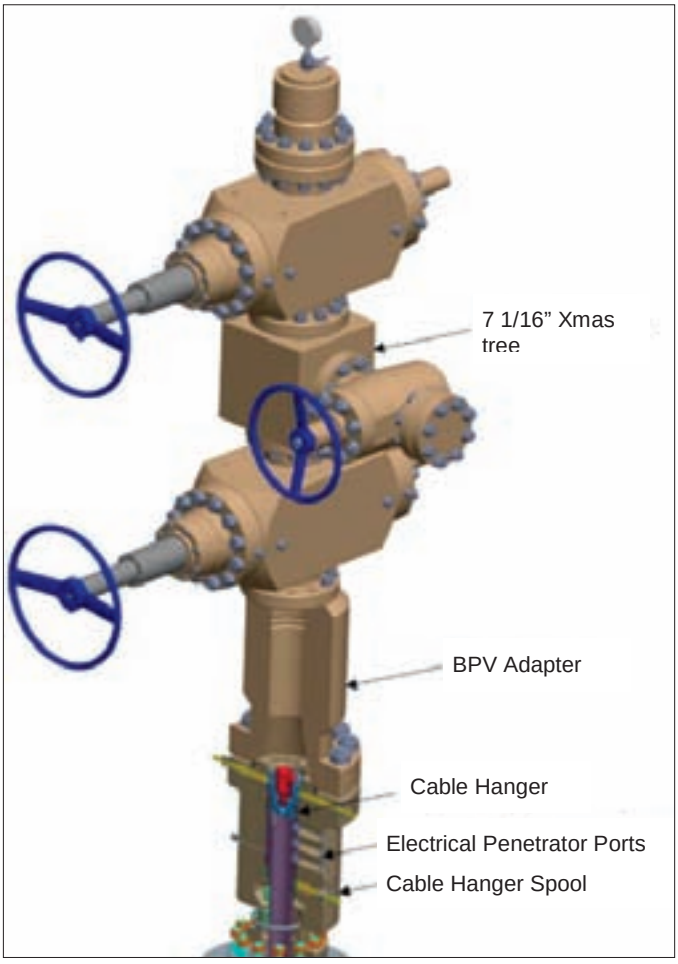

Fig. 2. Changes to the wellhead and Christmas tree[2].

5. Standard safety equipment — H_2S monitors, self-contained breathing apparatus, windsocks, eye wash and shower units, fire extinguishers, etc.
6. Radio communication systems; essential to have proper coordination between staff handling crane operations, equipment on top of CT tower, CT unit, pumping unit, return line monitoring, data acquisition, and main field coordinators.

Pressure Control Equipment Requirement for Rigless Operation

The candidate well has gas-oil ratio values that are less than 750 standard cubic ft/stock tank barrels and the SIWHP is below 1,500 psi. Moreover, the well location is not in a populated area. These conditions, which is typically the case for ESP wells, dictate that at least two independent barriers has to exist at all times during the operation. Independent means that failure in any of the barriers does not affect the function of the other[1].

At any point during the rigless part of the CD-ESP deployment, at least one of the two barriers has to be in effect:

Barrier 1: Kill brine (Nonmechanical): The hydrostatic pressure of the kill fluid column must exceed the reservoir pressure by at least 200 psi. Therefore, it is critical to ensure that the kill fluid always has the right density and the well is always topped up with this fluid.

Barrier 2: Stripper (and lubricator) (Mechanical – Surface – Closed): This barrier is used only when the cable is being run in hole. The ESP bottom-hole assembly (BHA) has nearly 6" of OD and heights exceeding 100 ft. This height and size limit the use of a lubricator as a barrier throughout the whole operation.

Barrier 3: Hydraulic blowout preventer (BOP), Fig. 3, (Mechanical – Surface – Closable): The BOP stack consists of:

- Annular BOP: The annular BOP is a qualified barrier to seal against different diameters, including a 5.62" motor and a 1.62" cable, as well as the blind.
- Variable Bore Rams (VBRs) and 5.62" Slip Rams: The upper combination has VBRs for the BHA sizes — seal against diameters between 5.13" and 5.78". The VBR is not a qualified barrier for this trial test and was part of the BOP stack as an additional contingency only. The slip rams will prevent axial movement of tools if the annular was closed during ESP section deployment.
- 1.62" BOP Stack: The lower combination — pipe/slip and shear/blind — is dressed for the ESP power cable — 1.62".

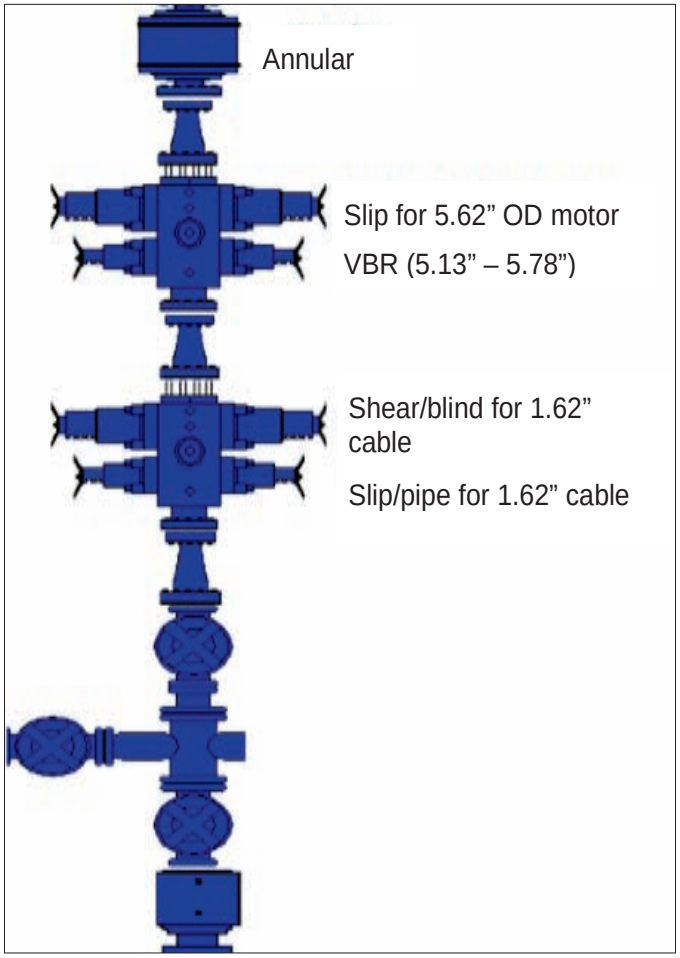

Fig. 3. Hydraulic BOP stack.

Figure 4 shows the main components of the ESP assembly to be run riglessly[1, 2].

Rigless ESP Installation Procedure

From a well control prospective, the rigless deployment procedure can be made up of the following phases. These are shown in Fig. 5.

1. Job Preparation. To minimize the working time with the well open, the following tasks are performed prior to the actual job:
   a. The cable connector, which connects the top of the ESP assembly to the cable, is installed at the end of the cable after feeding the cable through the injector head.
   b. The ESP motor and protector are pre-filled with dielectric oil, rather than filling them during deployment.
   c. A walk-through of the equipment is needed and other procedures are performed on the CT tower to minimize working time while the BOP is open.
2. Phase 1 — BHA deployment and connection to the cable: For this phase, a crane is used to place the ESP sections. C-plates are used to hang off sections from the tower.

During the lowering down of sections, the annular BOP is open. The annular BOP can be closed once a connection is being made or if a long work stop is required. Barriers 1 and 3 are effective in this phase. In more detail, the following steps will be performed:

a. The first two sections of the ESP assembly are connected together on the side of the tower, and then they are moved over the well and lowered down together after opening the BOP. These two sections are the stinger assembly section and the pump, motor and protector section. Running the first two sections as one minimizes the time the annular BOP is open.

b. The connection to the third section of the ESP assembly is made. The third section consists of the sensor gauge, connection chamber, primary shear sub, and stabilization gland.

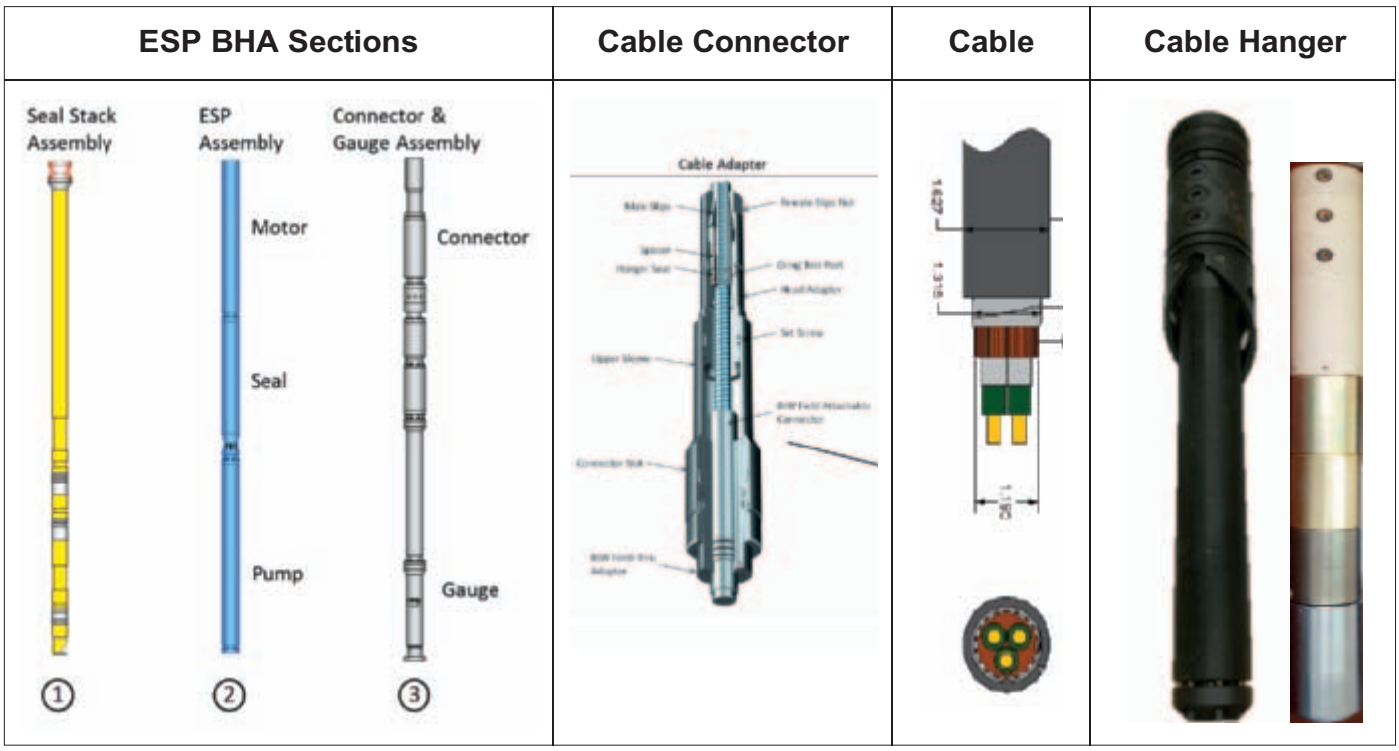

Fig. 4. Retrievable CD-ESP components[1, 2].

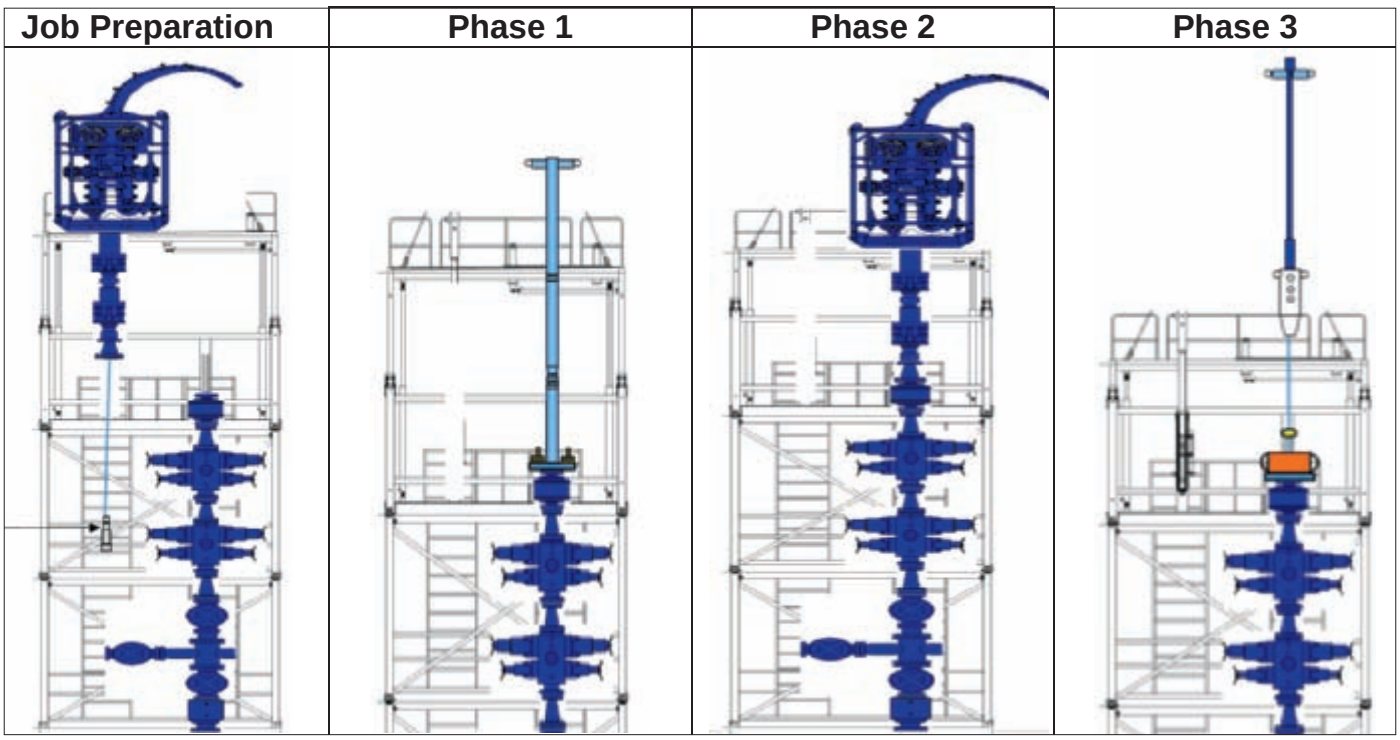

Fig. 5. Job phases.

c. The cable connector is made up to the BHA. The BHA is run down the hole several feet, and the 1.62" pipe and slip rams are engaged.

3. Phase 2 — Running the BHA to depth and performing the necessary space out: During this phase, the injector head and stripper will be closed on top of the annular BOP. With the stripper connection function tested, the well is contained in a closed system. Barriers 1 and 2 were effective in this phase. In more detail, the following steps where performed:
   a. The injector head and the stripper are made up on top of the annular BOP. The system is pressure tested and running in the hole commenced, limiting the run in speed to less than 25 ft/min.
   b. The ESP assembly stinger is landed inside the PBR as confirmed by the CT weight indicators. The necessary space out is made, taking into account the height of the wellhead with pressure control equipment and extra length, to leave enough space for the working envelope.

4. Phase 3 — Cutting the cable and connecting and landing of the cable hanger adapter: Barriers 1 and 3 are effective in this phase.
   a. With the annular BOP closed, the connection between the stripper and the annular BOP is broken.
   b. The power cable is cut based on space out made earlier and the cable hanger connecter with an electrical adapter is made at the end of the cable.
   c. The hydraulic GS tool is connected to the cable hanger, and with a means of a crane, the cable hanger is lowered down inside the cable hanger spool. Once landing is confirmed, the GS tool is released. The annular BOP is opened to lower down and retrieve the GS tool. The crown and master valve are closed after retrieval of the GS tool to secure the well.

5. Make up of the electrical surface connection and function test of the ESP.
   a. The horizontal electrical connectors to the cable are made up and connected to a temporary variable speed drive.
   b. The kill fluid is pumped off the well and the ESP is function tested.

Further details on the trial test can be found in Roth et al. (2017)[2].

KILLING OPERATIONS METHODOLOGIES AND FINDINGS

As previously mentioned, the operation for the CD-ESP installation and replacement is a critical and unique operation that requires a novel killing technique to be in place to ensure safety of personnel and equipment. The novelty of the killing operation introduced for this job is portrayed in these points:

- New design for kill line pipework, which implements a return loop to monitor kill fluid returns.
- Correct choice and close monitoring of kill fluid density.
- Close monitoring of return lines to measure loss rate and react accordingly.
- Accurate calculating and planning for kill fluid volumes required for the duration of the operation.
- The proper coordination of kill fluid pumping with the operation stages.
- Perceiving the effect of pumping kill fluid on tubing casing annulus (TCA) pressure.
- Perceiving the effect of pumping kill fluid on tensional forces on the cable while the ESP is inside the wellbore.

The following sections detail these seven items highlighting the major findings during the operation.

Kill Fluid Monitoring — Return Loop

During the permanent completion installation by the workover rig, a varying loss rate was recorded between 18 barrels per day (bpd) to 24 bpd. For the rigless operations, this meant that the well had to be continuously topped up with kill fluid to compensate for this loss rate.

The most critical phases of the operations are Phases 1 and 3, at which time the annular BOP has to be open to allow passage of the equipment to be lowered down the well. Additionally, closure of the annular BOP has to be minimized to avoid damaging the ESP system. The team worked on minimizing these critical periods. The pumping system design must account for long periods of the open annular BOP. The design has to allow pumping of the kill fluid, even when the annular BOP is open. The zero flaring and ESP function test equipment at the surface has been modified and used for this purpose, Fig. 6.

Both the kill line and return lines were connected to the wing valve using a T-joint connection. The T-joint could not be introduced above on the crown valve, as this would require an additional set of BOPs to be added between the T-joint and the crown valve. CT rig-up requirements have the BOP as the first piece of equipment that connects to the crown valve.

The pumped kill brine has three possible paths: either down the well, back to the return line — to surface tanks — or up through the annular BOP to the surface. The design of the surface pipework has been made, such that topping up the well with kill brine is the least resistance, or preferred path. Any excess to this will go to the return line, which avoids

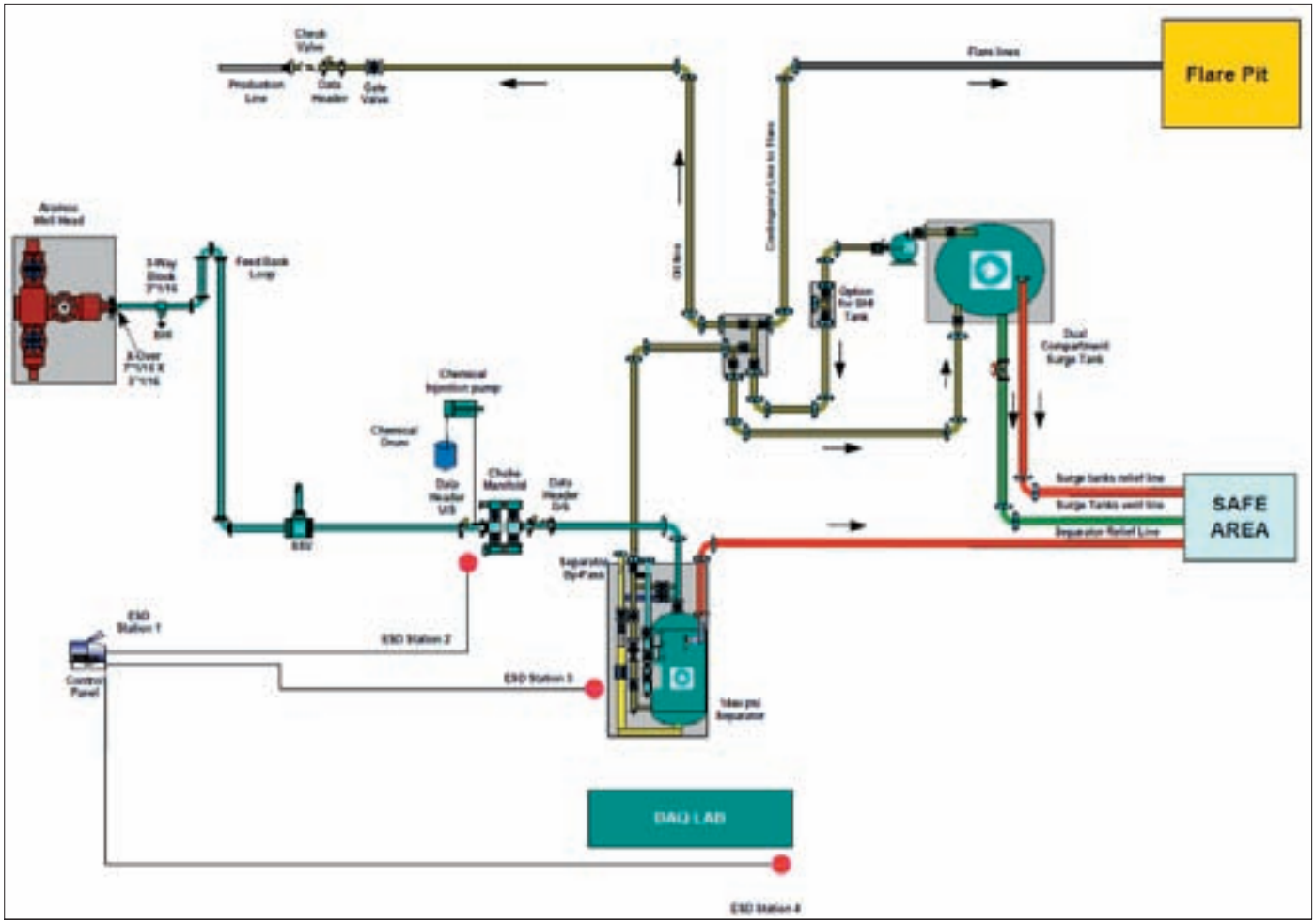

Fig. 6. Layout for surface kill brine return and ESP function test equipment.

moving up to the surface while the annular BOP is open. Therefore, additional elevation to the return line pipe — the kink in the pipework seen in Fig. 7 — has been introduced.

Such design allows kill brine to be supplied to the well at a rate equivalent to the loss rate and any excess will be monitored and captured by the return line. The loss rate of the well at any point in time can be estimated by gradually increasing the pumping rate until return is received. This system mimics some features of the circulation system in workover rigs. Measuring of the well's loss rate has to be performed regularly during different parts of the operation, to account for any changes in loss rate.

Kill Fluid Density (Overbalance)

To have an overbalance of 300 psi, a killing fluid with a density of 71.6 pounds per cubic foot (pcf) (9.57 pounds per gallon) was mixed. The same brine density used during the rig operation recorded a loss rate between 18 barrels per hour (bph) to 24 bph — 0.3 barrels per minute (bpm) to 0.4 bpm. The density of the kill brine was measured and recorded using a mud balance every one hour to ensure proper mixing. The loss rate depends highly on the density of the kill fluid with a proportional relationship between the two.

Change of Kill Fluid Density

Before commencing with the third phase of the rigless operation, the well condition changed. Negative values were recorded for wellhead pressure. This change was attributed to a sudden increase in loss rates. Even when the pumping rate was increased to values as high as 2 bpm, the wellhead pressure remained at negative values.

This condition was resolved by reducing the density of the kill fluid to 67 pcf — reducing the overbalance. Such a sudden change confirms the necessity to keep monitoring the loss rate of the well during the operation, to react accordingly by adjusting the kill fluid pumping rate or changing its density.

Volumes Required

Abundance of the supply of kill fluid is required to account for the whole operation. The operation started with bullheading one and a half wellbore volumes — 450 bbl — after which pumping at a rate similar to the well loss rate continued. Two 500 barrel tanks were on location. While one of the tanks is used for continuous pumping of kill fluid, the other is used for mixing and preparation to ensure continuous pumping.

It took 8 hours to drain the whole tank at a rate of 1 bpm,

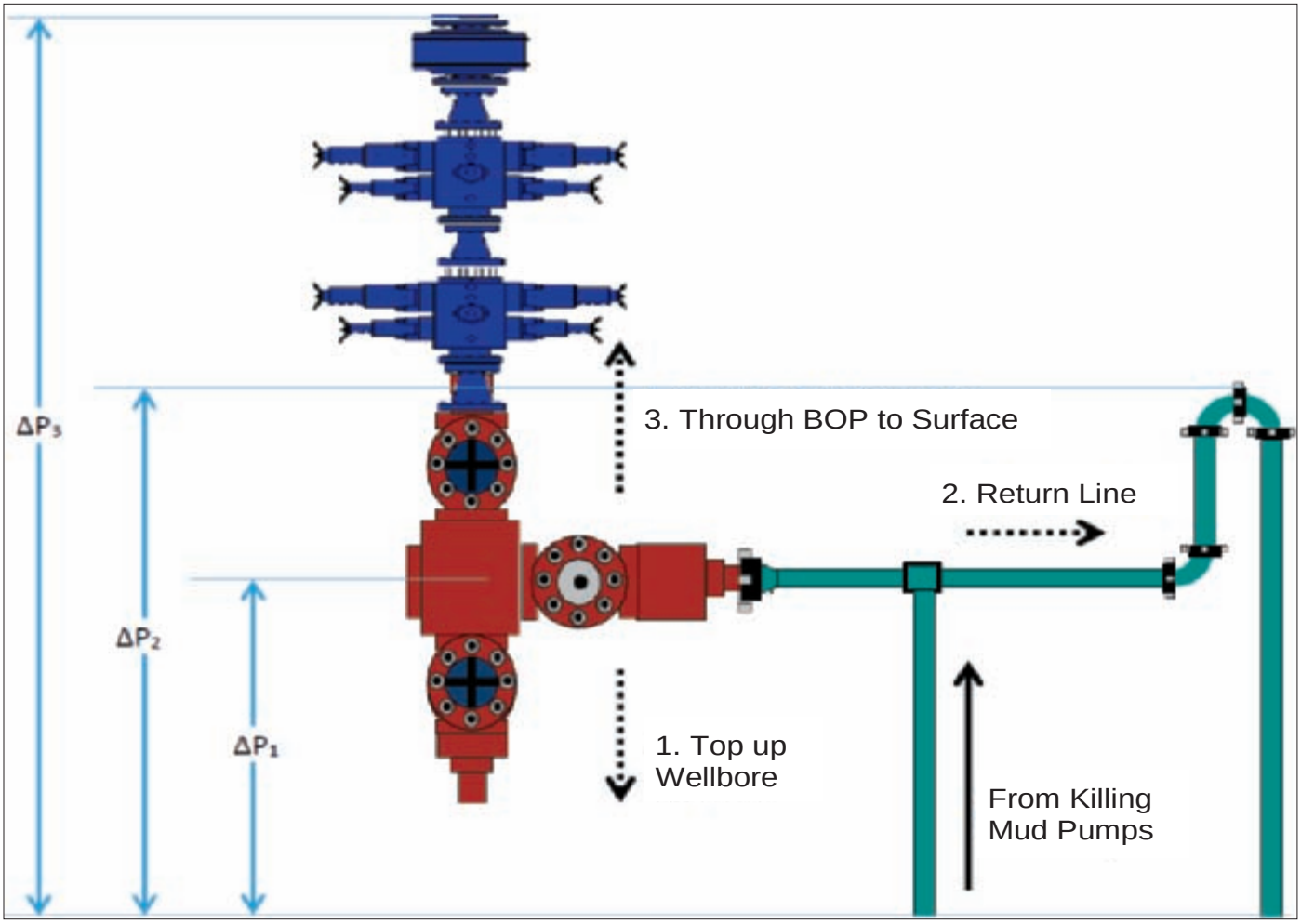

Fig. 7. Return loop design.

which was more than sufficient time to mix a new batch in the other tank. From the rate previously recorded by the rig operation, one can anticipate a scenario at which a pump rate of 0.5 bpm is required, dictating that two tanks shall be adequate for this job. Enough sodium chloride and water has to be continuously supplied to the location to ensure the continuation of kill brine mixing.

Coordination during Operation — When to Pump Kill Fluid?

It is vital to continue pumping at a rate equal to — or more than — the loss rate calculated at all times, even if the job is idle or the BOPs are closed. With the well on losses, the reduction in hydrostatic column height will eventually result in reaching a balanced state with reservoir pressure — no overbalance. The risk of hydrocarbon flow to the surface (kick) might be encountered if such a state is reached. The following calculation shows that if pumping is halted for more than an hour, then we might lose the 300 psi overbalance:

Overbalance Height (ft) = Overbalance (psi)/kill brine density (psi/ft)

Volume of Overbalance = Overbalance height (ft) × tubing capacity (bbl/ft)

Time to Balance = Volume of overbalance (bbl)/loss rate (bbl/hour)

Applying numbers from this trial test:

Density Conversion: 71.6 pcf → 9.57 ppg → 0.4977 psi/ft

Pipe Capacity (7" 26#) = 0.03826271 bbl/ft

Overbalance Height (ft) = 300/0.4977 = 602.77 ft

Volume of Overbalance = 602.77 × 0.03826271 = 23 bbl

$$\textit{Time to Balance} = \frac{23\ bbl}{24\ bbl/Hour} \cong 1\ Hour$$

These calculations assume that the loss rate is the same even at lower overbalance values, although fluid loss will decrease. Such assumption was made as a safety factor.

If more than an hour passes without pumping kill fluid, then the risk of hydrocarbon flow to the wellbore column might be encountered. Therefore, bullheading another 1.5 wellbore volumes is recommended to ensure consistent fluid density — all kill brine density — in the hydrostatic column.

During the time at which the annular BOP is open — Phase 1 and 3 — the return loop can be used by pumping continuously at a low rate to ensure the well is being topped up with kill fluid. The rate can be increased slowly until returns are monitored in the return line to ensure that pumping is in excess of the loss rate.

During Phase 2, and with the injector head and stripper made up and pressure tested on top of the annular BOP (closed system), a decision was made to stop pumping the killing fluid. After performing the required space out for the ESP system and removing the injector head, the well was bullheaded again with kill fluid followed by continuous pumping throughout the rest of Phase 3.

Effect on TCA Pressure

Pumping the kill fluid down the tubing caused substantial reduction in the TCA pressure, Fig. 8. Such observation is not due to wellhead integrity issues, i.e., no tubing and TCA communication issue, but it is rather associated with the tubing movement in the 4½" floating seal stinger assembly immediately above the production packer. Being at a temperature lower than the bottom-hole, the kill fluid cools the tubing string and causes it to contract (upward force). This upward temperature force dominates the piston forces, due to the hydrostatic pressure change in tubing. This upward tubing movement will increase the TCA volume, and along with TCA liquid cooling, can cause the TCA pressure value to drop significantly.

This means that the value of the TCA pressure depends on the amount of supply of cool kill fluid and not on the hydrostatic column of the kill fluid. Therefore, the TCA pressure cannot be used as a method to know if the well is fully topped up with kill fluid or not. Monitoring the return line with a gradual increase in pumping rate shall be used for this matter.

Another lesson learned from this observation is not to bleed the TCA at the start of the operation, even if high-pressure values are measured — unless they get close to the rated collapse pressure of the tubing. If the TCA pressure was reduced, then once pumping of the kill fluid commences, there will be a further reduction resulting in low-pressure values — vacuum, negative values — that might affect the wellhead integrity.

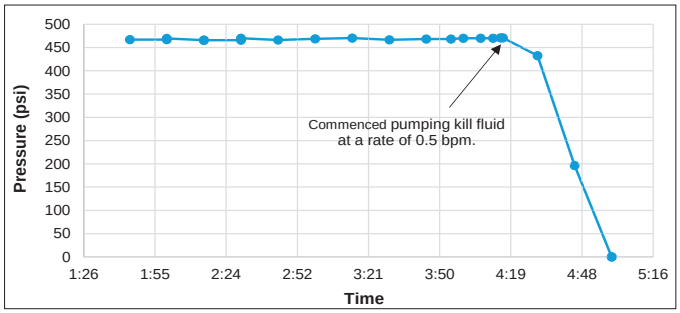

Fig. 8. TCA pressure drop during kill fluid pumping.

Effect of Pumping with ESP in the Wellbore (Piston Effect)

After lowering the ESP into the well (Phase 2), pumping kill fluid at high rates — 3 bpm — resulted in an increase in weight of the BHA as recorded by the CT weight indicator. This observation was traced back to the fact that the ESP assembly created a large piston system inside the tubing due to the small clearance between the two. The ESP motor had a total OD of 5.62" while the 7" tubing had an internal diameter of 6.276". In such a scenario, if tension forces increase beyond the primary shearing mechanism, then the pins might shear, leaving a fish in the hole. These shear pins were introduced as a contingency to detach the cable from the pump, to prepare for the fishing job in the emergency case of having a stuck pump in the well during deployment or retrieval.

Therefore, it is critical to adjust the pumping rate while monitoring the weight gauge of the CT or the crane, to limit the tension force below the shear values of the contingency shear sub.

LESSONS LEARNED

The following are key lessons learned from this successful trial test:

1. It is important to minimize the amount of work at the CT tower over the well, particularly when the annular BOP is open. Preparation tasks can be performed before the actual ESP deployment to reduce this time.
2. Coordination is key between all groups of the job, to include the pumping and mixing unit, CT operation, return line monitoring and data acquisition, and ESP build team.
3. It is important to start by bullheading the well, and then measure the loss rate through the return loop design introduced. Then pumping shall be maintained at a rate equivilant to the well loss rate. If the operation is to stop for a significant time — near one hour — then it is highly recommended to bullhead again to ensure that the hydrostatic column contains only the required kill brine.
4. It is critical to have all necessary logistics in place to ensure that there is enough of a supply of raw material, water and equipment (mixing tanks) to account for continuous pumping thoroughout the operation. Measurement of kill brine density shall be performed on regular intervals to ensure proper mixing.
5. It is important to regularly measure the loss rate to account for any changes in the well's condition.
6. Pumping pressure and rate shall be observed closely once the pump is placed inside the well. The pump might act as a piston that might generate high tension forces.
7. Pumping kill fluid might reduce the TCA pressure.

Therefore, TCA pressure shall not be bled initially unless near tubing collapse values are observed.

8. The kill line will be connected through the lower BOP. This eliminates the inverted U-tube in the return line, which had a tendency to trap air in the line.
9. The Christmas tree flow line will remain in place during subsequent installations. The return line and zero flare package will be connected to existing producing line connections. Check valves will be installed in the return line to flow back.
10. The requirement to continuously pump kill fluid might have a harmful effect on well productivity by changing the wettability in the near wellbore region. The amount of kill brine pumped will be reduceed as the operation becomes a practice that is performed at a faster pace. Future jobs can further incorporate using auto-degradable filter cakes to reduce the loss rate of the well.

CONCLUSIONS

A novel well killing technique and procedure was developed to allow CD-ESP systems to be safely deployed in wells, which have high reservoir pressure and can produce naturally to the surface. With a BOP and kill fluids, sufficient well control barriers are in place during all operational steps, making the CD-ESP rigless deployment not only more efficient, but also safer in comparison with the workover rig-based ESP deployment operations.

ACKNOWLEDGMENTS

The authors would like to thank the management of Saudi Aramco for their support and permission to publish this article.

This article was presented at the Abu Dhabi International Petroleum Exhibition and Conference, Abu Dhabi, UAE, November 13-16, 2017.

REFERENCES

1. Xiao, J.J., Roth, B.A., Lastra, R. and Sarawaq, Y.: "Well Control Strategy for ESP Rigless Deployment with Power Cable," SPE paper 185146, presented at the SPE Electric Submersible Pump Symposium, The Woodlands, Texas, April 24-28, 2017.
2. Roth, B.A., Xiao, J.J., Abdelaziz, M., Mack, J., et al.: "Field Deployment of a Rigless Cable Deployed ESP Using a Vertical Wellhead," SPE paper 183821, presented at the SPE Middle East Oil and Gas Show and Conference, Manama, Bahrain, March 6-9, 2017.

BIOGRAPHIES

Mohannad Abdelaziz is a Petroleum Engineer on the Production Technology Team of Saudi Aramco's Exploration and Petroleum Engineering Center – Advanced Research Center (EXPEC ARC). He has worked on several research and development projects in advanced well completions, well intervention, and artificial lift.

In 2015, Mohannad completed a one-year assignment working as a Production Engineer at the Safaniyah offshore field. He has filed three patents and has contributed to more than seven international publications. Mohannad won the 2016 Abu Dhabi International Petroleum Exhibition and Conference Young Engineer award.

He received his B.S. degree in Mechatronics Engineering from the University of Jordan, Amman, Jordan, and his M.S. degree in Mechanical Engineering from King Abdullah University of Science and Technology (KAUST), Thuwal, Saudi Arabia. Mohannad has a second M.S. degree, this one in Petroleum Engineering from Heriot-Watt University, Edinburgh, U.K.

Brian A. Roth is a Petroleum Engineer Specialist in the Production Technology Division of Saudi Aramco's Exploration and Petroleum Engineering Center – Advanced Research Center (EXPEC ARC). His focus is on R&D efforts with an emphasis on artificial lift technologies. Before joining Saudi Aramco in 2012, Brian spent over 25 years in engineering and leadership roles in large oil and gas service companies.

He has over 24 applied and granted patents, and has authored or coauthored several technical and journal papers.

Brian received his B.S. degree in Mechanical Engineering from the University of Texas at Austin, Austin, TX, and an MBA degree from Texas A&M University, College Station, TX.

Dr. Jinjiang Xiao is a Petroleum Engineering Consultant working in Saudi Aramco's Exploration and Petroleum Engineering Center – Advanced Research Center (EXPEC ARC). He is currently the focus area champion for artificial lift.

Prior to joining Saudi Aramco in 2003, Jinjiang spent 10 years with Amoco and later BP-Amoco, working on multiphase flow, flow assurance and deepwater production engineering.

He received both his M.S. and Ph.D. degrees in Petroleum Engineering from the University of Tulsa, Tulsa, OK.

SUBSCRIPTION ORDER FORM

To begin receiving the *Saudi Aramco Journal of Technology* at no charge, please complete this form.

Please print clearly.

Name _____

Title _____

Organization _____

Address _____

City _____

State/Province _____

Postal code _____

Country _____

E-mail address _____

Number of copies _____

TO ORDER

By phone/email:

Saudi Aramco Public Relations Department
JOT Distribution
+966-013-876-0498
william.bradshaw.1@aramco.com

By mail:

Saudi Aramco Public Relations Department
JOT Distribution
Box 5000
Dhahran 31311
Saudi Arabia

Current issues, select back issues and multiple copies of some issues are available upon request.

The *Saudi Aramco Journal of Technology* is published by the Saudi Aramco Public Relations Department, Saudi Arabian Oil Company, Dhahran, Saudi Arabia.

GUIDELINES FOR SUBMITTING AN ARTICLE TO THE SAUDI ARAMCO JOURNAL OF TECHNOLOGY

These guidelines are designed to simplify and help standardize submissions. They need not be followed rigorously. If you have additional questions, please feel free to contact us at Public Relations. Our address and phone numbers are listed on page 75.

Length

Varies, but an average of 2,500-3,500 words, plus illustrations/photos and captions. Maximum length should be 5,000 words. Articles in excess will be shortened.

What to send

Send text in Microsoft Word format via email or on disc, plus one hard copy. Send illustrations/photos and captions separately but concurrently, both as email or as hard copy (more information follows under file formats).

Procedure

Notification of acceptance is usually within three weeks after the submission deadline. The article will be edited for style and clarity and returned to the author for review. All articles are subject to the company's normal review. No paper can be published without a signature at the manager level or above.

Format

No single article need include all of the following parts. The type of article and subject covered will determine which parts to include.

Working title

Abstract

Usually 100-150 words to summarize the main points.

Introduction

Different from the abstract in that it "sets the stage" for the content of the article, rather than telling the reader what it is about.

Main body

May incorporate subtitles, artwork, photos, etc.

Conclusion/summary

Assessment of results or restatement of points in introduction.

Endnotes/references/bibliography

Use only when essential. Use author/date citation method in the main body. Numbered footnotes or endnotes will be converted. Include complete publication information. Standard is *The Associated Press Stylebook*, 52nd ed. and *Webster's New World College Dictionary*, 5th ed.

Acknowledgments

Use to thank those who helped make the article possible.

Illustrations/tables/photos and explanatory text

Submit these separately. **Do not place in the text.** Positioning in the text may be indicated with placeholders. Initial submission may include copies of originals; however, publication will require the originals. When possible, submit both electronic versions, printouts and/or slides. Color is preferable.

File formats

Illustration files with .EPS extensions work best. Other acceptable extensions are .TIFF, .JPEG and .PICT.

Permission(s) to reprint, if appropriate

Previously published articles are acceptable but can be published only with written permission from the copyright holder.

Author(s)/contributor(s)

Please include a brief biographical statement.

Submission/Acceptance Procedures

Papers are submitted on a competitive basis and are evaluated by an editorial review board comprised of various department managers and subject matter experts. Following initial selection, authors whose papers have been accepted for publication will be notified by email.

Papers submitted for a particular issue but not accepted for that issue will be carried forward as submissions for subsequent issues, unless the author specifically requests in writing that there be no further consideration. Papers previously published or presented may be submitted.

Submit articles to:

Editor
The *Saudi Aramco Journal of Technology*
C-11B, Room AN-1080
North Admin Building #175
Dhahran 31311, Saudi Arabia
Tel: +966-013-876-0498
Email: william.bradshaw.1@aramco.com.sa

Submission deadlines

Issue	Paper submission deadline	Release date
Winter 2018	August 16, 2018	December 31, 2018
Spring 2019	November 20, 2018	March 31, 2019
Summer 2019	February 21, 2019	June 30, 2019
Fall 2019	May 22, 2019	September 30, 2019

Toward a Method for Measuring Wettability in Porous Media by NMR Water Vapor Isotherm Technique

Dr. Hyung T. Kwak, Dr. Ahmad M. Harbi, Yan Song, Prof. Alfred Kleinhammes, and Prof. Yue Wu

ABSTRACT

The wettability of reservoir rocks is one of the most important factors in evaluating hydrocarbon reserves and producibility. Reservoir rocks contain considerable amounts of pore spaces to trap and transport fluids, including hydrocarbons and brine. Although those pore spaces are essential and beneficial for hydrocarbon production, the porous nature of reservoir rocks, on the other hand, poses difficulties for measuring the wettability. Macroscopic experiments, such as a contact angle determination, are of limited value because the wettability needs to be determined within the rock pore structure.

Smart Well Completion Optimization in Multilateral Wells

Dr. James O. Arukhe, Dr. Faisal T. Al-Khelaiwi, Obiomalotaoso L. Isichei, and Ammar A. Al-Dhubaiki

ABSTRACT

The ability of smart well completions (SWCs) to best function as intended in the field has led to renewed focus on SWC optimization opportunities. The action of inflow control valves (ICVs) is key to the improved management of flux imbalance and the premature production delay of unwanted fluids from contributing laterals of the intelligent wells. Difficulty with the use of ICVs includes the complexity to determine all possible combinations of valve settings — given 11 possible positions per valve on each lateral.

Effect of the Rotary Steerable System Steering Mechanism on Wellbore Tortuosity in Horizontal Wells

Victor Oliveira, Bader S. Al-Zahrani, Albaraa Al-Rushud, and Muntasar Mohammad

ABSTRACT

This article describes a new approach to evaluating the effectiveness of the rotary steerable system (RSS) steering mechanism on wellbore tortuosity in horizontal wells. Wellbore tortuosity in drilling applications is defined as any unwanted deviation from the planned well trajectory. As reservoir objectives become more complex and exact, operators increasingly perceive the wellbore tortuosity as a serious concern in the process of drilling, completing, and producing wells.

Successful Implementation of Multi-modal, Self-Assembling, Self-Degradable and Environmentally Friendly Solids Particulates as Diverter in Acid Stimulation Treatments in Carbonate Reservoirs

Ataur R. Malik, Mohammed A. Asiri, Tolulope M. Ogundare, and Mohamed Khalifa

ABSTRACT

This article focuses on the evaluation of novel diversion technology based on self-degradable solids particulates that were applied in the complex carbonate reservoirs. The well performance results were compared in this article between wells stimulated with novel and conventional diversion technologies as part of the evaluation.